Observations of Plasma Waves at the Earth's Dayside Magnetopause

A DISSERTATION
SUBMITTED TO THE FACULTY OF THE GRADUATE SCHOOL
OF THE UNIVERSITY OF MINNESOTA
BY

Xiangwei Tang

IN PARTIAL FULFILLMENT OF THE REQUIREMENTS
FOR THE DEGREE OF
Doctor of Philosophy

Cynthia A. Cattell, Advisor

April, 2015

Acknowledgments

The work presented in this thesis would not have been possible had I not been given the chance to do the research involved. Thus, I am sincerely grateful to my advisor Cynthia Cattell for giving me the opportunity to prove myself. Her knowledge, enthusiasm and perseverance make it difficult to overstate my gratitude.

I would like to thank V. Angelopoulos for use of data from the THEMIS Mission, specifically: J. W. Bonnell and F. S. Mozer for use of EFI data; D. Larson and R. P. Lin for use of SST data; C. W. Carlson and J. P. McFadden for use of ESA data; A. Roux and O. LeContel for use of SCM data; and K. H. Glassmeier, U. Auster and W. Baumjohann for the use of FGM data.

Many people were instrumental in my understanding of space plasma physics and computational methods. I would especially like to thank professors Robert Lysak, John Wygant and Thomas Jones for their guidance and useful physics discussions, without which this paper would not have been possible. As the members of both my preliminary exam and thesis committee, they provided great assistance evaluating my work.

This work has benefited from discussions with other researchers, also. John Dombeck was instrumental in my understanding of programing in IDL. Lynn Wilson provided very useful softwares and helped me modify papers. Aaron Breneman and Scott Thaller were very helpful whenever I have questions. Their humerousness brightend our lives in the office. Steve Monson was so nice and provided a lot of help on modifying my papers and thesis. Yan Song was very considerate and always gave me help and advice. I would also like to thank the following people for their help and useful physics discussions: Paul Kellogg, Keith Goetz, Kris Kersten, Adam Hupach, Sheng Tian, Chris Colpitts, Jianbao Tao, Jesse Woodroffe, Alyssa Hamre, Joshua Lynch and Charles Godfrey. I must not forget to thank all the people whom I have encountered with during my graduate school

career, including: Qing Xu, Tianran Chen, Jie Yang, Xin Zhang, Chen Hou and Shanxu Shi.

The last, but definitely not the least note of acknowledgment goes to my family. I would like to thank both of my parents for their understanding and support. I would like to thank my husband Lei Dai for keeping me honest and supporting my efforts. My lovely daughter Siqi Dai has brought a lot of happiness to me and brightened my life. I would not have made it through the graduate school if both my parents and Lei's parents had not crossed the Pacific Ocean to take care of Siqi. Same thanks to my sister for her understanding and support.

This research was supported by NNX08AF28, NNX13AE16G and the Dr. Leonard Burlaga/Arctowski Medal Fellowship.

Abstract

Plasma waves near the magnetopause are of considerable interest due to the possible role which wave-particle interactions may play in the diffusion and transport of plasma across the magnetopause and the possible effects of plasma turbulence on energy dissipation and magnetic reconnection. Large amplitude plasma waves in a variety of frequency bands are often observed during crossings of the magnetopause current sheet when diagnostics indicate that reconnection is occurring.

The studies herein were performed using plasma wave electric and magnetic fields and particle data primarily from the Time History of Events and Macroscale Interactions during Substorms (THEMIS) satellite to investigate the possible generation mechanisms of different wave modes and the roles that the wave modes play in the process of magnetic reconnection and magnetopause boundary layer formation. The main advantages of the THEMIS data set are the long intervals of high time resolution three-dimensional electric and magnetic field burst waveforms.

The work began with observations of large amplitude waves in a well-defined electron diffusion region at the subsolar magnetopause. These waves identified as whistler-mode waves, electrostatic solitary waves, lower-hybrid waves and electrostatic electron cyclotron waves, are observed in the same 12 s waveform capture and in association with signatures of active magnetic reconnection. The large amplitude waves in the electron diffusion region are coincident with abrupt increases in electron parallel temperature suggesting strong wave heating. The whistler-mode waves are at the electron scale and enable us to probe electron dynamics in the diffusion region. The energetic electrons ($\sim$30 keV) within the electron diffusion region have anisotropic distributions with $T_{e\perp}/T_{e\parallel} > 1$ that may provide the free energy for the whistler-mode waves. The energetic anisotropic electrons may be produced during the reconnection process. The whistler-mode waves propagate away from the center of the "X-line" along magnetic field lines, suggesting that the electron diffusion region is a possible source region of the whistler-mode waves.

Another study was the identification of large amplitude electrostatic ion cyclotron

waves near the Earth's dayside magnetopause at MLT of ~ 14. The electrostatic ion cyclotron waves were identified in a boundary layer in the magnetosphere adjacent to the magnetopause where reconnection was occurring. The electrostatic ion cyclotron wave power was primarily at $2f_{cH}$ (where f_{cH} is the hydrogen cyclotron frequency) and simultaneously observed with perpendicular ion heating. The electrostatic ion cyclotron waves had electric field amplitudes as large as 30 mV/m peak-to-peak with significant power both perpendicular and parallel to the magnetic field. These amplitudes were greater than those of previously observed ion cyclotron harmonics at the nightside magnetopause. The electrostatic ion cyclotron waves occurred during an interval of enhancements in the quasi-static electric field and fluctuations in the background magnetic field, plasma density and temperatures. The observations indicate that a plasma density gradient is a possible source of free energy for the electrostatic ion cyclotron waves. The observed flow shears are not large enough to drive the waves. Whistler-mode waves were identified near the electrostatic ion cyclotron wave region but closer to the magnetopause in a region with slightly higher ion and electron temperatures.

Further investigation was on simultaneous observations of these waves at the low-latitude boundary layer of the Earth's magnetopause. The waves were identified through auditory analysis in the high resolution (16384 samples/s) electric field burst data and occurred at the same time as large fluctuations of plasma density and temperature (at time scales of $\sim$3 to 4 minutes) at a location of 9.3 Re, 14.4 magnetic local time, and 5.8 degrees magnetic latitude. Large fluctuations in the interplanetary magnetic field and solar wind flow speed were observed associated with this wave event and could be responsible for the variations seen in the low-latitude boundary layer. The particle distribution functions show that lower-energy ions (<1.3 keV) are anisotropic with $T_{i\perp} > T_{i\parallel}$ while lower-energy (<300 eV) electrons are anisotropic with $T_{e\perp} < T_{e\parallel}$. In addition, electrons show a double-peaked distribution, i.e., bi-streaming beams. These distributions are consistent with instability mechanisms proposed for the observed waves. The results provide insights into wave coupling near the magnetopause and suggest that coupling processes may be more important than usually thought.

The work presented in this thesis has helped increase understanding of the microphysics of reconnection and boundary layer formation through investigation of the role of waves.

Contents

List of Figures

Chapter 1

Introduction

1.1 The Earth's Magnetosphere

After the discovery of the Van Allen radiation belts in 1958, Thomas Gold proposed the term magnetosphere in 1959. A magnetosphere is the region surrounding a planet, where the motion of particles is governed by the planet's magnetic field. The shape of the Earth's magnetosphere is the direct result of being blasted by the particles from the Sun, carried in the solar wind. An illustration of the Earth's magnetosphere is shown in Figure 1.1 (Illustration by Steele Hill). Due to the Sun-Earth coupling, the magnetosphere is a very dynamic environment for many plasma phenomena. Satellites have been launched to probe the Earth's magnetosphere since 1960, making the magnetosphere a natural laboratory for studies of various plasma processes.

Kellogg [71] predicted the existence of the bow shock based on the interplanetary plasma flow measured by means of Explorer 10. A bow shock develops where supersonic solar wind is slowed down to subsonic speed. The solar wind flow is deflected at the bow shock and streams around the magnetosphere, forming the magnetosheath. Most of the solar wind particles are heated and slowed at the bow shock and detour around the Earth. Thus the Earth's magnetosphere prevents most of the solar wind particles from hitting the Earth and protects life on the Earth. The Explorer 12 spacecraft in 1961 led to the observation by Cahill and Amazeen in 1963 [15] of a sudden decrease in the strength of the magnetic field at about 8.2 R_E (where R_E is the radius of the

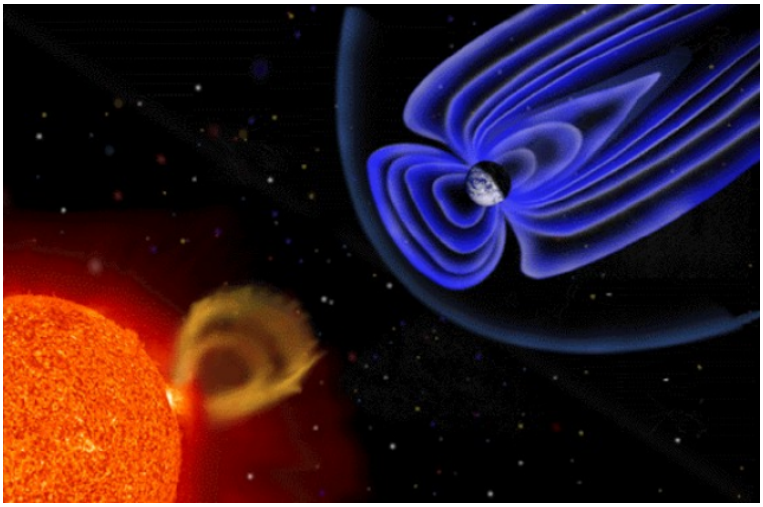

Figure 1.1: An artist's view of the Sun-Earth connection through the solar wind and magnetic fields (Illustration by Steele Hill).

Earth), later named the magnetopause. As shown in Figure 1.2 [81], the thin boundary between the shocked solar wind plasma and the magnetospheric plasma is the Earth's magnetopause. Moving towards the Sun, we would detect this boundary at a distance of about 10 R_E. The interaction of the Earth's magnetic field and the solar wind drags out the night-side magnetosphere to possibly 1000 R_E. This extension of the magnetosphere is known as the magnetotail.

The Earth's magnetopause is formed by the interaction of solar wind with the Earth's magnetic field. It forms where the pressure in the magnetosphere equals the pressure in the magnetosheath. The pressure in the magnetosphere is mainly magnetic pressure while the pressure in the magnetosheath is the sum of thermal pressure and magnetic pressure. The two pressures are in approximate equilibrium. The magnetopause is very sensitive to plasma conditions in the magnetosheath so it varies from crossing to crossing, even as the magnetopause is being crossed. By applying Ampere's law across the boundary, we find that the boundary must carry the currents flowing into and out of the plane as shown in Figure 1.2. In addition, these currents must provide the current needed so that the $\vec{j} \times \vec{B}$ force can deflect the solar wind plasma.

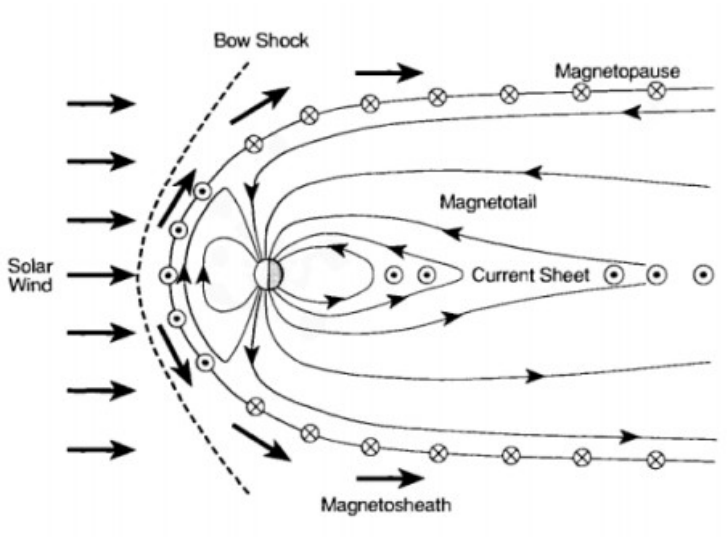

Figure 1.2: A simple sketch of the Earth's magnetosphere in the noon-midnight meridian from Kivelson and Russell [81].

1.2 Magnetopause and Boundary Layer

1.2.1 Introduction

The first extensive observations of the magnetopause were made by the ISEE 1 and 2 spacecraft. It was found that magnetic field direction and magnitude change abruptly from their magnetosheath to their magnetospheric values at the magnetopause [15]. However, the adjoining plasma boundary layer, a thin region located just inside the magnetopause, was discovered much later [65, 41]. OGO-5 observations show that in the boundary layer the magnetic field has substantial fluctuations and depressed field magnitude. The boundary layer contains plasma with characteristics similar to, but not identical with, the magnetosheath plasma. The plasma boundary layer immediately Earthward of the magnetopause at low latitudes is called the low-latitude boundary layer. A schematic drawing of the magnetopause surface and the boundary layers is shown in Figure 1.3 [82]. The light blue outer surface is the magnetopause, its boundary layers are shown in darker blue. Magnetic field lines are shown in blue, electric currents in yellow. The polar region where the magnetic field lines converge is the polar cusp.

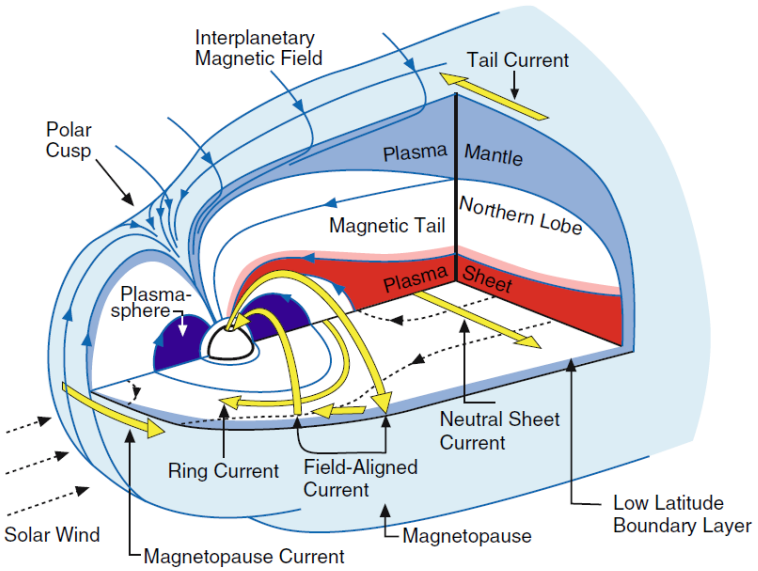

Figure 1.3: A schematic drawing of the magnetopause surface and the boundary layers from Kivelson and Russell [82].

1.2.2 The Structure of the Magnetopause and Boundary Layer

The earliest concept of the magnetopause was that of a boundary between an unmagnetized, cold flowing plasma (solar wind) and a uniform vacuum magnetic field (magnetosphere). This simplest approximation is shown in Figure 1.4 [81]. A cold beam of ions and electrons flows from the left and turns around and returns to the left. Since the electron is much lighter than the proton, its gyro radius is much smaller than that of the proton and it will turn around in a narrow layer near the outer edge of the current layer. In the absence of any electric field that might accelerate the particles, both particles carry half of the current because they have the same velocity and charge. Thus half the current flows in a very narrow layer of one electron gyro radius and the other half of the current flows in a layer one proton gyro radius wide. If a charge separation electric field arises, the electron will be accelerated toward the more massive ion, increase in velocity, penetrate further and carry a larger fraction of the current. Thus, most of the current would be carried by electrons in a layer that is less than an ion gyro radius thick.

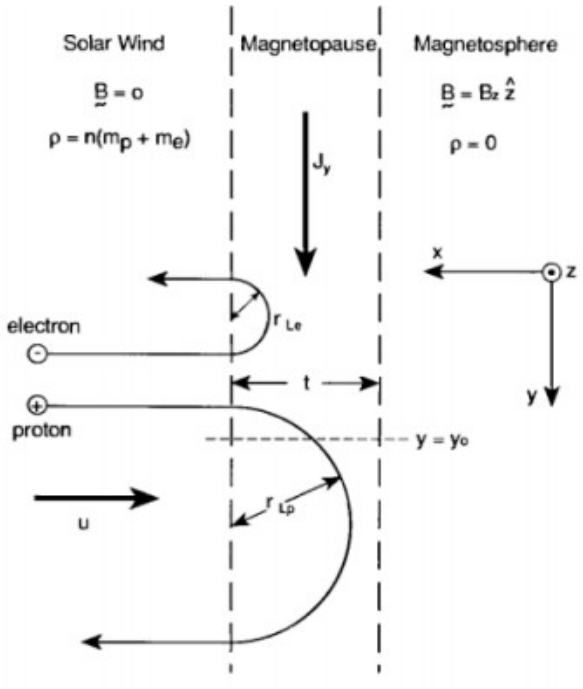

Figure 1.4: Chapman-Ferraro current layer from Kivelson and Russell [81].

Assuming a one-dimensional model of the local magnetopause structure and that the orientation of the magnetopause current layer doesn't change during the satellite crossing time, the condition $\nabla \cdot \mathbf{B} = 0$ implies that the magnetic field component perpendicular to the magnetopause remains constant during the satellite crossing. The normal direction to the magnetopause is that along which the projected magnetic field component has minimum variance. For many magnetopause crossings the magnetopause normal direction and normal magnetic field component may be determined from single satellite magnetic field data by using Minimum Variance Analysis [76].

The magnetopause is constantly in motion due to changing solar wind conditions, resulting in boundary velocities greater than that of any of the observing spacecraft. This velocity is often periodic leading to multiple crossings. Multi-spacecraft missions have shown that the magnetopause is almost always in rapidly changing inward-outward

motion with typical speeds of tens of km/s. The region near the subsolar point is important for the understanding of magnetospheric dynamics since it is the preferred site of plasma entry in all theoretical work ever since the original proposal by Dungey [39]. Chapman and Ferraro [26] first introduced the concept of magnetopause location which depends on the solar wind dynamic pressure. Fairfield [43] recognized that the interplanetary magnetic field orientation can also affect the magnetopause location. Song et al. [135] showed that magnetopause is composed of a sheath transition layer, outer boundary layer and inner boundary layer near the subsolar point when the interplanetary magnetic field was northward.

1.2.3 Formation of the Low-Latitude Boundary Layer

The magnetopause boundary layer is a site of continual transfer of plasma, momentum and energy from the magnetosheath to the magnetosphere. Observations have shown evidence for the existence of the boundary layer [41]. However, how solar wind plasma, momentum and energy are transferred to the magnetosphere has been a critical question of magnetospheric physics. Possible mechanisms include magnetic reconnection [39], diffusive entry [139], and the Kelvin-Helmholtz instability [98].

Diffusive processes at the magnetopause are required to either explain the existence of the low-latitude boundary layer during cases of northward interplanetary magnetic field or to locally provide the resistivity to drive reconnection. Eastman and Hones [40] conclude that diffusive as well as nondiffusive processes contribute to the entry of magnetosheath plasma into the boundary layer. Observations reported by Phan et al. [117] suggest that low-latitude magnetopause reconnection during northward interplanetary magnetic field is not responsible for the formation of the adjacent low-latitude boundary layer; it might be in the process of eroding a pre-existing low-latitude boundary layer that was created either by diffusive entry or by non-simultaneous double-cusp reconnection.

Under comparatively stable solar wind parameters, the existence of high level fluctuations of plasma and magnetic field parameters in the magntosheath is suggested to be

important for low-latitude boundary layer formation [126]. The jets of magnetosheath plasma which formed under these conditions can penetrate inside the magnetosphere due to the absence of pressure balance. This process is suggested to lead to low-latitude boundary layer formation and magnetic reconnection.

Early studies suggested that the strength of local anomalous dissipation is too weak (see reviews by Coroniti [30]). Tsurutani and Thorne [154] suggested that electrostatic waves at frequencies of ion cyclotron frequency may be capable of inducing the required rapid inward diffusion of typical magnetosheath ions. Treumann et al. [153] calculated the diffusion expected from the quasi-linear theory of the lower-hybrid drift instability at the Earth's magnetopause. They found that the lower-hybrid drift instability yields sufficiently high diffusion rates to account for the production and maintenance of the magnetopause boundary layer. Treumann et al. [152] conclude that high frequency electrostatic waves are unable to provide the diffusion coefficients needed for forming the low-latitude boundary layer. Very low frequency electric and magnetic waves can provide sufficiently large diffusion to form the low-latitude boundary layer. Cattell et al. [22] presented observations of low-frequency waves at the magnetopause and also suggested that lower-hybrid drift waves provide enough resistivity required for magnetopause reconnection to occur.

1.3 Magnetic Reconnection

1.3.1 Introduction

The entry of solar wind plasma onto geomagnetic field lines earthward of the magnetopause is one of the outstanding problems of magnetospheric physics. One of possible dominant entry mechanisms is magnetic reconnection [39].

Magnetic reconnection is the process during which magnetic field lines of opposite polarity reconfigure to a lower-energy state by releasing magnetic energy to the surroundings. Magnetic reconnection is considered to be an important energy conversion process [39] that occurs in a variety of plasma environments such as solar flares [109],

planetary magnetospheres [130], the solar wind [57, 116] and fusion experiments in laboratories [14]. In the magnetosphere, reconnection can occur both in the magnetopause and magnetotail. At the magnetopause, it facilitates the entry of solar wind plasma and electromagnetic energy into the magnetosphere. During this process of breaking and reconnection of magnetic field lines, particles can be accelerated to high energies, plasma jets are formed, heat is released, and energy can be transferred into the surrounding region. Magnetic reconnection is also known as a source of electromagnetic radiation [137, 163].

Observationally, magnetic energy is released in bursts, driving explosive phenomena such as solar flares and magnetospheric substorms. When sunspots erupt, intense x-ray flares can be released on a time scale of minutes with as much as 10^{25} joules of electromagnetic energy - equivalent to all the energy stored in fossil fuels on Earth or 10 million times as much energy as that released from a volcanic explosion. A large amount of experimental evidence for magnetic reconnection is also found in fusion devices in laboratories. Magnetic reconnection phenomena are investigated in fusion devices (like Tokamaks) to gain better magnetic confinement. Yamada [164] and Ji et al. [67] reviewed laboratory experiments dedicated to the study of the fundamental physics of magnetic reconnection. Laboratory experiments are useful for understanding the fundamental physics of magnetic reconnection since they can provide well-correlated plasma parameters at multiple plasma locations simultaneously.

Examples of the magnetic geometry of the interaction between the solar and terrestrial magnetic fields during reconnection near the equator at a variety of scale sizes are shown in Figure 1.5 [104]. Figure 1.5a illustrates the magnetic field interactions between the Sun and the Earth in the noon-midnight meridian plane. The purple curves represent the interplanetary magnetic field lines that start and end at the Sun without passing through the Earth. The blue curves represent the Earth's magnetic field lines. The green curves represent the magnetic field lines that pass through both the Earth and the Sun. Figure 1.5b shows a smaller scale view of the white shaded area in Figure 1.5a. The interplanetary field lines (in purple) and the Earth's field lines (in blue) reconnect in a small region (yellow shaded) where the plasma becomes demagnetized,

creating open field lines (in green) extending from the Earth into the solar wind. Figure 1.5c shows a magnified view of the yellow shaded area in Figure 1.5b. Reconnection occurs between the interplanetary field lines and the Earth's closed field lines, forming an "X-line" which is extended in the Y direction at the thin magnetopause current sheet. Plasma and fields flow into the reconnection region from the right and the left and flow out of the top and bottom as electromagnetic energy is converted into particle kinetic energy. The gray rectangle represents a sheet of current flowing out of the page, which is associated with the curl of magnetic fields.

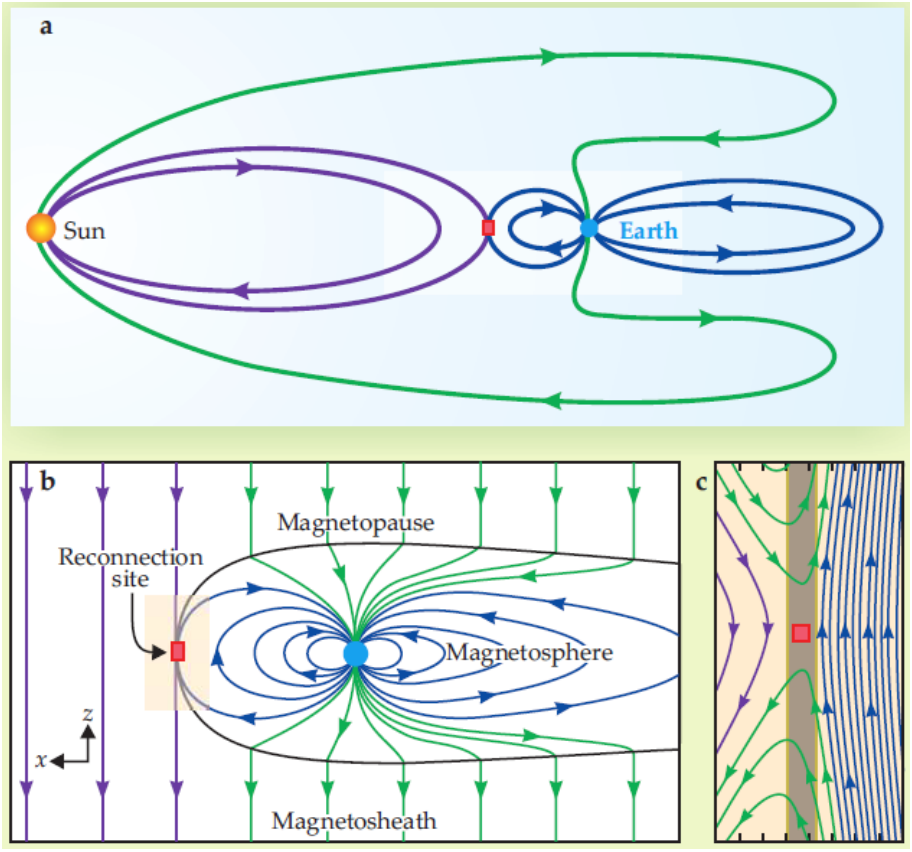

Figure 1.5: Magnetic-field interactions between the Sun and the Earth in the noon-midnight meridian plane [104]. (a) The magnetic field interactions between the Sun and the Earth in the noon-midnight meridian plane. (b) A smaller scale view of the white shaded area in (a). (c) A magnified view of the yellow shaded area in (b).

Applying reconnection geometries to the dayside magnetopause results in the sketch shown in Figure 1.6 [58]. The field lines marked S1 and S2 are reconnected across the magnetopause which form the "X-line". Magnetosheath and magnetospheric particles enter from the left and right, respectively. Plasma crossing the current layer is accelerated away from the subsolar region by the force. The plasma, on reconnected flux tubes, flows out of the figure toward the top and bottom to form the boundary layer. For comparable energies, electrons are faster than ions, so they move closest to the Earth, almost defining the last closed field line. Ions have an inner edge that is closer to the current layer defined by time-of-flight effects and the convection of plasma toward the current layer.

1.3.2 Models of Reconnection

Theoretical studies of reconnection have resulted in the development of many reconnection models. The physics of energy conversion is crucial in magnetic reconnection theories. The time scale of reconnection plays an important role as an experimental check for theoretical models. The most frequently studied models can be categorized into three types: two classical models of steady-state reconnection (Sweet-Parker [142] and Petschek [114]) and more recent models that focus on collisionless reconnection.

Sweet-Parker Model

The Sweet-Parker model is based on resistive magnetohydrodynamics (MHD). This model consists of two different regions: the convection region (electric field $\vec{E} = -\vec{V} \times \vec{B}$) and the diffusion region (electric field $\vec{E} = \vec{j}/\sigma$, where σ is conductivity of plasma). Figure 1.7 [81] shows the two-dimensional reconnection layer, in which the magnetic field lines with opposite directions but same strength B_0 reconnect and create new field lines with strength B_1. The shaded region, which has a width 2L in the Z direction and a thickness 2δ in the X direction, is the diffusion region surrounded by the convection region. In the convection region, the ideal MHD (frozen-in condition) assumption holds while the resistivity has to be considered in the diffusion region. Ideal MHD assumes that the conductivity of plasma is infinitely large and the equation $\vec{E} + \vec{V} \times \vec{B} = 0$ can be

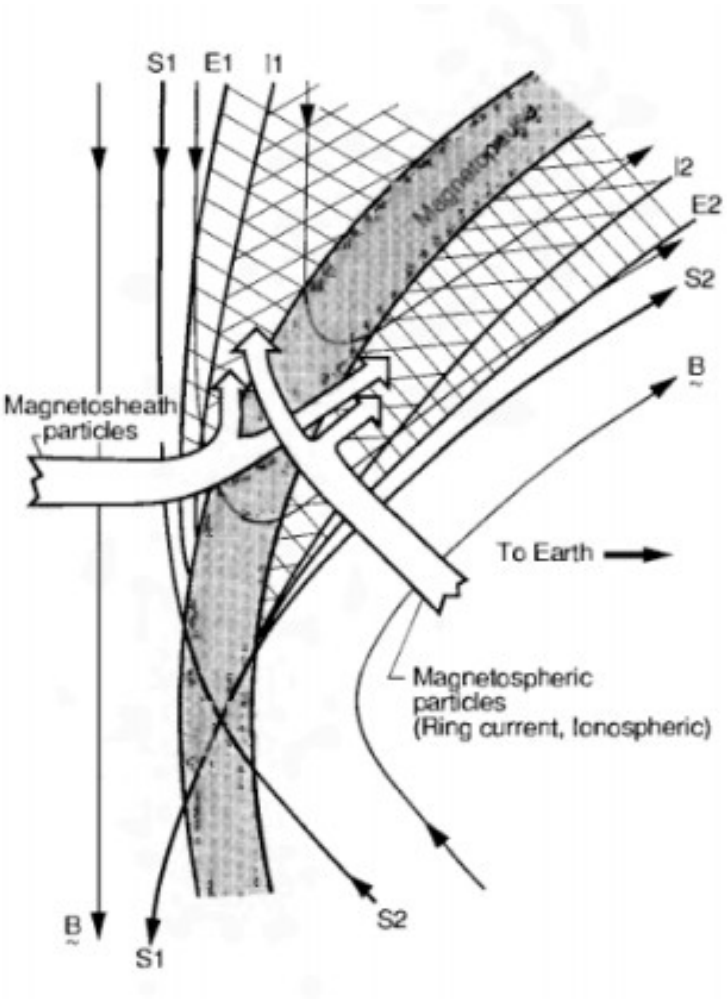

Figure 1.6: Geometry of magnetopause reconnection at an "X-line" [58]. S1 and S2 represent magnetic field lines. The shaded region bounded by lines E1 and E2 are those regions accessible to accelerated electrons while the shaded region bounded by lines I1 and I2 are those regions accessible to accelerated ions.

derived from Ohm's law. The resistivity is zero in ideal MHD. Another interpretation of the frozen-in condition is that the magnetic flux through any enclosed area remains constant as the area is transported with the fluid. The convection electric fields $\vec{E} = -\vec{V} \times \vec{B}$ are in the same direction (points out of the page) on both sides of the "X-line" which is extended in the Z direction. The $E \times B$ drift due to the convection electric fields makes plasma flow toward the diffusion region from both the top and the bottom with a velocity u_i and flow out of the left and the right of the picture with a velocity u_0. According to Faraday's law, $\nabla \times \vec{E} = 0$ holds in steady state. Thus the electric fields must be uniform over the entire reconnection region, i.e. the same electric field must also be present in the region where the magnetic fields switch sign. Therefore, the ideal MHD assumption must break down in the diffusion region and resistivity cannot be neglected in that region. The reconnection rate is usually defined as the inflow speed and equals the magnetic diffusion speed $\frac{\eta}{\mu_0 \delta}$, where η is the resistivity of plasma and μ_0 is the permeability of free space. The reconnection rate in the Sweet-Parker model depends on the existence of finite resistivity and is too low to explain fast dissipative events [114].

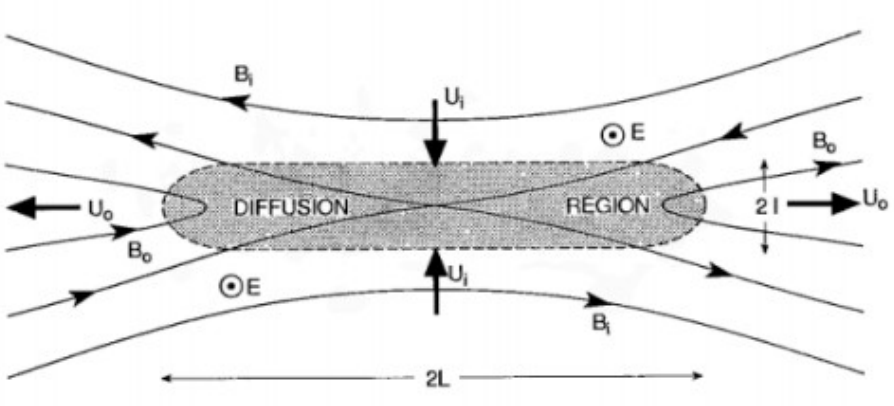

Figure 1.7: Schematic of Sweet-Parker reconnection [81].

Petschek Model

To resolve the discrepancy of the time scale of reconnection, Petschek [114] came up with a reconnection model which involves slow mode shock propagation as well as resistive MHD. The Petschek model consists of two regions as shown in Figure 1.8 [151].

One region is the diffusion-dominated region, which is equivalent to a Sweet-Parker current sheet. In this region, the reconnection rate depends on the resistivity of plasma. The other region is the shock-propagation-dominated region. In this region, the reconnection rate depends on shock wave propagation velocity which is independent of the plasma resistivity and can be much larger than the rate predicted by the Sweet-Parker model.

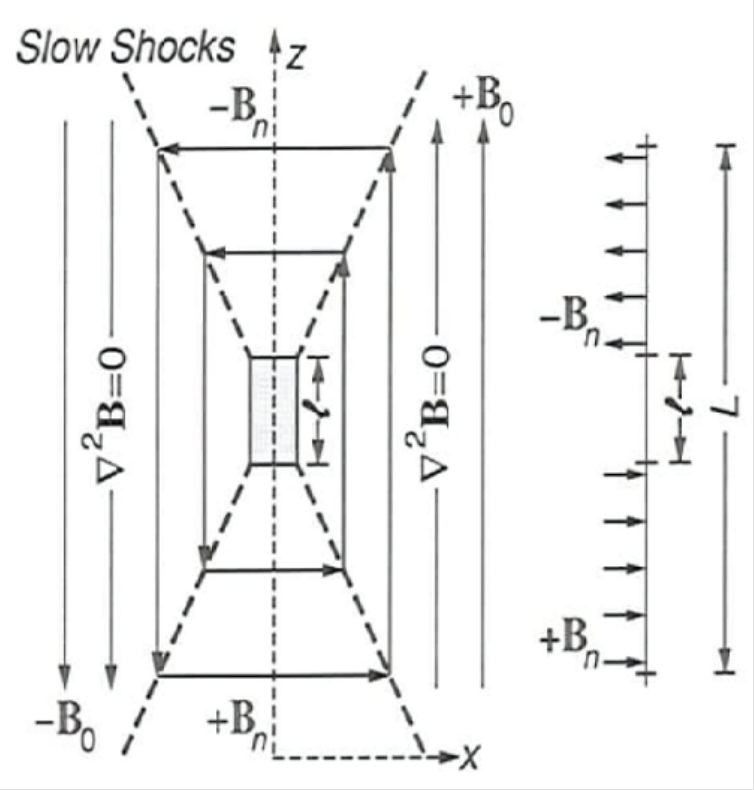

Figure 1.8: Schematic of Petschek reconnection [151].

As was discussed in the context of the Sweet-Parker and Petschek reconnection models, the collisional resistivity is far below the required resistivity to explain the observed energy release rate of fast dissipative events. Ji et al. [69] performed an experimental test of the Sweet-Parker model of magnetic reconnection in a laboratory plasma. They found that the observed reconnection rate can be explained by a generalized

Sweet-Parker model which incorporates compressibility, downstream pressure, and the effective resistivity. This generalized model was valid in certain two-dimensional cases and enhanced the resistivity over its classical values in the collisionless limit.

Collisionless Reconnection

Recent research has focused on collisionless reconnection. However, the mechanism of magnetic reconnection in a collisionless plasma is not yet well understood. One example of collisionless reconnection is anomalous resistivity due to wave turbulence [34]. Theoretical studies have suggested that plasma waves, such as lower-hybrid drift waves [66] and ion acoustic waves, may also be a source of this anomalous resistivity. Che et al. [28] performed two-dimensional and three-dimensional PIC simulations and came up with current filamentation as a mechanism for breaking magnetic field lines during reconnection. Che et al. [28] found that when the current layers that form during magnetic reconnection become too intense, they disintegrate and spread into a complex web of filaments that causes the rate of reconnection to increase abruptly. It was suggested by Che et al. [28] that the filamentation of current was possibly driven by right-hand circularly polarized electromagnetic waves (whistler/electron cyclotron branch) or a current density gradient.

1.3.3 Evidence for Reconnection

The first direct, convincing in-situ evidence for quasi-steady state magnetic reconnection came with plasma and magnetic field observations from the ISEE spacecraft. Early in situ evidence for reconnection at the Earth's magnetopause was provided by Paschmann et al. [111], Russell and Elphic [129], Sonnerup et al. [140] and Gosling et al. [56]. The primary observed evidence of reconnection includes a change in magnetic field configuration and enhanced plasma flow speed from the reconnection sites.

Reconnection models predict that the dayside magnetopause is a rotational discontinuity - a current layer across which a non-zero normal magnetic field component is constant and the tangential component changes direction by an arbitrary angle [111].

The rotational discontinuity is in fact a large amplitude Alfvén wave since the plasma flows across the magnetopause sheet with the modified Alfvén speed. To access quantitatively the level of agreement between this reconnection prediction and the observed flow acceleration, the Walén test is suggested by Paschmann et al. [111]. In the spacecraft frame, the Walén relation $\Delta\vec{v} = \pm\Delta\vec{v}_A$ states that the observed flow velocity change across the magnetopause equals the predicted modified Alfvén velocity change. $\vec{v}_A = \vec{B}\sqrt{(1-\alpha)/(\mu_0\rho)}$ is the modified Alfvén velocity, where α represents the pressure anisotropy factor defined by $\alpha = (p_{\parallel} - p_{\perp})\mu_0/B^2$ and ρ represents the mass density of the plasma. The positive and negative signs indicate that the observed difference vector should be parallel ($B_n < 0$) and antiparallel ($B_n > 0$) to the predicted difference vector, respectively.

Wygant et al. [163] reported detailed characteristics of the current sheet during the process of magnetic reconnection in the near-earth magnetotail measured by the CLUSTER. They investigated the structure and dynamics of electric and magnetic fields responsible for the acceleration of ions and the formation of the electron current layer. Overviews of the insights into the magnetic reconnection have been provided by Vaivads et al. [158], Yamada et al. [165], Fuselier and Lewis [49], and Paschmann et al. [110].

1.3.4 Properties of Reconnection

In reality, the reconnection site usually has a more complicated structure, consisting of multiple X-lines and exhibiting a three-dimensional configuration. However, in many cases the simple two-dimensional picture is a sufficient approximation to a reconnection site. Simulations have been performed to investigate the effects of diamagnetic drift [143], guide magnetic field [119] and dissipation mechanism [6] on collisionless asymmetric reconnection. In this section, we focus on properties of collisionless reconnection.

Influences of Interplanetary Magnetic Field

The factors that control the rate of reconnection are not completely understood. The orientation of the interplanetary magnetic field, which controls the rate of reconnection,

is thought as the most important factor affecting the features of the magnetopause. A southward direction of the interplanetary magnetic field is critical to enabling reconnection with the dayside low-latitude magnetosphere, resulting in magnetic flux transfer to the magnetotail. It is expected that reconnection occurs most strongly when the interplanetary magnetic field is antiparallel to the geomagnetic field. Figure 1.9 shows measurements of the magnetic field and plasma near the subsolar magnetopause during different interplanetary magnetic field conditions [135, 136]. The panel on the left of Figure 1.9 shows a pass through the subsolar magnetopause on ISEE-1 during northward interplanetary magnetic field. The outer boundary layer where density decreases and magnetic field increases is probably the plasma depletion layer. The inner boundary layer is probably due to magnetosheath plasma entering the magnetosphere from reconnection at high latitudes where reconnection is occurring. The righthand panel of Figure 1.9 shows a pass through the subsolar magnetopause when interplanetary magnetic field is southward and reconnection is occurring near the subsolar point. There are external and internal current layers.

Symmetric and Asymmetric Reconnection

The situation at the magnetopause differs from the simplest approximation discussed in the previous section because plasma properties are asymmetric on the two sides of the magnetopause. Reconnection in the magnetotail exhibits stronger symmetry as the plasmas on both sides of the tail current sheet have similar densities and temperatures. The magnetosheath consists of shocked solar-wind plasma and is relatively dense ($n_e \sim 10\ cm^{-3}$) and warm (T$\sim$100 eV). Inside the magnetosphere, the density is typically 1 cm^{-3}. There are two particle populations: the trapped energetic particles that constitute the ring current (several keV) and cold plasma (T$\sim$1 eV) of ionospheric origin. A number of simulations have been performed to explicitly investigate collisionless magnetic reconnection in asymmetric systems [125, 118, 63]. Recently Yoo et al. [166] reported the first quantitative analysis of asymmetric antiparallel reconnection in a laboratory plasma.

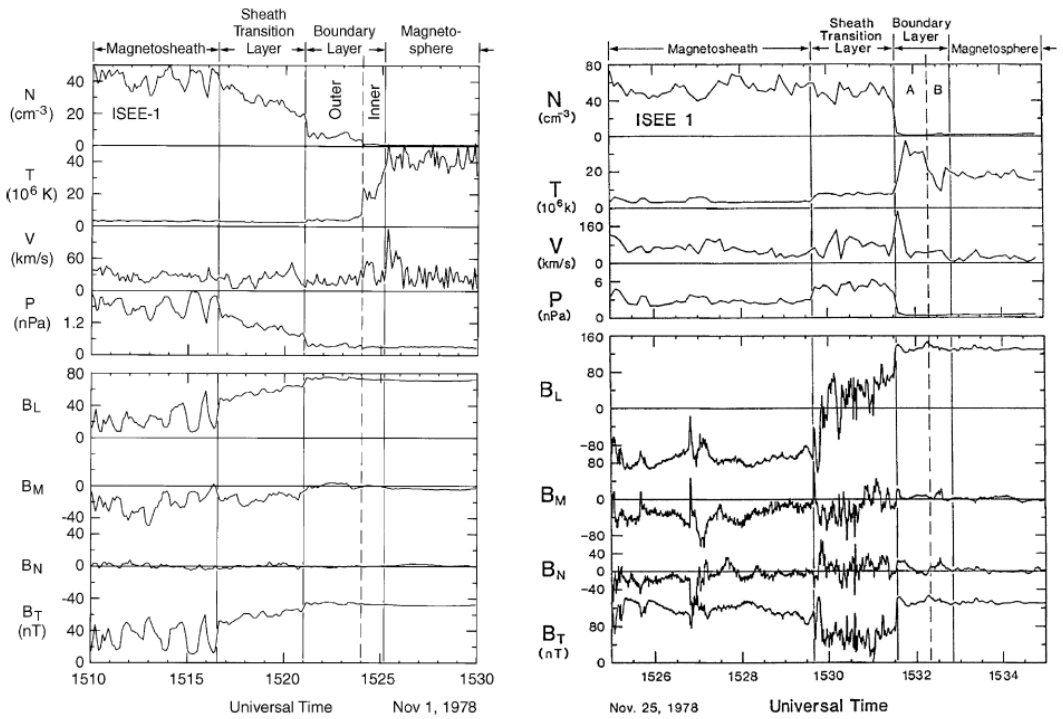

Figure 1.9: Observations of magnetic field and plasma near the subsolar magnetopause made by ISEE. (Left) During northward interplanetary magnetic field conditions [135]; (Right) During southward interplanetary magnetic field conditions [136].

Effects of the Guide Field

The initiation of reconnection appears to be at locations where the magnetic fields on either side of the magnetopause are antiparallel, i.e, shear-angles of 180°. So at the reconnection point there is a magnetic null point. This condition is referred to as "antiparallel reconnection". In the scenario of "antiparallel reconnection", the line of reconnection is determined by the location of antiparallel fields. The reconnection configuration at the magnetopause is usually characterized by highly asymmetric conditions on the two sides of the current layer as discussed in the previous subsection. The magnetic shear across the magnetopause reflects the variations of the interplanetary magnetic field orientation. Reconnection occurs along a specific line and the magnetic fields on either side of this line are not exactly oppositely directed [138]. The case when the magnetic field component along the "X-line" is nonzero is referred to as guide-field reconnection. In the scenario of "component reconnection" there is a significant guide field. Observations have shown that magnetopause reconnection can occur in the presence of strong guide fields [121, 120]. There is essentially no guide field in magnetotail reconnection since the boundary conditions are nearly symmetric as discussed in the previous subsection.

Diffusion Region of Magnetic Reconnection

As we discussed in the previous section, the ideal MHD (frozen-in condition) assumption holds in the convection region of reconnection while it must break down in the diffusion region. The physics of reconnection occurs on the larger spatial scale (ion diffusion region) and on the smaller scale (electron diffusion region) that are associated with the ion and electron dynamics, respectively. In most theoretical scenarios, the ion diffusion region has a scale size typically comparable to an ion inertial length and the electron diffusion region is within a smaller region embeded within the ion diffusion region. Properties of collisionless asymmetric reconnection have been compared to those of symmetric reconnection on ion-scale physics [118] and electron-scale physics [105] and references therein. A recent view of the diffusion region in magnetic reconnection has been presented by Hesse et al. [64].

Mozer et al. [101] first reported evidence of diffusion regions at a subsolar magnetopause crossing made by the Polar satellite. Figure 1.10 [101] shows that ions are decoupled from the electrons and magnetic field in the ion diffusion region, creating the Hall magnetic and electric field patterns. Electrons are demagnetized in the electron diffusion region. The out-of-plane quadrupole magnetic field and the in-plane bipolar electric field are two signatures of collisionless reconnection. Graham et al. [59] have recently investigated the electron distributions in the ion diffusion region of an asymmetric reconnection at the subsolar magnetopause. They concluded that parallel electric fields can trap and heat the magnetosheath electrons parallel to the magnetic field.

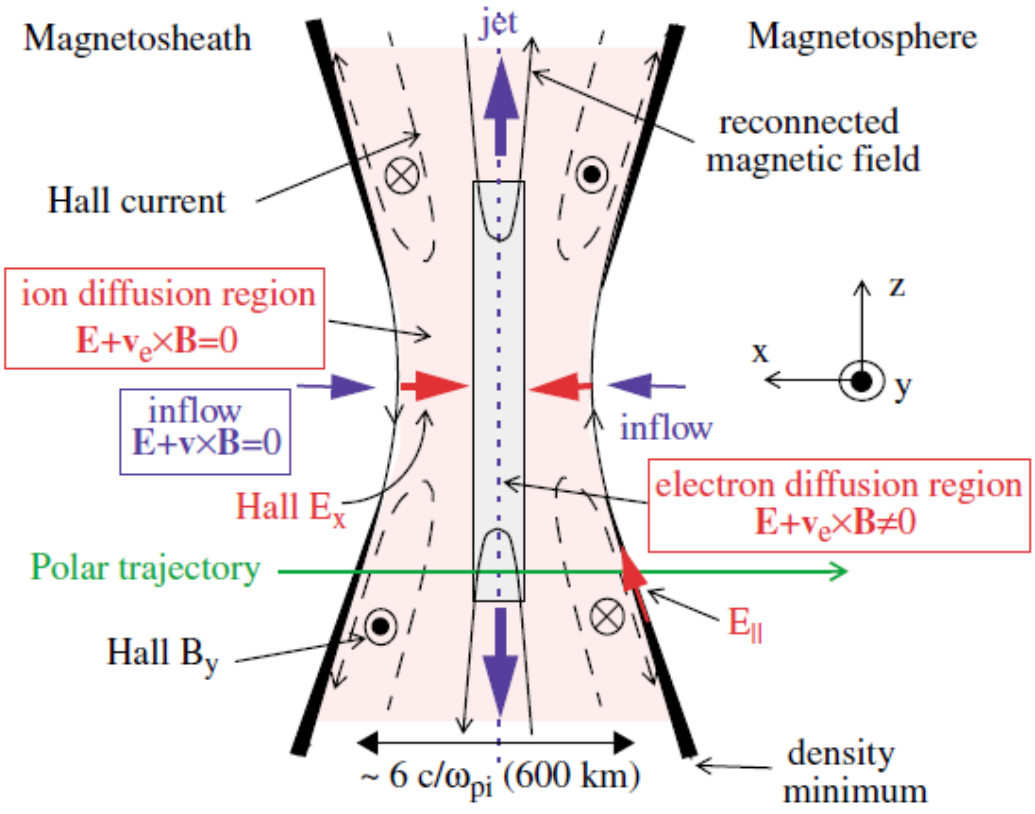

Figure 1.10: The geometry of the reconnection region with Hall effects [101].

The efficiency of collisionless asymmetric reconnection is controlled by the physics

in the electron diffusion region. Observations of the electron diffusion region have been made by Polar at the subsolar magnetopause [102], by Wind in the magnetotail [107] and by Cluster in the magnetosheath [115]. Recent simulations and observations of electron diffusion regions during collisionless antiparallel reconnection in the Earth's magnetotail [106] report that the diffusion region is characterized by a narrow extended layer containing electron jets. It is shown that the jets in the layer are driven by electron pressure anisotropy $\mathrm{P}_{e\parallel} \gg \mathrm{P}_{e\perp}$ and the anisotropy is responsible for the structure of the electron diffusion region [106]. Mozer [100] has identified electron diffusion regions on the basis of the non-zero parallel electric field, a large perpendicular electric field compared to the reconnection electric field, a large electromagnetic energy conversion rate and accelerated electrons, and a topological boundary that separates regions having different $\mathbf{E} \times \mathbf{B}/B^2$ flows with thickness of the order of the electron skin depth.

We concentrate on a specific way to identify the electron diffusion region described by Scudder et al. [133] who report spatially resolved diagnostic signatures of a demagnetized electron diffusion region observed by Polar at the Earth's magnetopause. The criteria for being in an electron diffusion region should be electron specific since electrons are locally disrupted in the electron diffusion region. The four dimensionless scalar diagnostics that were used to find the electron diffusion region are peak electron thermal Mach numbers $\mathrm{M}_{e\perp} \equiv |\mathbf{U}_e|/\langle w_{e\perp}\rangle > 1.5$ (where $\mathbf{U}_e$ represents electron bulk velocity and $\langle w_{e\perp}\rangle$ is the electron thermal speed derived from the average perpendicular temperatures), electron temperature anisotropy $\mathrm{An}_e \equiv \mathrm{T}_{e\parallel}/\langle T_{e\perp}\rangle > 7$, calibrated agyrotropy of electron pressure tensor $\mathrm{A}\phi_e = 2|\,1-\alpha\,|/(1+\alpha) > 1$ (where $\alpha \equiv \mathrm{P}_{e\perp,1}/\mathrm{P}_{e\perp,2}$) and strong ($\gtrsim$150 eV) increases in electron temperature [133]. The electron pressure agyrotropy is a measure of the departure of the pressure tensor from cylindrical symmetry about the local magnetic field and it reflects the demagnetization of the thermal electrons which enables collisionless reconnection.

1.4 Wave Modes associated with Magnetic Reconnection

1.4.1 Introduction

Wave modes associated with magnetic reconnection are briefly introduced in this section. Previous studies on these wave modes will be discussed in Chapter 3.

Reconnection sites are regions of strong wave activity covering a broad range of frequencies from below the ion gyrofrequency to above the electron plasma frequency. Density and temperature gradients as well as non-Maxwellian particle distribution functions in the vicinity of a reconnection site could generate various plasma wave modes. Wave modes frequently found near reconnection sites are: lower-hybrid waves, whistler-mode waves, electron cyclotron waves, Langmuir/upper hybrid waves, and solitary waves. Different wave modes are suggested to provide the necessary diffusion to sustain the low-latitude boundary layer in the absence of reconnection or to provide anomalous resistivity in the diffusion region required to break the magnetic field frozen-in condition, decoupling the motion of ions and electrons allowing magnetic reconnection. In situ observations of the wave generation and wave-particle interactions at the reconnection sites can be used as a probe of the microphysics of reconnection.

Labelle and Treumann [85] have summarized the role of wave turbulence in providing sufficient diffusion to support reconnection or boundary layer formation. Based on the review of twenty years of wave measurements at the dayside magnetopause they concluded that the anomalous diffusion due to various microscopic plasma waves was always too small to explain boundary layer formation. Treumann et al. [152] concluded that low frequency electric and magnetic waves could provide sufficiently large diffusion to form the low-latitude boundary layer. Tsurutani and Thorne [154] suggested that electrostatic waves at frequencies $\sim f_{ci}$ could induce the required rapid inward diffusion of typical magnetosheath ions. Cattell et al. [22] provided observational evidence of examples of these waves with sufficient amplitude to support this theory. Ji et al. [68] found laboratory evidence for a positive correlation between the magnitude of electromagnetic fluctuations up to the lower-hybrid frequency range and enhancement of reconnection rates.

Recent simulation has revealed the Čerenkov emission of quasiparallel whistlers by fast electron phase-space holes during magnetic reconnection [54]. The dynamics and structure of whistler-mode waves relevant to electron acceleration in the Earth's outer radiation belt has been recently explored with simulations [36]. It was found that the whistler-mode waves can scatter electrons and the electrons can drive spikes of intense parallel electric fields. The resulting parallel electric fields trap and heat the precipitating electrons [36].

1.4.2 Lower-Hybrid Drift Waves

Emissions with the strongest electric fields are often detected near or below the lower-hybrid frequency f_{lh}. Some of these emissions have both strong electric and magnetic field components while some of them only have a strong electric field. The largest amplitude lower-hybrid waves seem to be located in the regions of steepest density gradients. Simulations suggest that the observed waves are lower-hybrid drift waves even though the modified two-stream instability could generate waves with similar properties. More detailed studies are required in order to confirm the lower-hybrid drift nature of the observed waves.

The lower-hybrid drift waves are characterized by a broadband spectrum extending from frequencies well below to well above f_{lh}, short wavelengths $k\rho_e \sim 1$, wave numbers $k_\perp >> k_\parallel$, a phase velocity of the order of the ion thermal velocity, and a coherence length of the order of one wavelength.

1.4.3 Electrostatic Ion Cyclotron Waves

The electrostatic ion cyclotron wave is an electrostatic plasma wave mode with frequency structure related to the ion cyclotron frequency f_{ci}. This wave mode was first observed by Motley and D'Angelo [99] in a laboratory plasma. Electrostatic ion cyclotron waves are of great importance in space plasmas as they occur in the same

spatial region as field-aligned currents, electrostatic shocks, upflowing ions, and downflowing electrons associated with auroral arcs [103, 79, 149, 148, 21, 18]. Although these waves have been frequently observed in the auroral zone, they have not been previously observed near the dayside magnetopause to the best of our knowledge.

1.4.4 Whistler-Mode Waves

Whistler-mode waves are a type of transverse electromagnetic wave which is right-handed circularly polarized. Whistler-mode waves are identified in the frequency range between the lower-hybrid frequency and the local electron cyclotron frequency $f_{lh} < f < f_{ce}$. For whistler-mode waves, the higher frequencies travel at a faster speed than lower frequencies. Thus, at a distant location, higher frequency whistler-mode waves are received first.

1.4.5 Electrostatic Electron Cyclotron Waves

Electron cyclotron waves were first observed in the magnetosphere between 0000 and 1200 LT and at $4 < L < 10$ at low-latitudes [74]. The emissions occur just slightly above electron cyclotron frequency f_{ce}, near $(n + \frac{1}{2})f_{ce}$ (where n is a positive integer) and well above f_{ce}. The most commonly occurring frequency is $f \sim \frac{3}{2}f_{ce}$.

1.4.6 Langmuir/Upper Hybrid Waves

Strong electric fields are found near the electron plasma frequency f_{pe}. These emissions are usually believed to be Langmuir waves or upper hybrid waves (if oblique). It has been found that the wave electric fields are often polarized at large angles with respect to the ambient magnetic field ($E_\perp >> E_\parallel$) indicating that the observed waves are upper hybrid waves [44].

1.4.7 Electrostatic Solitary Waves

Electrostatic Solitary Waves have a signature that is a bipolar pulse in the wave electric field parallel to the ambient magnetic field. They are structures generated out of nonlinear instabilities and processes. They are almost always found in boundary/current layers and turbulent plasmas. The electron mode solitary waves are called electron holes. They are localized, nonlinear plasma structures, consisting of a positive-potential spike which has trapped a population of electrons.

1.5 Thesis Overview

This thesis describes research in magnetospheric physics related to the process of magnetic reconnection and associated plasma waves.

Chapter 1 gives a brief introduction to the magnetosphere, the structure of the Earth's magnetopause and boundary layer, magnetic reconnection and associated waves and the structure of the thesis.

Chapter 2 describes the instruments on board THEMIS satellites and the data analysis methods for the studies in the thesis.

Chapter 3 contains a brief introduction to previous studies of magnetic reconnection and the associated waves at the magnetopause.

Chapter 4 provides a case study of observations of the magnetopause electron diffusion region and associated large amplitude waves and heated electrons.

Chapter 5 describes a case study of observations of electrostatic ion cyclotron waves and associated ion heating.

Chapter 6 presents a case study of simultaneous observations of lower-hybrid, whistler-mode, electrostatic solitary, and electron cyclotron waves in the magnetopause boundary

layer.

Chapter 7 concludes the thesis by reviewing the major findings described, discussing the importance of these findings to the growing understanding of the microphysics of magnetic reconnection and looking at future topics of study that are suggested by the findings presented in the thesis.

Chapter 2

Instrumentation and Analysis Techniques

2.1 Introduction

In this chapter, the Time History of Events and Macroscale Interactions during Substorms (THEMIS) satellite and the relevant instruments and analysis techniques needed for studies of magnetopause reconnection and waves are described. The five THEMIS spacecraft have highly elliptical orbits and cover a broad region in the magnetosphere. The primary advantages of the THEMIS dataset include continuous high time resolution three-dimensional electric field waveform data as well as high time resolution magnetic burst data which can last for more than 10 seconds. Additionally, the THEMIS dataset includes a large number of sub-solar magnetopause crossings. The electric field data is provided by the Electric Field Instrument (EFI). The magnetic field data is provided by the Flux Gate Magnetometer (FGM) and Search Coil Magnetometer (SCM). Particle data is provided by the Electrostatic Analyzer (ESA) and Solid State Telescope (SST).

2.2 THEMIS satellites and instruments

The THEMIS mission was launched on February 17, 2007 to determine the trigger and large-scale evolution of substorms [5]. An artistic view of the THEMIS spacecraft

is shown in Figure 2.1 [147]. THEMIS consists of five identically-instrumented spacecraft. The five spin-stabilized (spin period equals 3 seconds) THEMIS spacecraft were placed in highly elliptical orbits where the spacecraft line up at apogee every four days. Three inner probes are at about 10 R_E while two outer probes are at 20-30 R_E. The five THEMIS spacecraft carry comprehensive packages of plasma and field instruments. A schematic diagram of the THEMIS spacecraft, including body- and boom mounted sensors is shown in Figure 2.2 [13].

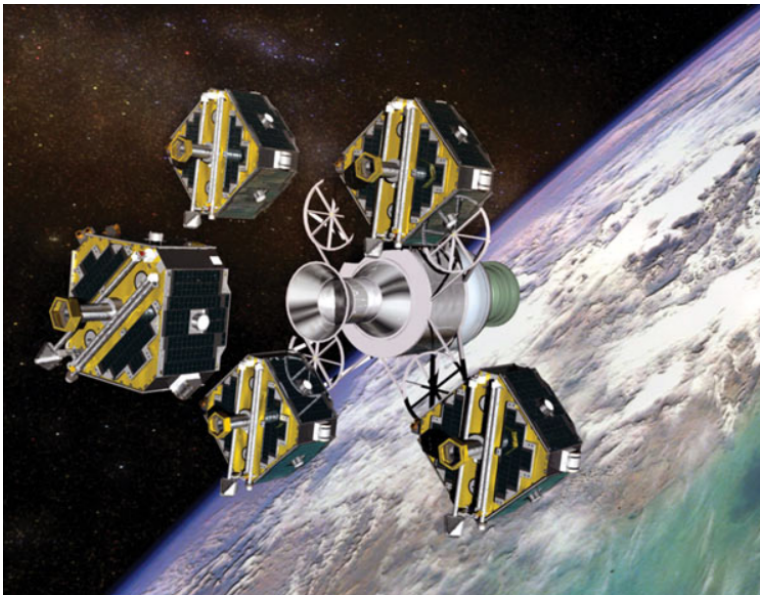

Figure 2.1: An artistic view of THEMIS spacecraft [147]

2.2.1 Electric Field Instrument

The Electric Field Instrument (EFI) provides for waveform and spectral three-axis measurements of the ambient electric field from DC up to 8 kHz [13]. Individual sensor potentials are also measured, providing for on-board and ground-based estimation of spacecraft floating potential and high-resolution plasma density measurements. The wave burst mode electric fields are either at 8192 samples/s or 16384 samples/s. The booms are 50 m and 40 m tip to tip in the spin plane, and 6.9 m along the spin axis. Because the measured quasi-static electric field component along the spin axis has large

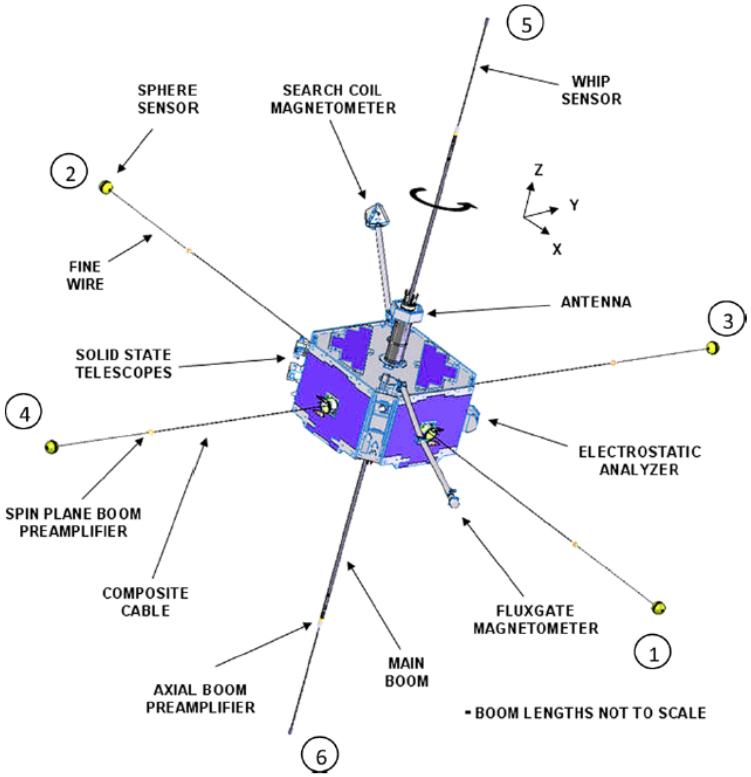

Figure 2.2: Schematic diagram of THEMIS spacecraft [13]

uncertainty due to the short boom along the spin axis we use $\mathbf{E} \cdot \mathbf{B} = 0$ to determine the electric field and to calculate the $\mathbf{E} \times \mathbf{B}/B^2$ velocity. Electric fields in the spin-axis component are reliable for high time resolution electric field wave burst data.

2.2.2 Magnetic Field Instrument

The Flux Gate Magnetometer (FGM) measures the three-dimensional background magnetic field and its low frequency fluctuations (up to 64 Hz) [7]. The THEMIS FGM uses an updated technology (digital fluxgate technology) developed in Germany. It has two specific features: a single sensor on a 2 m boom and the compact integrated instrument concept. These features result in higher sensitivity, lower mass and improved robustness compared to magnetometers installed on previous missions. The THEMIS FGM is capable to detect variations of the magnetic field with amplitudes of 0.01 nT and measures magnetic fields in a range extending over six orders of magnitude. The sampling rate of the magnetic field data is 128 samples/s in the high rate mode or 4 samples/s in the low rate mode.

The Search Coil Magnetometer (SCM) measures low-frequency magnetic field fluctuations and waves in three directions [127]. The SCM measures the frequency range from 0.1 Hz to 4 kHz. The wave burst mode data is sampled at 8192 samples/s. Thus the wave electric and magnetic fields are sampled at the same rate during wave bursts. The bursts provide the main data set for this study.

2.2.3 Particle Detectors

Ion and electron distribution functions are measured by the Electrostatic Analyzer (ESA) [94] and by the Solid State Telescope (SST) [5]. The ESA measures plasma over the energy range of a few eV up to 30 keV for electrons and 25 keV for ions. The SST measures superthermal particles within the energy range from 25 keV to 6 MeV for electrons and 900 keV for ions. The measured spacecraft potential is used in analysis of the particle data.

The ESA sensor consists of a pair of top-hat electrostatic analyzers that measure ion and electron energy per charge [147]. Both sensors have a $180° \times 6°$ field of view that sweep out 4π steradians each 3 s spin period. Particles are detected by microchannel plate detectors and binned into six distributions whose energy, angle, and time resolution depend upon the instrument mode.

The SST are packaged into two instrument heads [147]. Each head consists of two double-sided telescopes measuring ions on one side and electrons on the other side. The telescopes are arranged side-by-side looking in opposite directions, such that each head is measuring ions and electrons on both sides [147].

2.3 Coordinate Systems

The coordinate systems used in this paper include geocentric solar magnetospheric (GSM) coordinates, local boundary normal (LMN) coordinates and field-aligned coordinates (FAC).

The GSM coordinate basis is defined as: the positive X-axis points from the Earth towards the Sun; the Z-axis is perpendicular to the X-axis and parallel to the projection of the negative dipole moment on a plane perpendicular to the X-axis (the northern magnetic pole is in the same hemisphere as the tail of the magnetic moment vector); and the Y-axis completes a right-handed coordinate system.

The LMN coordinate basis is defined as: the positive N-axis is parallel to the outward magnetopause normal; the M-axis is defined by $N \times Zgsm$; and the L-axis completes the orthogonal right-handed basis.

In FAC, the positive Z-axis points in the direction of the magnetic field B_0 at the spacecraft's location; the Y-axis is defined by $Z \times Xgsm$; and the X-axis completes the orthogonal right-handed system. In our event, the X-axis points almost noonward and

the Y-axis points almost duskward in FAC.

2.4 Analysis Techniques

2.4.1 Minimum Variance Analysis

Minimum Variance Analysis (MVA) utilizes a property of plane polarized linear electromagnetic waves which allows one to assume that fluctuations in the electric and magnetic fields are in a plane orthogonal to the direction of propagation [76]. Assuming a one-dimensional model of the local magnetopause structure and the orientation of the magnetopause current layer doesn't change during the crossing, the condition $\nabla \cdot \mathbf{B} = 0$ requires the normal magnetic field component to be constant during the magnetopause crossing. The normal direction is that along which the component of the magnetic field has minimum variance.

2.4.2 Wavelet Analysis

A wavelet is a mathematical function used to divide a given function or continuous-time signal into different scale components. A wavelet transform is the representation of a function by wavelets. Wavelet transforms have advantages over the traditional Fast Fourier transforms(FFT) for representing functions that have discontinuities and sharp peaks. Morlet wavelet transforms [150] are utilized for dynamic waveform analysis throughout this thesis due to the advantages of wavelet over a windowed FFT.

2.4.3 Wave Auto-Identification Technique

The THEMIS dataset includes a large number of sub-solar magnetopause crossings. We have surveyed all the available waveform bursts obtained by THEMIS from 2007 to 2014. More than 1000 bursts have been identified during sub-solar magnetopause crossings. We use an auto-identification program for THEMIS waveform data. This wave

identification program is based on calculation of wave coherence and wave frequency.

Chapter 3

Previous Studies of Wave Modes associated with Reconnection

In this chapter, we introduce previous theoretical and observational studies on wave modes associated with magnetic reconnection. We focus on the study of waves near the Earth's dayside magnetopause.

3.1 Introduction

The plasma waves observed at the magnetopause can play many important roles in the physical processes occurring at the magnetopause. In this section, we focus on the plasma wave modes associated with the dayside magnetopause. Past studies of plasma waves near the magnetopause [60, 4, 85] have indicated intense electrostatic and electromagnetic waves. Strong wave turbulence covering a broad range of frequencies has been frequently observed near the reconnection site [25, 122, 157, 75, 20, 161]. More specifically, these wave modes include the whistler-mode waves [35, 112], electrostatic solitary waves [44, 92], lower-hybrid waves [24, 8], kinetic Alfvén waves [27] and Langmuir/upper hybrid waves [44]. Different wave modes are suggested to play important roles in the reconnection process [22, 123, 113]. The effect of different wave modes on the reconnection process has been a problem of longstanding interest for their role in

anomalous resistivity, particle acceleration, energy transport and formation of reconnection sites [66, 85, 153, 37, 128].

3.2 Lower-Hybrid Drift Waves in association with Reconnection

It was demonstrated that the most suitable instability exciting the observed waves near the lower-hybrid frequency at the dayside magnetopause was the lower-hybrid drift instability, driven by a diamagnetic current that arises from density and magnetic field gradients [52]. Observations of lower-hybrid drift waves have been made in the near-earth magnetotail plasma sheet [24, 20] and in the magnetopause current sheet [60, 22, 19, 8, 156].

The lower-hybrid drift waves can accelerate electrons parallel to the magnetic field to MeV energies and this process might be associated with acceleration in the reconnection region [89]. The phase velocity of lower-hybrid drift waves in the direction perpendicular to the magnetic field is comparable to the ion thermal speed while the phase velocity along the magnetic field is comparable to the electron thermal velocity. Thus the lower-hybrid drift waves can resonate with thermal electrons and efficiently accelerate these electrons.

The lower-hybrid drift waves interact efficiently with both ions and electrons and could cause a significant anomalous resistivity and corresponding anomalous diffusion. It has been suggested that the lower-hybrid drift waves can produce the necessary anomalous resistivity for reconnection [66]. Observational evidence of examples of these waves with sufficient amplitude to support this theory have been provided by Cattell et al. [24, 22]. Bale et al. [8] show that the contributions of the lower-hybrid drift waves anomalous resistivity in the diffusion region during one reconnection event at the magnetopause are negligible for reconnection. Daughton [33] suggests that the fastest growing lower-hybrid drift waves (electrostatic fluctuations) cannot produce resistivity in the center of the current sheet as it is localized on the edge of the sheet and has a

limited penetration length due to the effects of finite plasma beta. Longer wavelength lower-hybrid drift wave modes, which have a significant electromagnetic component, are suggested to influence reconnection as they can penetrate into the central region [33].

More recent simulations have shown that the lower-hybrid drift waves can affect reconnection through current sheet bifurcation, thinning and reconnection onset [132]. It was suggested that the lower-hybrid drift waves contributes to reconnection onset through its effect on the tearing mode instead of anomalous resistivity [70]. Simulations have shown that lower-hybrid drift waves have an important effect on reconnection by heating electrons anisotropically, by peaking and bifurcating the current sheet, and by causing ion velocity shear [124].

3.3 Electrostatic Ion Cyclotron Waves in association with Reconnection

Most theoretical studies suggest ion beams or field-aligned currents as possible sources of free energy to drive the electrostatic ion cyclotron instability [38]. Kindel and Kennel [77] have shown that the electrostatic ion cyclotron wave is the most easily destabilized current-driven instability for currents carried by a Maxwellian electron distribution. Observations reported by Kintner et al. [80] and Cattell [17] have confirmed the hypothesis that electrostatic ion cyclotron waves are driven by a combination of ion beams and electron drift [62]. Kintner [78] distinguished the electrostatic ion cyclotron mode from ion cyclotron harmonic waves and suggested that ion conics could generate ion cyclotron harmonic waves at high ($\gtrsim 3$) harmonics of f_{ci}. Ungstrup et al. [155] and Lysak et al. [90] suggested that the ion conics could be heated at a lower altitude by electrostatic ion cyclotron waves.

Ganguli et al. [50] suggested a new mechanism that can explain the occurrence of short wavelength turbulence around f_{ci} in the presence of a nonuniform electric field perpendicular to the external magnetic field. This wave is expected to be broad band

electrostatic noise and efficient for heating the ions. In order to study the role of transverse electric fields in the generation of ion cyclotron waves, Ganguli et al. [51] used a kinetic approach and suggested a mechanism based on the coupling of the negative energy ion Bernstein modes in the region where DC electric field is present, with the positive energy ion Bernstein modes in the region where DC electric field is absent. Laboratory observations [2, 83] confirmed that ion cyclotron waves can be driven unstable by sheared plasma flow transverse to the magnetic field resulting from an inhomogeneous, transverse electric field. Laboratory experiments [162, 3] have shown evidence of a correlation between sheared cross-field flow, velocity-shear-driven ion-cyclotron waves and perpendicular ion heating.

Blecki et al. [12] observed strong wave activity at frequencies $f_{ci} < f \lesssim f_{lh}$ (where lower-hybrid frequency $f_{lh} \simeq f_{pi}/\sqrt{1 + f_{pe}^2/f_{ce}^2}$, f_{pi} and f_{pe} are ion and electron plasma frequency, respectively, f_{ce} is electron cyclotron frequency) in plasma clouds close to the high-latitude nightside magnetopause. These magnetosheath-like plasma clouds have fairly sharp boundaries and strong plasma density and temperature variations. Blecki et al. [12] did not clarify if the observed waves were purely electrostatic or have ion cyclotron harmonics due to limitations of the instrument. They concluded that the lower-hybrid dirft instability was most likely given the observation of a secondary maximum around f_{lh} and that the wave amplitude agrees well with the estimated saturation level ($\sim$ 5mV/m) for the lower-hybrid drift instability. Unlike those reported by Blecki et al. [12], Belova et al. [9] did observe ion cyclotron harmonics (peaked at $\sim f_{ci}$ with some at $2f_{ci}$ also). Belova et al. [9] modeled the results from Blecki et al. [12] and concluded that the ion cyclotron harmonics were due to gradients in the magnetic-field-aligned ion drift velocity. Belova et al. [9] excluded the ion cyclotron drift instability because the instability caused by the variation in the ion velocity has no threshold and the theoretical estimates of saturation amplitude and the shape of the spectrum based on a shear driven instability agree well with the experimental data. This shear driven instability is the same mechanism as Koepke et al. [84] showed in a laboratory study and that was originally proposed by Lakhina [88]. For the plasma parameters at the magnetopause the most suitable instabilities driving waves in the frequency range of 1-100 Hz are the ion cyclotron drift [53] and lower-hybrid drift instabilities [52]. Primarily,

these two instabilities can be excited by the presence of sufficiently large transverse gradients in the plasma density [12]. The ion cyclotron drift instability requires the ratio $\rho_i/L \gtrsim 0.025$ while the lower-hybrid drift instability requires a steeper gradient $\rho_i/L \gtrsim 0.25$ (where ρ_i is the ion Larmor radius and L is the characteristic length scale of the density gradient) [12].

Ion heating by the electrostatic ion cyclotron instability was first observed in a laboratory plasma [131]. Protons can be energized up to energies of ∼100 eV perpendicular to the magnetic field by electrostatic ion cyclotron waves in the topside ionosphere [155]. A theory of the ion heating due to coherent electrostatic ion cyclotron waves in the auroral zone was presented by Lysak et al. [90]. They considered the effects of ion heating in the presence of the magnetic gradient force and parallel electric fields and concluded that perpendicular energies over 100 eV were easily attainable from a 1 eV source plasma. It has been suggested that perpendicular heating in the absence of a parallel electric field yields conical ion distributions, which in the presence of an electric field and/or due to the mirror force become field-aligned beams [90].

3.4 Whistler-Mode Waves in association with Reconnection

Whistler-mode waves are one of the most ubiquitous wave modes observed in space plasmas. They have been frequently observed in regions that are related to magnetic reconnection, such as the plasma sheet boundary layer [61], the magnetopause [85, 35, 141], and the magnetotail [24]. Whistler-mode waves are an important candidate for the anomalous resistivity, particle acceleration and heating.

Whistler-mode waves may be driven unstable by superthermal electrons with temperature anisotropies of $T_{e\perp}/T_{e\parallel} > 1$ in the magnetosphere [73], current-driven plasma instabilities [61], energetic electron beams [168, 170] or anisotropic electrons in plasma

bubbles [169] in the magnetotail, or modified two-stream instabilities in laboratory experiments [68]. Electron anisotropy, due to compression of the magnetopause or lower-hybrid drift waves, may be the generation mechanism of whistler-mode waves in the magnetopause current sheet [70]. It is believed that whistler-mode waves in the reconnection neutral line region would scatter electrons and thus destabilize the tearing mode [29]. The generation of the out-of-plane component of the magnetic field is suggested to be a signature of whistler mediated reconnection [91]. It has also been suggested that the strongest whistler emissions are observed on the most recently opened magnetospheric flux tubes due to magnetic reconnection [159]. One recent simulation study concludes that whistler-mode waves do not control the dissipation processes of reconnection but are generated as a result of the reconnection processes [48]. Whistler-mode waves in the electron diffusion region may play a significant role in the microphysics of reconnection as they are excited on electron scales. Laboratory experiments show that the reconnection rate correlates with the amplitude of obliquely propagating broadband whistler-mode waves inside the reconnecting current sheet [68]. We have recently identified intense whistler-mode waves inside an electron diffusion region and concluded that the source of free energy was electron temperature anisotropy of $T_{e\perp}/T_{e\parallel} > 1$ for electrons with energies above 20 keV [144]. Recent simulation performed by Goldman et al. [54] has revealed the Čerenkov emission of quasiparallel whistlers by fast electron phase-space holes during magnetic reconnection.

3.5 Electrostatic Electron Cyclotron Waves in association with Reconnection

Electron cyclotron waves are usually observed in the inner regions of the magnetosphere, such as the cusp, polar magnetosphere, and auroral zone [46, 95, 97]. They have been typically observed during crossings of the plasma sheet near the magnetic equator [134]. Electron cyclotron wave emissions at the magnetopause were reported by [4]. Matsumoto and Usui reported observations of intense bursts of electron cyclotron waves at the dayside equatorial magnetopause region [93]. Intense electron cyclotron waves were intermittently observed superimposed on weak diffuse electron cyclotron waves.

The intermittently appearing intense electron cyclotron waves had harmonic components even above the local plasma frequency and their frequency peaked at $\sim \frac{3}{2} f_{ce}$ and $\frac{5}{2} f_{ce}$. The diffuse emission had a rather weak amplitude and broad frequency band. Theoretical studies have suggested that the electrostatic electron cyclotron waves are generated by microscopic instabilities due to anisotropic electron velocity distributions based on the assumption of linear dispersion [167]. A review of theoretical studies on electrostatic electron cyclotron waves was published by Kennel and Ashour-Abdalla [72].

Electron cyclotron waves have been observed in association with flux transfer events [4, 87], energetic plasma [61] and regions where the DC electric field was small and quiet [25] in the magnetotail. Both electrostatic and electromagnetic cyclotron waves have been observed at the magnetopause [4]. It has been reported that during a flux transfer event, quasi-periodic electron cyclotron harmonics correlated with ∼1 Hz magnetic fluctuations [4]. Observations in the cusp and close to the magnetopause indicate that electron cyclotron waves tend to be generated on open field lines [96]. Menietti et al. [96] also show that there is a close correspondence between observations of electron cyclotron waves and solitary waves.

Different generation mechanisms have been discussed by LaBelle and Treumann [86]. Electron cyclotron waves can be generated by transverse temperature anisotropies or loss cones which excite diffuse electron cyclotron waves between the harmonic bands. In case of electron beams, a cold electron population is needed in order for the waves to become unstable. However, direct measurements of the cold electron population in relation to reconnection are not found [96].

The presence of electron cyclotron waves in association with flux transfer events as well as being mainly on open field lines indicates that the reconnection process is important in creating unstable electron distribution functions. However, electron cyclotron waves have not been observed close to the reconnection site. The electron beams which generate electron cyclotron waves are suggested to be from the reconnection region.

3.6 Langmuir/Upper Hybrid Waves in association with Reconnection

Cattell et al. [25] reported the first observations of upper hybrid waves occurring at multiples of the electron cyclotron frequency. These waves occurred in a region where $\beta < 1$ and the density was large and the ion temperature was low. They are associated with regions where the DC electric field was small ($\leq$0.5 mV/m) and quiet, and the plasma flows were $\leq$100 km/s [25]. Simulations suggest that Langmuir modes are usually driven by the weak-beam instability [108]. Upper hybrid waves can be generated by beams as well as loss cone and shell distributions. Large amplitudes ($>$ 40 mV/m) obliquely-propagating upper hybrid bursts were observed near a reconnection "X-line" in the geomagnetic tail [44]. It was suggested that the energetic electron beams flowing along the separatrix may generate the upper hybrid waves and the waves act to thermalize the beams into the plateau football-shaped distribution [45].

3.7 Electrostatic Solitary Waves in association with Reconnection

Electrostatic solitary waves are also associated with reconnection. Electrostatic solitary waves at the subsolar, equatorial magnetopause were first identified by Cattell et al. [19]. Observations of electrostatic solitary waves in association with reconnection have been made by Wind in the magnetotail [44], Geotail at the magnetopause [92], Cluster in the magnetotail [20] and magnetic reconnection experiments in the laboratory [47].

It is believed that electrostatic solitary waves are generated by the electron two-stream instability [108] or the Buneman instability [37, 55]. Comparisons of three-dimensional particle simulations of reconnection [37] to Polar observations at the magnetopause [19] have provided evidence that the electron holes and lower-hybrid waves can cause strong electron scattering associated with anomalous resistivity as well as produce energetic electrons. Drake et al. [37] conclude that intense electron beams that form near the magnetic "X-line" and separatrices can drive the development of

turbulence. The turbulence may collapse into localized three-dimensional nonlinear structures in which the electron density is depleted. Their predictions agree with satellite observations at the magnetopause. The birth and death of these electron holes and their associated intense electric fields lead to strong electron scattering and energization. This may explain why magnetic explosions release energy so quickly and produce many energetic electrons. Recent observations suggest that electron holes could be generated due to injections of highly-anisotropic plasma sheet electrons into the outer radiation belt [160].

3.8 Reason for the Study in the Thesis

In this thesis, I used plasma wave electric and magnetic fields and particle data from the THEMIS satellites to investigate the possible generation mechanisms of different wave modes and the roles that the wave modes play in the process of magnetic reconnection and magnetopause boundary layer formation. The main advantages of the THEMIS data set are the long intervals of high time resolution three-dimensional electric and magnetic field burst waveforms with simultaneous high time resolution and accurate plasma measurements. In addition, the multiple spacecraft allow comparisons of magnetopause structures closely spaced in time and/or space. This allows us to determine the time scale and spatial sizes over which specific wave types are seen. We focus on wave observations near the subsolar magnetopause region as the subsolar region should be the simplest region to understand with the simplest geometry. At the subsolar magnetopause, there should be less complex motions, the flow should be slowest and the region should be least affected by dynamic events elsewhere at the magnetopause.

Chapter 4

Observations of the Magnetopause Electron Diffusion Region: Large Amplitude Waves and Heated Electrons During the 27 August 2009 Event

An example of a reconnection event at the subsolar magnetopause observed by one THEMIS satellite is presented in this chapter. The results of this study have been published [144].

4.1 Introduction

This chapter presents an example of large amplitude waves in a well-defined electron diffusion region based on the criteria described by [133] at the subsolar magnetopause using data from one THEMIS satellite. These are the first observations, in a well-defined electron diffusion region, with waveform capture electric and magnetic field data so that

wave modes can be definitely identified, and compared to high resolution particle distributions. These waves, identified as whistler-mode waves, electrostatic solitary waves, lower-hybrid waves and electrostatic electron cyclotron waves, are observed in the same 12 s waveform capture and in association with signatures of active magnetic reconnection. The large amplitude waves in the electron diffusion region are coincident with abrupt increases in electron parallel temperature suggesting strong wave heating. The whistler-mode waves, which are at the electron scale and which enable us to probe electron dynamics in the diffusion region were analyzed in detail. The energetic electrons (∼30 keV) within the electron diffusion region have anisotropic distributions with $T_{e\perp}/T_{e\parallel} > 1$ that may provide the free energy for the whistler-mode waves. The energetic anisotropic electrons may be produced during the reconnection process. The whistler-mode waves propagate away from the center of the "X-line" along magnetic field lines, suggesting that the electron diffusion region is a possible source region of the whistler-mode waves.

4.2 Overview of Event

Figure 4.1 shows a 5.5 min interval of the field and plasma observations made by probe E of the THEMIS mission on 27 August 2009. The boundary normal direction (determined from MVA on the ambient magnetic field) was [0.99, 0.015, -0.12] in GSM coordinates and almost identical to the GSM-X direction, consistent with the spacecraft being near the subsolar point (indicated by the position parameters at the bottom of Figure 4.1). The spacecraft travels from the outer magnetosphere (SP) through the magnetopause (MP, indicated by two light green shaded bands) into the magnetosheath (SH). The purple shaded band shows a ∼12 s interval of magnetic burst data capture.

The magnetopause crossing can be seen in the change in B_z from positive to negative (Figure 4.1a). The differential energy flux of electrons in Figure 4.1j shows that in the magnetosphere, where B_z was positive, higher-energy electrons were encountered; while in the magnetosheath, where B_z was negative, lower-energy electrons were measured. The spacecraft passed from the lower plasma density magnetosphere to the high-density (factor of 100) magnetosheath via a region of mixed magnetosheath/magnetospheric

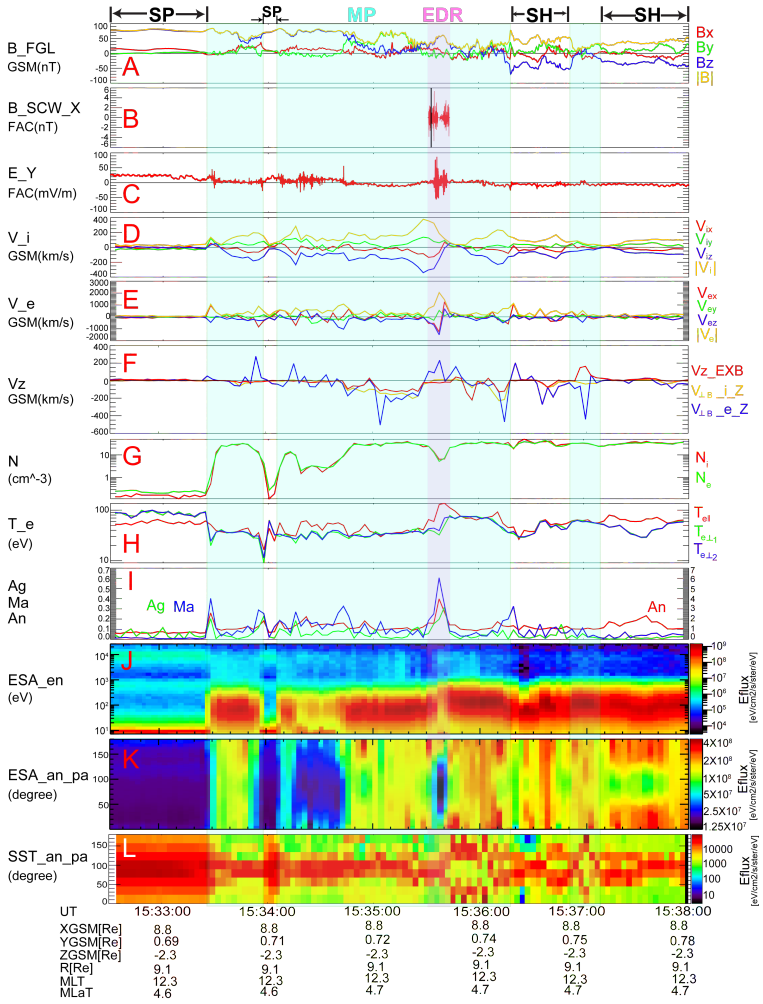

Figure 4.1: A reconnection event at the subsolar magnetopause observed by THEMIS-E on 27 August 2009. (a) 4 samples/s magnetic field data in GSM. (b) Perpendicular X component of the burst magnetic field at 8192 samples/s in FAC. (c) Perpendicular Y component of the electric field at 128 samples/s in FAC. (d and e) Ion and electron bulk flow velocity in GSM, respectively. (f) Comparisons of GSM-Z component of the $\mathbf{E} \times \mathbf{B}/B^2$ velocity with the GSM-Z component of ion and electron perpendicular flow velocity with respect to the ambient magnetic field, respectively. (g) Ion and electron densities. (h) Electron temperatures. (i) Electron agyrotropy and Mach number (scale to the left) and temperature anisotropy (scale to the right). (j) Differential energy flux for electrons measured by ESA. (k and l) Electron pitch angle spectra for lower engery (7 eV - 26 keV) electrons measured by ESA and higher energy (31 keV - 719 keV) electrons measured by SST, respectively.

plasmas comprising the low-latitude boundary layer as shown in Figure 4.1g. This observation is evidence for the transport of solar wind plasma across the magnetopause. The presence of accelerated plasma flow is seen through the magnetopause current sheet as shown in Figures 4.1d and 4.1e. The spacecraft crossed the magnetopause south of the separator, as suggested by the negative GSM-Z component of ion flow velocity and the result of Walén test [140].

Based on the prediction that the magnetopause should be a rotational discontinuity if reconnection is occurring [111], the Walén test [140] states that the observed flow velocity change between a point in the magnetopause and a reference point in the adjacent magnetosheath equals the predicted modified Alfvén velocity change. The ratios of magnitudes between the observed flow velocity change and the theoretically predicted modified Alfvén velocity change range from 0.30 to 0.66 which is reasonable within the range of uncertainty. The angle deviations between the observed and the predicted velocity changes are almost 180° for this event. This antiparallel relation indicates that the normal magnetic field component B_n is positive and thus the spacecraft crossed south of the separator [140]. This result is consistent with the positive polarity of the GSM-X component of the magnetic field, which is an approximation for B_n shown in Figure 4.1a (around 15:35:30 UT). The encounter with the magnetopause current sheet is associated with fast ion jetting consistent with the Walén relation and fast electron flows, indicating that reconnection is occurring. Magnetic reconnection is generally considered to be the primary mechanism through which transport of plasma and energy across the magnetopause occurs.

4.3 Identification of Electron Diffusion Region

Enhanced wave activity can be seen associated with the magnetopause crossing from Figures 4.1a (ambient magnetic field), 4.1b (burst magnetic field), and 4.1c (electric fluctuations). We note that the electric fluctuations maximize during the magnetic burst interval. During this interval, the electron flow speed (Figure 4.1e), anisotropy, agyrotropy and Mach number (Figure 4.1i) also maximize. These enhanced amplitudes

are coincident with the abrupt increases in electron parallel temperature $T_{e\|}$ shown in Figure 4.1h suggesting strong wave heating. As will be discussed in more detail in section 4.5, the observed intense waves may provide the observed electron heating. All these features, along with the fact that the electron perpendicular flow velocity is not consistent with the $\mathbf{E} \times \mathbf{B}/B^2$ velocity during the magnetic burst interval (Figure 4.1f), provide evidence for the detection of an electron diffusion region. These signatures are consistent with the simulation and observations of Scudder et al. [133].

It should be noted that the small peaks in the electron thermal parameters correspond to entries of topological boundaries of the magnetic field. For example, the peaks around 15:33:30 UT are due to the entry into the magnetopause boundary layer. A density cavity can be seen in Figure 4.1g (purple shaded band). The density inside the density cavity decreases to 16% of the magnetopause boundary level (30 cm^{-3}) which might indicate the center of the electron diffusion region. This density cavity is not a signature of magnetospheric separatrix as the density inside the density cavity does not drop with respect to its magnetospheric level. From the deviations of ion perpendicular flow velocity from the $\mathbf{E} \times \mathbf{B}/B^2$ velocity (Figure 4.1f), it can be seen that the ion diffusion region was encountered probably during the following two time intervals: 15:34:40 - 15:36:20 UT and 15:36:50 - 15:37:10 UT.

4.4 Distributions of Electrons

Figures 4.1k and 4.1l show the electron pitch angle spectra for lower-energy electrons measured by ESA and higher-energy electrons measured by SST, respectively. The magnetic field (Figure 4.1a) and electric field (Figure 4.1c) fluctuations enhance in the magnetopause boundary layer and in the magnetosheath with field-aligned and counterstreaming lower-energy electrons as shown in Figure 4.1k. However, the higher-energy electron pitch angle (Figure 4.1l) enhances around 90° in the boundary layer and in the magnetosheath, especially during the purple shaded magnetic burst interval. Distinct from the electron distributions in the boundary layer and in the magnetosheath, the

higher-energy electron pitch angle enhances at 0° and 180°, and the lower-energy electrons are more isotropic near the current sheet center around 15:36:00 UT and 15:37:00 UT. The lower-energy electrons in the identified electron diffusion region in Figure 4.1k can be seen streaming away from the "X-line" (antiparallel to the local magnetic field). These electrons are associated with Hall current parallel to the magnetic field. This indicates that the identified electron diffusion region is close to the "X-line".

4.5 Observations of Waves

Figure 4.2 shows an example of the identified whistler-mode waves at the time indicated by a black vertical line in Figure 4.1b. It can be seen from Figures 4.2a and 4.2b that the waves have frequencies from 0.1 to 0.6 f_{ce} with amplitudes up to 3 nT (peak-peak). As can be seen from Figure 4.2c, the wave Poynting flux is mostly antiparallel to the ambient magnetic field. The wave vector (k =[-0.23,-0.09,0.97] in FAC), determined from MVA on band pass-filtered wave magnetic field, is nearly along the background magnetic field. The wave propagation angle with respect to the ambient magnetic field θ_{kB} is ∼166° since the Poynting flux is mostly antiparallel to the magnetic field.

An expanded view of the whistler-mode waves can be seen in Figures 4.2d and 4.2e which respectively show the filtered (200 - 2000 Hz) waveforms of the burst magnetic and electric field data over the time interval indicated by the purple bar in Figure 4.2a. Figure 4.2f shows that the whistler-mode waves are circularly right-handed polarized with respect to the ambient magnetic field as expected. The electron distribution functions observed at times close to and/or concurrently with the whistler-mode waves are shown in Figures 4.2g and 4.2h. The lower-energy electrons (∼100 eV) shown in Figure 4.2g have anisotropic distributions with $T_{e\perp}/T_{e\parallel} < 1$. However, the energetic electrons (∼30 keV) shown in Figure 4.2h have anisotropic distributions with $T_{e\perp}/T_{e\parallel} > 1$. Broad-banded emissions with strong electric (∼10 mV/m) and magnetic (∼40 nT) field fluctuations below the ion cyclotron frequency (∼1 Hz) and electric (∼30 mV/m) and magnetic (∼20 nT) field fluctuations below the lower-hybrid frequency (∼30 Hz) are also detected during this magnetopause crossing (not shown). The < 1 Hz waves

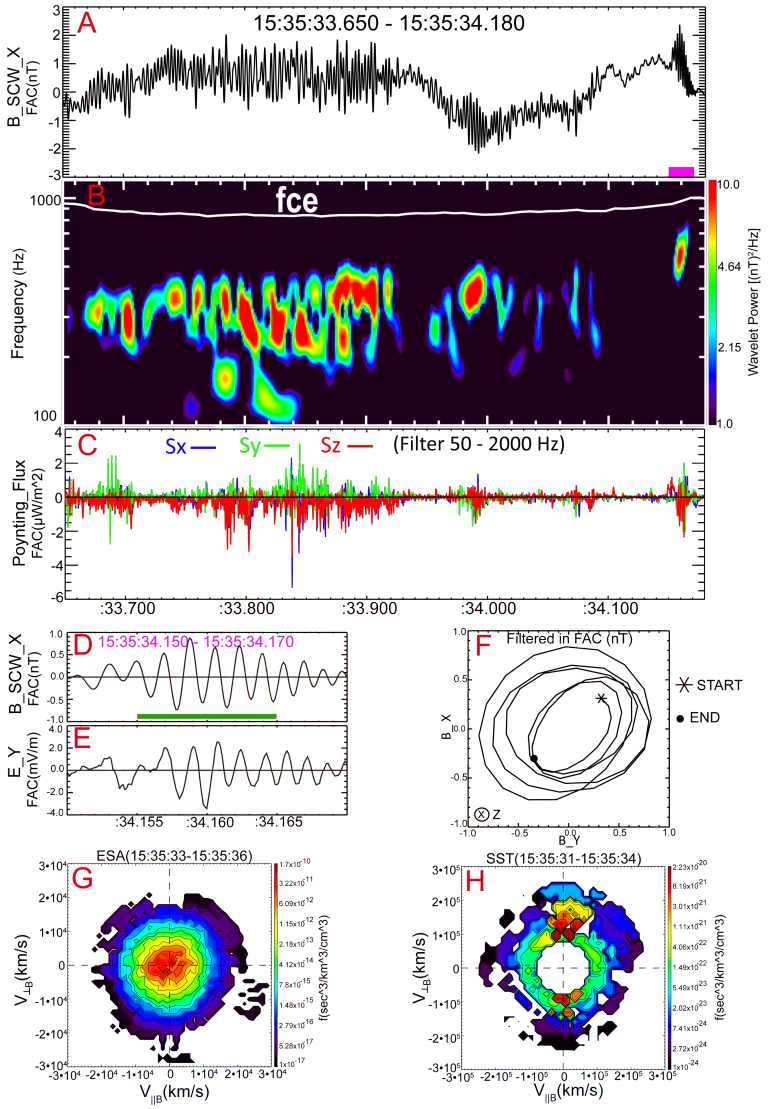

Figure 4.2: Example of whistler-mode waves within the electron diffusion region. (a, b, and c) A 0.53 sec interval in FAC of perpendicular X component of the burst magnetic field, associated wavelet power spectrum, and whistler Poynting flux, respectively. (d and e) Expanded views of the filtered whistler waveforms of the perpendicular X component of the burst magnetic field and the perpendicular Y component of the electric field over the time interval indicated by the purple bar in Figure 4.2a. (f) Hodogram of the filtered burst magnetic field waveforms in FAC for the interval indicated by the green bar in Figure 4.2d. The black star and dot mark the beginning and ending of the wave field, respectively. (g and h) Distribution functions of lower-energy electrons (up to 20 keV) measured by ESA and higher-energy electrons (20-700 keV) measured by SST observed at times close to the whistler-mode waves, respectively. The horizontal axis is parallel to the ambient magnetic field and the bulk velocity defines the plane.

may be kinetic Alfvén waves, and the 10s of Hz waves are consistent with lower-hybrid waves. These intense wave emissions may provide the observed electron heating associated with the magnetopause crossing.

Figure 4.3 shows examples of electrostatic waves at a time preceding the waves in Figure 4.2 by 0.05 s. Whistler-mode waves at a frequency of ∼0.3 f_{ce} are observed in the magnetic fluctuations in Figure 4.3a from 15:35:33.650 UT to 15:35:33.700 UT. This time interval overlaps with that of the electrostatic solitary waves, suggesting a possible coupling of whistler-mode waves and electrostatic solitary waves. Electrostatic solitary waves (up to 30 mV/m) indicated by the magenta arrows in Figure 4.3b have a broad spectrum which extends from 200 to 3000 Hz shown in Figure 4.3c. The high-frequency electrostatic waves (up to 35 mV/m) labeled by light blue arrows in Figure 4.3b have power that peaks at f_{ce}, which can be seen from both the wavelet power spectrum in Figure 4.3c and the Fourier power in Figure 4.3g. During this time interval, there is no power in the wave magnetic field at f_{ce} (not shown). This wave mode is linearly polarized, as shown in the hodograms in Figures 4.3d, 4.3e, and 4.3f in FAC with an interval indicated by the light blue arrows below Figure 4.3c. Occasionally, these high-frequency emissions are seen associated with clear harmonics, possibly suggesting electrostatic electron cyclotron waves.

4.6 Discussion and Conclusions

We have presented the first observations of intense waves in the electron diffusion region in a subsolar magnetopause reconnection region. The identification of the electron diffusion region in this event is based on the occurrence of signatures of strong electron heating, large electron thermal anisotropy, agyrotropy, and Mach number and electron velocity not consistent with the $\mathbf{E} \times \mathbf{B}$ velocity, consistent with the simulation and observations of Scudder et al. [133]. The lower-energy electrons (∼100 eV) with anisotropic distributions of $T_{e\perp}/T_{e\parallel} < 1$ within the electron diffusion region may have been heated by the observed waves with frequency below the lower-hybrid frequency, consistent with the suggestion that lower-hybrid waves lead to electron heating in the

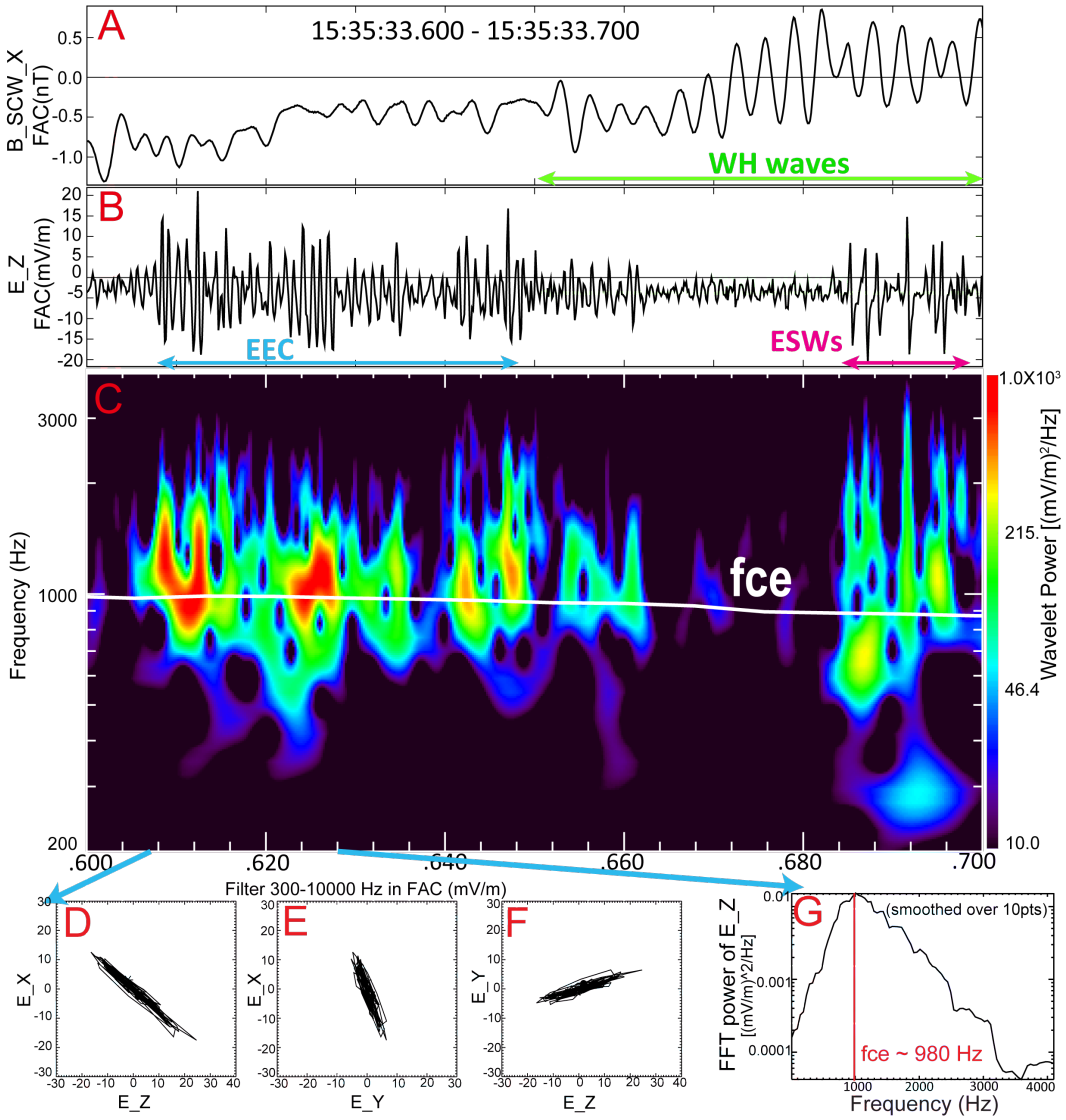

Figure 4.3: Example of electrostatic waves within the electron diffusion region. (a, b, and c) A 0.1 s interval of the perpendicular X component of the burst magnetic field, the parallel Z component of the electric field waveform capture and the associated wavelet power spectrum of the parallel electric field in FAC, respectively. (d, e, and f) Hodograms of the electric field waveforms with an interval indicated by the light blue arrows below Figure 4.3c. (g) Fourier wave power versus frequency with the same time interval as the hodograms.

parallel direction [16].

We identified intense whistler-mode waves inside the electron diffusion region. This is inconsistent with reported simulation results that indicated whistler-mode waves are only driven downstream of an electron diffusion region [48]. The whistler-mode waves seen by THEMIS in the electron diffusion region propagate almost antiparallel to the ambient magnetic field and the Poynting flux indicates that the whistler-mode waves propagate away from the center of the "X-line" along magnetic field lines. The observed electron temperature anisotropy of $T_{e\perp}/T_{e\parallel} > 1$ for energies above 20 keV may be the source of free energy for the generation of the whistler-mode waves. The energetic electron anisotropy may be produced by adiabatic heating in the perpendicular direction as the locally intensified magnetic field can accelerate electrons in the perpendicular direction [48]. On the field lines directly connected to the electron diffusion region, the energetic electron anisotropy may also be due to higher-energy field-aligned electrons (accelerated by the reconnection process) being lost to the magnetosheath [141]. Whistler-mode waves can scatter the electrons in pitch-angle distribution and relax the temperature anisotropy. Studies of large amplitude whistlers in the inner magnetosphere have provided evidence for rapid scattering and/or energization [23]. Whistler-mode waves may play a significant role in the microphysics of reconnection through the enabling of a current sheet instability, the decoupling of electrons, the acceleration and heating of particles, and the transport of energy away from the reconnection region.

A possible coupling of electrostatic electron cyclotron waves and electrostatic solitary waves with whistler-mode waves is often seen during magnetopause reconnection. The growth of the electrostatic waves may reduce the electron temperature anisotropy and reduce the growth rate of whistler-mode waves. Recent simulation performed by Goldman et al. [54] suggested that electron phase-space holes can generate whistler-mode waves during magnetic reconnection. However, the propagation properties of the whistler-mode waves in this case study are not consistent with those reported by Goldman et al. [54]. The generation mechanism of the whistler-mode waves in this event is different from that suggested by Goldman et al. [54]. The physics of the wave coupling process is important to understand the effect of wave-wave interactions on the

reconnection process and will be investigated in a future study. This study provides further evidence that the plasma waves can play a significant role in the microphysics of magnetic reconnection at the Earth's magnetopause.

Chapter 5

Observations of Electrostatic Ion Cyclotron Waves and associated Ion Heating During the 08 September 2010 Event

In this chapter, we describe observations of electrostatic ion cyclotron waves and whistler-mode waves and the associated particle distribution functions near one magnetopause crossing by three satellites of THEMIS. The results of this case study have been published [146]. These observations provide the first definitive identification of electrostatic ion cyclotron waves in the magnetopuase boundary layer and evidence for associated ion heating. We show that the waves are observed in a boundary layer of plasma in the magnetosphere adjacent to the magnetopause. We suggest that the electrostatic ion cyclotron waves can be a source for providing perpendicular ion heating at the Earth's magnetopause and therefore be important for understanding the boundary layer.

5.1 Introduction

This chapter presents an example of large amplitude electrostatic ion cyclotron waves near the Earth's dayside magnetopause at MLT of ~ 14 using data from THEMIS satellites. The electrostatic ion cyclotron waves were identified in a boundary layer in the magnetosphere adjacent to the magnetopause where reconnection was occurring. The electrostatic ion cyclotron wave power was primarily at $2f_{cH}$ (where f_{cH} is the hydrogen cyclotron frequency) and simultaneously observed with perpendicular ion heating. The electrostatic ion cyclotron waves had electric fields with significant power both perpendicular and parallel to the magnetic field. These amplitudes (30 mV/m) were greater than those of previously observed ion cyclotron harmonics (16 mV/m) at the nightside magnetopause [9]. The electrostatic ion cyclotron waves occurred during an interval of enhancements in the quasi-static electric field and fluctuations in the background magnetic field, plasma density and temperatures. The observations indicate that a plasma density gradient is a possible source of free energy for the electrostatic ion cyclotron waves. The observed flow shears are not large enough to drive the waves. Whistler-mode waves were identified near the electrostatic ion cyclotron wave region but closer to the magnetopause in a region with slightly higher ion and electron temperatures. The amplitude and frequency of the whistler-mode waves in this event are different from those observed in the electron diffusion region presented in Chapter 4.

5.2 Overview of Event

Examples of magnetopause crossings made by the THEMIS mission around 18:27:00 UT on 8 September 2010 at a local time of $\sim$14 MLT are shown in this section. THEMIS-A, D and E crossed the magnetopause with nearly simultaneous waveform burst data available. All three spacecraft observed both electrostatic ion cyclotron waves and whistler-mode waves during the crossing. For all three spacecraft the encounter with the magnetopause current sheet is associated with fast ion jetting consistent with the Walén relation and fast electron flows, indicating that reconnection was occurring.

Spacecraft locations and magnetic fields mapped with the Tsyganenko T01 Model in

GSM X-Z and Y-Z planes at 18:30:00 UT on 08 September 2010 are shown in Figure 5.1. Figures 5.1c and 5.1d are zoomed-in portions of Figures 5.1a and 5.1b. The distances of the satellites from the Earth are $r_A > r_E \simeq r_D$, $r_A \simeq 11.0R_e$, $r_E \simeq r_D \simeq 10.9R_e$, where R_e is the Earth radius. THEMIS-D and THEMIS-E encountered the magnetopause around 18:26:00 UT while THEMIS-A encountered the magnetopause about one minute later. This is consistent with the observations that both THEMIS-D and THEMIS-E had multiple magnetopause crossings while THEMIS-A had a single crossing from unambiguous magnetosheath to unambiguous magnetosphere. The magnetopause was generally moving sun-ward, sometimes bouncing back and forth. The OMNI magnetic field and solar wind plasma data shows that the solar wind dynamic pressure and the magnitude of the Bz-GSM component of the interplanetary magnetic field started to decrease at $\sim$ 17:20:00 UT. This sudden change in the solar wind led to an expansion of the magnetosphere and might explain why the magnetopause was generally moving outward during 18:25:00-18:30:00 UT.

Figures 5.2, 5.3 and 5.4 present overviews of field and moment data obtained by THEMIS-A, D and E, respectively. THEMIS-A, D and E traveled from the magnetosheath (SH) through the magnetopause (MP) into the magnetosphere (SP). The magnetopause crossings can be seen in the change in B_l from negative to positive (Figures 5.2a, 5.3a and 5.4a). Magnetopause crossings were also indicated by ion and electron differential energy flux as shown in Figures 5.2i and 5.2k, 5.3i and 5.3k, and 5.4i and 5.4k. There is a boundary layer (BL) of plasma adjacent to the magnetopause on the magnetospheric side. The start time of the boundary layer is the time of the onset of the rise in proton temperature (Figures 5.2g, 5.3g and 5.4g) and the end time is the time of the last temperature rise accompanied by a density drop (Figures 5.2d, 5.3d and 5.4d). The overall density gradient across the magnetopause and boundary layer is in the opposite direction from the overall ion and electron temperature gradients. The magnetic field in Figures 5.2a, 5.3a and 5.4a show that the field strength within the boundary is larger than that in the magnetosheath or in the magnetosphere and the field within the boundary is more irregular than it is later in the magnetosphere. Figures 5.2b, 5.3b and 5.4b show that magnetic burst data was available for all three spacecraft within the same time interval ($\sim$ 18:28:40-18:29:04 UT) on the magnetospheric side right after the

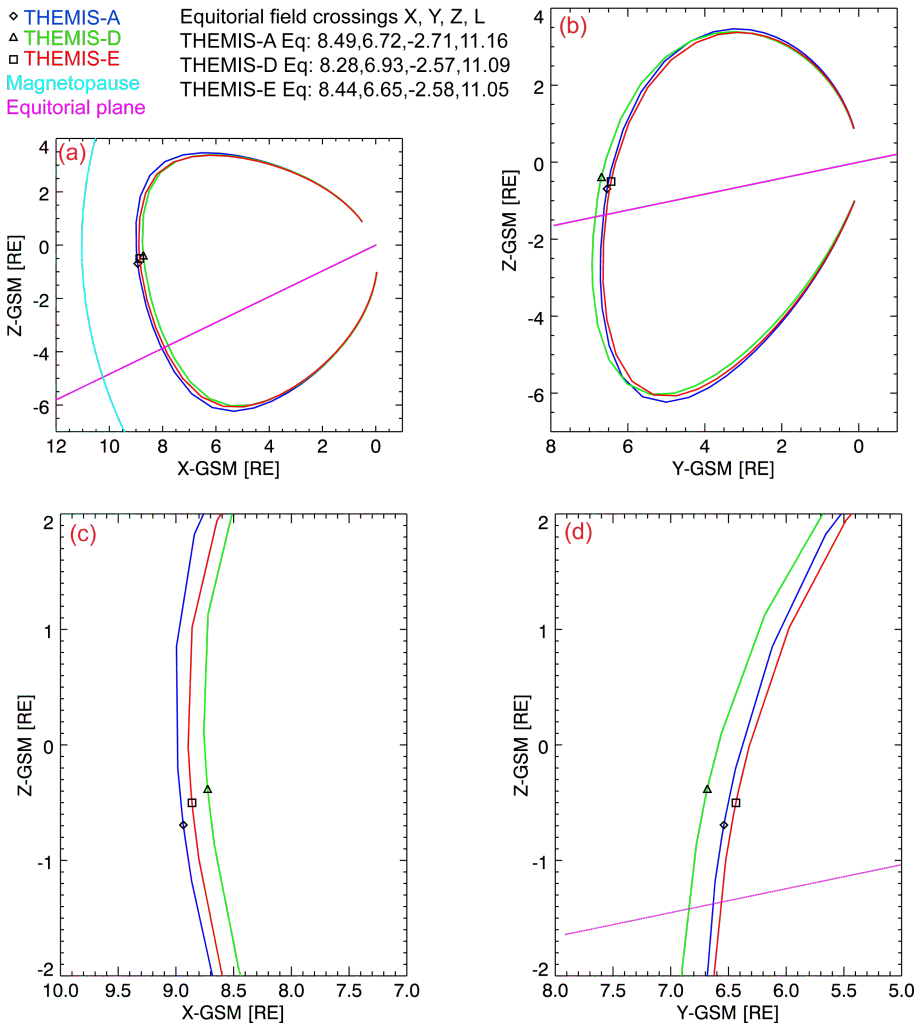

Figure 5.1: (a and b) Spacecraft locations and magnetic fields mapped with Tsyganenko T01 Model in GSM X-Z and Y-Z planes at 18:30:00 UT on 08 September 2010. (c and d) Zoomed-in portions of (a) and (b)

magnetopause crossing. All the three spacecraft observed low-frequency electrostatic ion cyclotron waves in the electric field (shaded pink) and whistler-mode waves in both magnetic and electric field (shaded blue, and occurring closer to the magnetopause) in the boundary layer in Figures 5.2, 5.3 and 5.4. It can be seen from the ion flow velocity in Figures 5.2e, 5.3e and 5.4e and the ion pitch angle distributions in Figures 5.2j, 5.3j and 5.4j that within the magnetopause layer with respect to the ambient magnetic field the ions are almost antiparallel before ion flow reversal while almost parallel after the flow reversal.

5.3 Electrostatic Ion Cyclotron Waves

The electrostatic ion cyclotron waves were observed in the 128 samples/s survey electric field (around 18:30:00 UT, shaded pink) in the boundary layer as shown in Figures 5.2, 5.3 and 5.4. During the electrostatic ion cyclotron wave intervals: (1) The ambient B_l and $|B|$ decreases slightly while B_m fluctuates (Figures 5.2a, 5.3a and 5.4a). (2) The DC electric field is largest as shown in Figures 5.2c, 5.3c and 5.4c. (3) There is a big shear in the $\mathbf{E} \times \mathbf{B}/B^2$ velocity. The GSM-Y components of the $\mathbf{E} \times \mathbf{B}/B^2$ velocity are shown in Figures 5.2f, 5.3f and 5.4f. (4) The ion density is higher than in the adjacent regions of the magnetosphere, but lower than in the magnetosheath and magnetopause (Figures 5.2d, 5.3d and 5.4d). (5) The ion temperature is higher than in the magnetosheath and magnetopause, but lower than in the adjacent regions of the magnetosphere (Figures 5.2g, 5.3g and 5.4g). (6) Lower-energy ions (< 100 eV) can be seen in the ion differential energy flux as shown in Figures 5.2i, 5.3i and 5.4i. (7) More specifically, the lower-energy ions were mainly in the perpendicular direction as shown in Figures 5.2m, 5.3m and 5.4m. The ion and electron distribution functions will be discussed later. (8) The ratio of electron temperature to ion temperature T_e/T_i is generally less than 0.1. The ratio of the parallel to perpendicular electron temperature $T_{e\parallel}/T_{e\perp}$ is ~ 1. Plasma β is ~ 0.5.

Figure 5.5 shows examples of the electrostatic ion cyclotron waves. Figures 5.5a-5.5f show the waveforms and associated wave power spectra of the electrostatic ion cyclotron

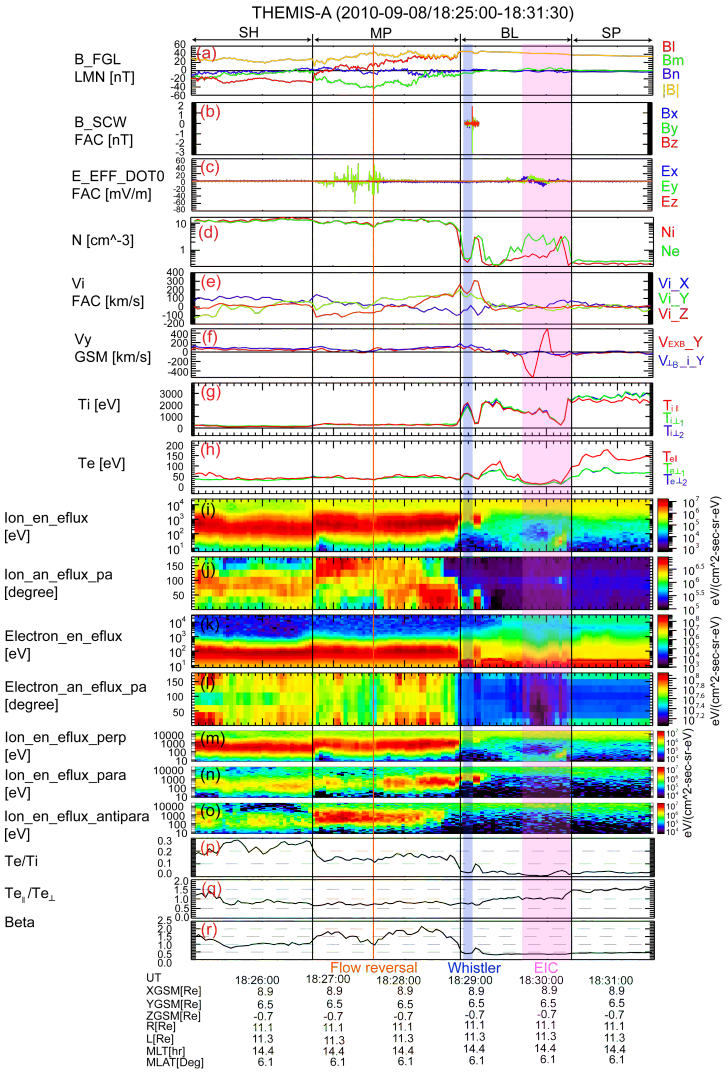

Figure 5.2: Observations made by THEMIS-A from 18:25:00 UT to 18:31:30 UT on 08 September 2010. (a) 4 samples/s magnetic field data in LMN. (b) Burst magnetic field at 8192 samples/s in FAC. (c) Fast survey electric field using $E \cdot B = 0$ at 128 samples/s in FAC. (d) Ion and electron density. (e) Ion bulk flow velocity in FAC. (f) Comparisons of GSM-Y component of the $\mathbf{E} \times \mathbf{B}/B^2$ velocity with the GSM-Y component of ion perpendicular flow velocity with respect to the ambient magnetic field (g and h) Ion and electron temperatures, respectively. (i) Ion differential energy flux. (j) Ion pitch angle spectra. (k) Electron differential energy flux. (l) Electron pitch angle spectra. (m, n, and o) Ion differential energy flux in perpendicular, parallel and antiparallel directions, respectively. (p and q) Ratios of T_e/T_i and $T_{e\|}/T_{e\perp}$, respectively. (r) Plasma beta. The position parameters are shown at the bottom.

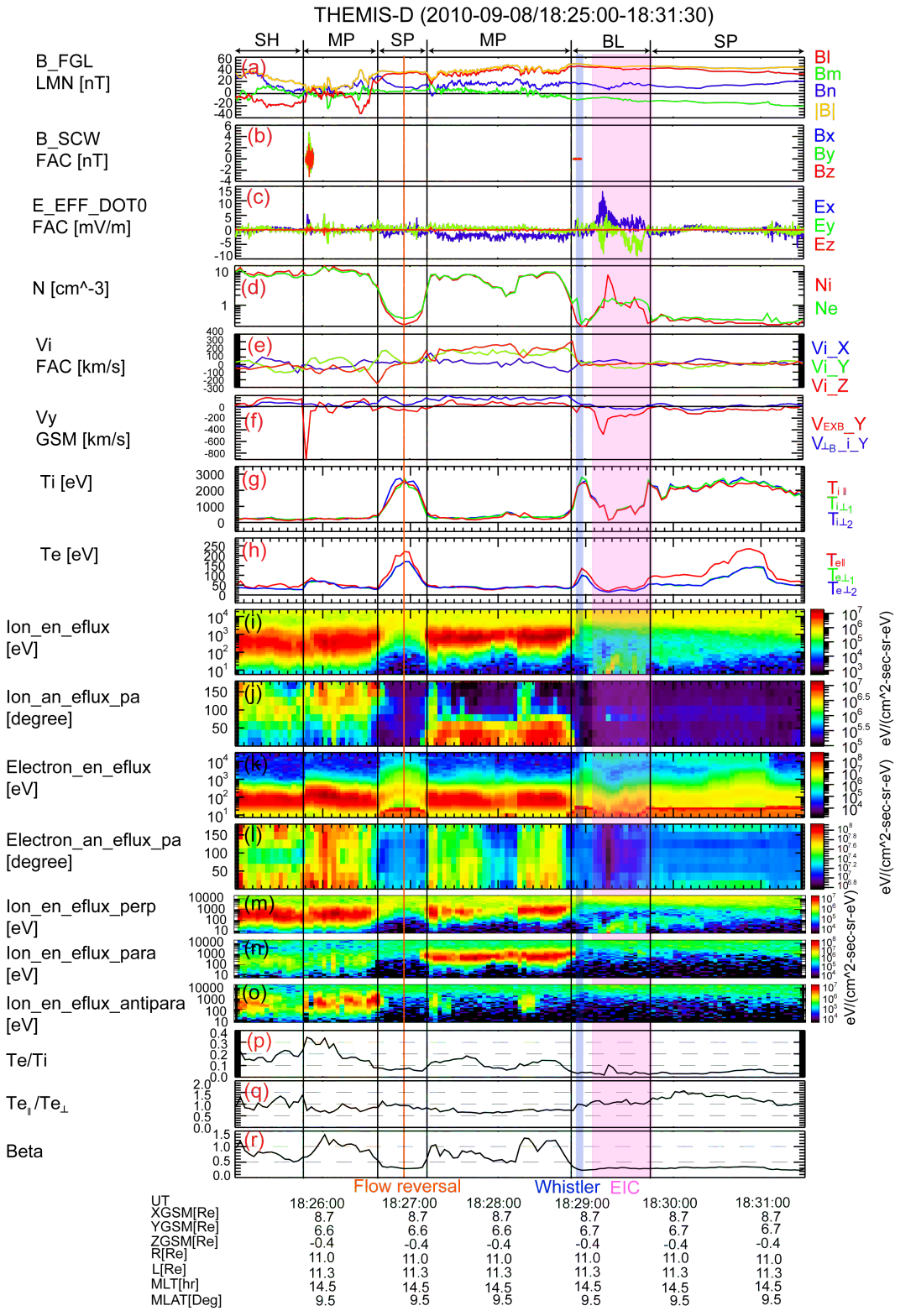

Figure 5.3: Observations made by THEMIS-D from 18:25:00 UT to 18:31:30 UT on 08 September 2010. Caption is the same as that of Figure 5.2.

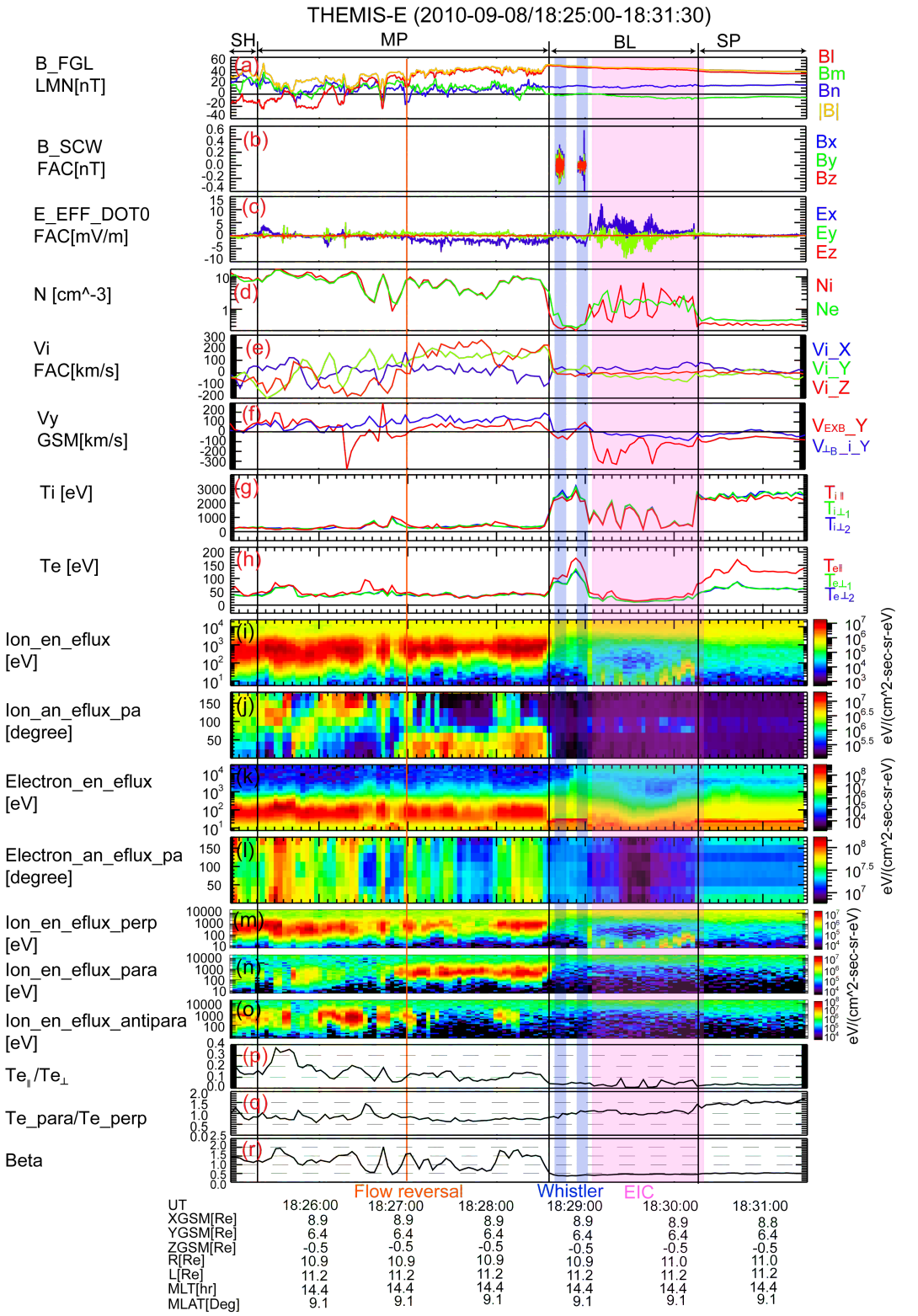

Figure 5.4: Observations made by THEMIS-E from 18:25:00 UT to 18:31:30 UT on 08 September 2010. Caption is the same as that of Figure 5.2.

waves observed by THEMIS-A, D and E during the time intervals shaded by pink in Figures 5.2, 5.3 and 5.4. It can be seen from Figures 5.5b, 5.5d and 5.5f that the wave power in the electric field enhances near $\sim 2f_{cH}$, f_{cH} and $0.5f_{cH}$. The enhancement is clearer near $2f_{cH}$ than f_{cH} and $0.5f_{cH}$. The lower hybrid frequency f_{LH} is $\sim$ 28 Hz, well above the hydrogen cyclotron frequency f_{cH} of 0.65 Hz. It can be seen from Figures 5.5b, 5.5d and 5.5f that the wave power in the electric field enhances near $\sim 2f_{cH}$, f_{cH} and $0.5f_{cH}$. The enhancement is clearer near $2f_{cH}$ than f_{cH} and $0.5f_{cH}$. The lower hybrid frequency f_{LH} is $\sim$ 28 Hz, well above the hydrogen cyclotron frequency f_{cH} of 0.65 Hz. It can be seen that both ends of the electric field spectrum plotted for the wave intervals on THEMIS-A (Figure 5.5b) and THEMIS-D (Figure 5.5d) are affected by the spin tone (0.33 Hz) although they are not affected during the time intervals of the electrostatic ion cyclotron waves. The waves observed by THEMIS-E have a longer duration and are more coherent as shown in Figure 5.5e. So the influence of the spin tone on both ends of the electric field spectrum observed by THEMIS-E (Figure 5.5f) is much smaller than those observed by THEMIS-A (Figure 5.5b) and THEMIS-D (Figure 5.5d). Therefore the wave power dominates near $2f_{cH}$ as shown in Figure 5.5f. Doppler effect is negligible as the average magnitude of the bulk flow velocity is very small (less than 50 km/s) during the time intervals of the waves as shown in Figures 5.2e, 5.3e and 5.4e. It indicates that the frequency can only be shifted by 0.2 Hz at most, which is small compared to the dominant frequency of the waves ($\sim$ 1.3 Hz). These waves are electrostatic as there is no wave power enhancement near f_{cH} in the magnetic field (not shown). The wave power enhancement near $0.5f_{cH}$ in the electric field may be due to ion cyclotron waves associated with He++ that has diffused (or been accelerated) across the magnetopause boundary. Helium and oxygen are often seen inside the magnetopause and adjacent to it; however, the THEMIS mission does not make ion composition measurements to distinguish different ion species. Figures 5.5g and 5.5h show the perpendicular Y and parallel Z components of the electric field observed by THEMIS-A in FAC, respectively. The waves are up to 30 mV/m (peak-peak) and last for $\sim$40-75 s on each spacecraft. The waveforms of the electrostatic ion cyclotron waves observed by THEMIS-A, D, and E have little coherence as shown in Figures 5.5a, 5.5c and 5.5e. The ratio of the parallel to perpendicular wave vector calculated from both wave amplitude and MVA is consistently $k_{\parallel}/k_{\perp} \sim 1.5$ for the observed electrostatic ion

cyclotron waves.

The ion and electron distributions at times preceding and succeeding the electrostatic ion cyclotron waves look different from those at times of electrostatic ion cyclotron waves. It can be seen from Figure 5.5i that the ion distribution at times of electrostatic ion cyclotron waves elongate in the perpendicular to ambient magnetic field direction - consistent with the idea that ions with energy less than 100 eV were heated by the electrostatic ion cyclotron waves in the perpendicular direction. The electron distribution at times of electrostatic ion cyclotron waves shows a temperature anisotropy of $T_{e\parallel} > T_{e\perp}$ at energies larger than 50 eV, see Figure 5.5j.

5.4 Whistler-Mode Waves

THEMIS-A, D and E all observed whistler-mode waves near the magnetopause close to the electrostatic ion cyclotron waves. Figure 5.6 presents an example of the identified whistler-mode waves observed by THEMIS-E during the magnetopause crossing with the time interval indicated by the blue band on the left of Figure 5.4. Figures 5.6a and 5.6c show that the wave amplitudes (peak-to-peak) are up to 0.5 nT in magnetic fluctuations and 20 mV/m in electric fluctuations. These amplitudes are smaller than those observed within the electron diffusion region shown in Chapter 4. It can be seen from Figures 5.6b and 5.6d that the wave power enhances in the frequency band of 400-1000Hz where the electron cyclotron frequency f_{ce} is $\sim$ 1300 Hz. The frequency of the whistler-mode waves in this event is primarily in the upper band ($f > 0.5f_{ce}$) while the frequency is primarily in the lower band ($f < 0.5f_{ce}$) for the whistler-mode waves observed in the electron diffusion region presented in Chapter 4. As can be seen from Figure 5.6e that the wave Poynting flux is mostly antiparallel to the ambient magnetic field. The wave vector (k =[-0.16,0.15,-0.97] in FAC), determined from MVA on bandpass filtered wave magnetic field, is nearly along the background magnetic field. The wave propagation angle with respect to the ambient magnetic field θ_{kB} is determined as $\sim$167° since the Poynting flux is mostly anti-parallel to the magnetic field. THEMIS-E was at the south of the magnetic separator during the time interval when

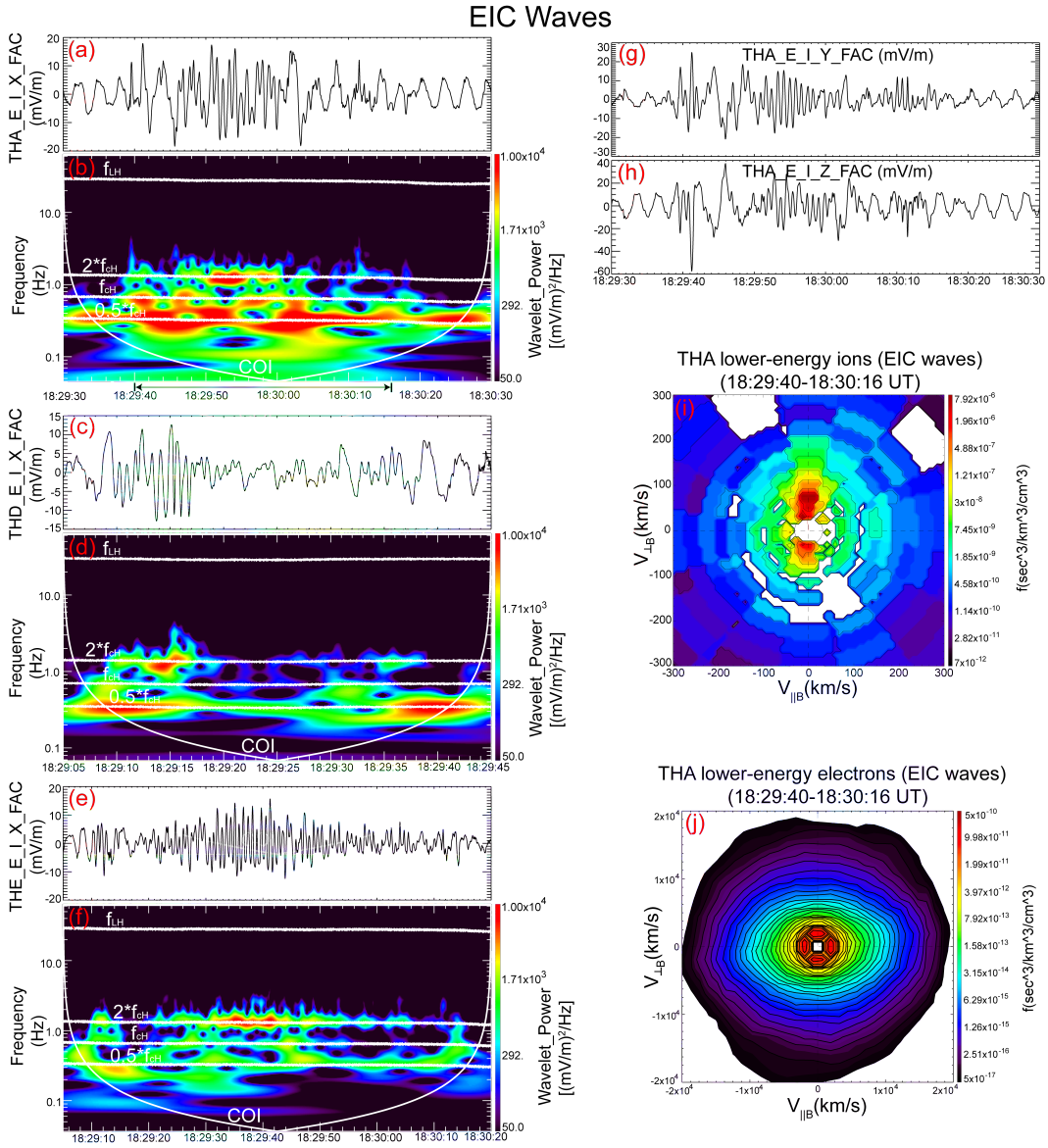

Figure 5.5: Examples of electrostatic ion cyclotron waves observed by THEMIS-A, D and E on 08 September 2010. (a, b; c, d; e, f) Perpendicular X component of the electric field in FAC and associated wave power spectrum by THEMIS-A, D and E, respectively. The white lines on the power spectrums indicate: f_{LH}(lower hybrid frequency); $2f_{cH}$, f_{cH}, $0.5f_{cH}$(hydrogen cyclotron frequency); COI(cone of influence under which data is subjected to edge effect). (g and h) Perpendicular Y and parallel Z components of the electric field by THEMIS-A in FAC, respectively. (i and j) Distribution functions of lower-energy ions and electrons measured by ESA on THEMIS-A for the time interval indicated at the top of each panel and indicated by the arrows in the wave power spectrum. The horizontal axis is parallel to the ambient magnetic field and the bulk velocity defines the plane.

the whistler-mode waves were observed, as suggested by the positive B_n component. It indicates that the whistler-mode waves propagate away from the reconnection region along magnetic field lines, consistent with observations of the electron diffusion event in Chapter 4. Figure 5.6f shows that the waves are circularly right-handed polarized with respect to the ambient magnetic field as expected. The electron distribution functions observed at times concurrently with the whistler-mode waves are shown in Figure 5.6g and 5.6h. The lower-energy ($\sim$ 100 eV) electrons shown in Figure 5.6g has anisotropic distribution with $T_{e\perp}/T_{e\parallel} < 1$ while the higher-energy electrons ($\sim$ 30 keV) shown in Figure 5.6h has anisotropic distribution with $T_{e\perp}/T_{e\parallel} > 1$.

5.5 Discussions and Conclusions

THEMIS-D observed electrostatic ion cyclotron waves first, followed within 5 seconds by THEMIS-E, and finally THEMIS-A. This sequence is consistent with the relative spacecraft locations and with the observed relative times of the observed magnetopause crossings on the three spacecraft. The magnetopause was generally moving sun-ward, sometimes bouncing back and forth. Electrostatic ion cyclotron waves were observed and very likely generated within the boundary layer of the magnetopause. Signatures of strong plasma inhomogeneity were observed within the boundary layer. During the electrostatic ion cyclotron wave intervals the plasma density and temperature are quite variable with highest values on the side adjacent to the magnetopause. These signatures are very similar to those observed by [12] in what they called plasma clouds near the high-latitude nightside magnetopause. The power spectrum of the electrostatic ion cyclotron waves is similar to that of the observation made by [9] that has ion cyclotron harmonic peaks. However, the wave power does not decrease with increasing ion cyclotron harmonics as reported by [9]. During the time intervals of the electrostatic ion cyclotron waves, T_e/T_i is generally less than 0.1, $T_{e\parallel}/T_{e\perp}$ is $\sim$ 1, and β is $\sim$ 0.5. The ratio of ion Larmor radius over the scale length of the plasma density gradient within the boundary layer is comparable to the threshold value for the ion cyclotron drift instability, which is $\sim$ 0.025 [12]. Therefore, the gradients in the plasma density are possible sources of free energy for the electrostatic ion cyclotron waves observed near the dayside

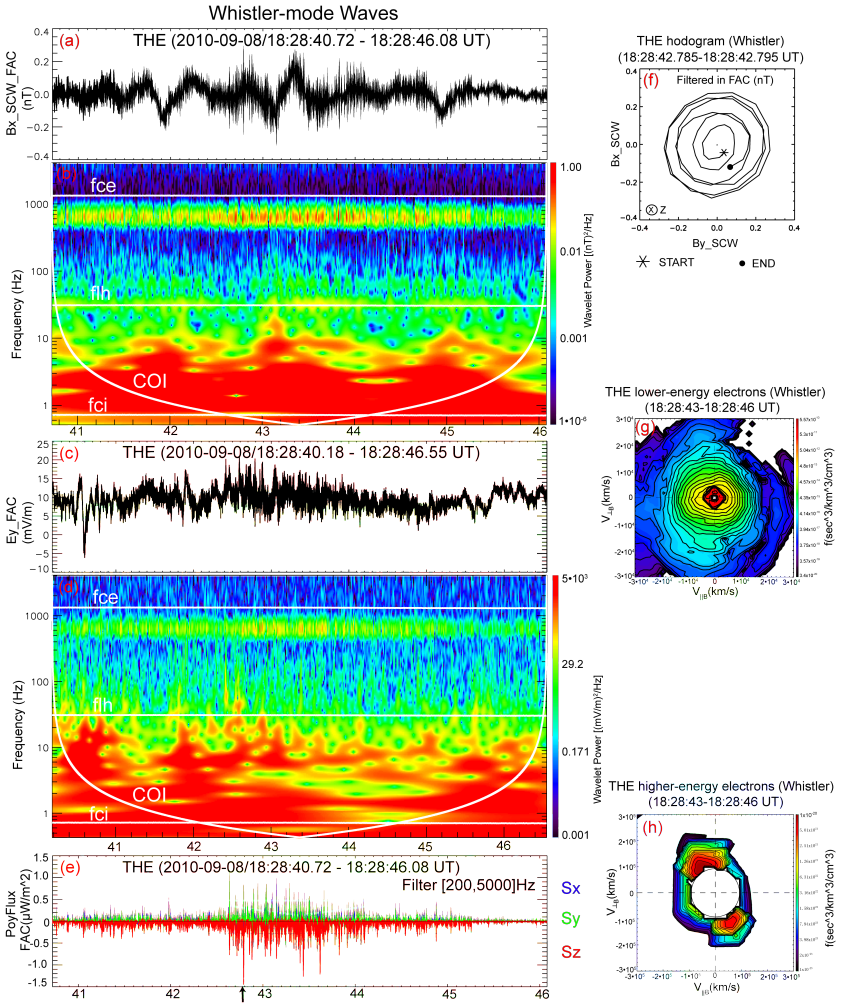

Figure 5.6: Examples of whistler-mode waves observed by THEMIS-E on 08 September 2010. (a and b) Perpendicular X component of the burst magnetic field in FAC and associated wave power spectrum. (c and d) Perpendicular Y component of the electric field in FAC and associated wave power spectrum. (e) Whistler Poynting flux in FAC with magnetic field and electric field data filtered between 200 Hz and 5000 Hz. (f) Hodogram of the filtered burst magnetic field waveforms in FAC for the time indicated by the black arrow in Figure 5.6e. The black star and dot mark the beginning and ending of the wave field, respectively. (g) Distribution function of lower-energy electrons measured by ESA for the time interval indicated at the top of the panel. The horizontal axis is parallel to the ambient magnetic field and the bulk velocity defines the plane. (h) Distribution function of higher-energy electrons measured by SST for the time interval indicated at the top of the panel.

magnetopause at MLT of ~ 14. [9] concluded that the threshold value depends on the number of ion cyclotron harmonics. A steeper density gradient is required for increasing number of ion cyclotron harmonics.

The parallel shear instability mechanism is very unlikely to explain the waves as there is no big shear in the parallel ion flow velocity during the time intervals of electrostatic ion cyclotron waves (shaded pink in Figures 5.2e, 5.3e and 5.4e). Large shears were seen in the $\mathbf{E} \times \mathbf{B}/B^2$ velocity (Figures 5.2f, 5.3f and 5.4f) by all three spacecraft; however, the scale length of the sheared $\mathbf{E} \times \mathbf{B}$ flows ($\sim 8000km$) is much larger than the ion gyroradius ($\sim$ 70 km in this case). It indicates that based on prior work [51] the perpendicular shear instability mechanism is also unlikely.

The waveforms of the electrostatic ion cyclotron waves observed by THEMIS-A, D, and E have little coherence. It indicates that the wavelength of the electrostatic ion cyclotron waves are much less than the smallest spacecraft separation ($\sim$ 1400 km). This estimate is reasonable since the electrostatic ion cyclotron wavelengths are generally on the order of an ion gyroradius ($\sim$ 70 km in this case). The estimated electrostatic ion cyclotron wavelengths are much shorter than those of the very-low frequency ion waves [32, 31] which have wavelength and coherence over several thousand of kilometers in the current sheet boundary.

The waves have $k_{\parallel}/k_{\perp} \sim 1.5$ which is very different from the typically observed value of $\lesssim 0.2$ for electrostatic ion cyclotron waves on auroral field lines [10, 21]. The observation indicates that there might be a coupling of electrostatic ion cyclotron waves with ion acoustic waves. Linearly unstable electrostatic ion cyclotron waves may decay into stable daughter electrostatic ion cyclotron and ion acoustic modes as suggested by [11]. This three-wave decay is possible as long as the electrostatic ion cyclotron waves are of sufficient amplitude to exceed the threshold for decay to weakly damped electrostatic ion cyclotron modes. This possibility will require further theoretical study, which is beyond the scope of this paper.

The presence of electrostatic ion cyclotron waves in the magnetopause boundary

layer may contribute to maintaining the layer. The He++ in the magnetosheath may be transported inward by resonating with the electrostatic ion cyclotron waves as suggested by [154] who theorized that electrostatic ion cyclotron waves were capable of inducing the required rapid inward diffusion of typical magnetosheath ions. Hydrogen ions may also be heated and diffused by these waves.

Whistler-mode waves were observed close to the electrostatic ion cyclotron waves. Both wave modes were observed in a boundary layer of plasma in the magnetosphere adjacent to the magnetopause, but the electrostatic ion cyclotron waves were farther from the magnetopause. The particle distribution functions show that lower-energy ion temperature anisotropy of $T_{i\perp} > T_{i\parallel}$ is associated with the electrostatic ion cyclotron waves while higher-energy electron temperature anisotropy of $T_{e\perp}/T_{e\parallel} > 1$ is associated with whistler-mode waves. Unlike the whistler-mode waves reported by Tang et al. [144] and discussed in Chapter 4, the frequency of the whistler-mode waves observed in this event is in the upper band ($f > 0.5 f_{ce}$). In addition, the whistler-mode waves in the former event have larger amplitudes than those in the latter event. The former event was in the electron diffusion region at the subsolar magnetopause, whereas the latter event was in the magnetopause boundary layer and at post-noon ($\sim$14 MLT).

We have presented the first observations of large amplitude ($\sim$ 30 mV/m) electrostatic ion cyclotron waves near the Earth's magnetopause. The properties of the identified wave frequency and wavelength agree with those of electrostatic ion cyclotron waves. Perpendicular heating of low energy ions, consistent with heating by electrostatic ion cyclotron waves, was observed in the event. The gradients in plamsa density within the low latitude boundary layer are possible sources of free energy for the electrostatic ion cyclotron waves. The large value of $k_\parallel/k_\perp$ indicates that there might be coupling of electrostatic ion cyclotron waves with ion acoustic waves. The magnetosheath particles were transported inward by resonating with the electrostatic ion cyclotron waves. Thus, the presence of electrostatic ion cyclotron waves in the magnetopause boundary layer may contribute to maintaining the boundary layer.

Chapter 6

Simultaneous Observations of Lower-Hybrid, Whistler-Mode, Electrostatic Solitary, and Electron Cyclotron Waves During the 23 August 2010 Event

An example of simultaneous observations of four wave modes is presented in this chapter. The results of this case study are to be submitted to Geophysical Research Letters [145].

6.1 Introduction

As discussed in earlier chapters, wave modes including lower-hybrid waves, whistler-mode waves, electrostatic solitary waves and electron cyclotron waves have been frequently observed in the Earth's magnetosphere and at the Earth's magnetopause. We present the first simultaneous observations of these waves at the low-latitude boundary layer of the Earth's magnetopause using data from the THEMIS-E satellite. The waves

were identified through auditory analysis [1] in the high resolution (16384 samples/s) electric field burst data and occurred at the same time as large fluctuations of plasma density and temperature (at time scales of ∼3 to 4 minutes) at a location of 9.3 Re, 14.4 magnetic local time, and 5.8 degrees magnetic latitude. Large fluctuations in the interplanetary magnetic field and solar wind flow speed were observed associated with this wave event and could be responsible for the variations seen in the low-latitude boundary layer at THEMIS-E. The particle distribution functions show that lower-energy ions (<1.3 keV) are anisotropic with $T_{i\perp} > T_{i\parallel}$ while lower-energy (<300 eV) electrons are anisotropic with $T_{e\perp} < T_{e\parallel}$. In addition, electrons show a double-peaked distribution, i.e., bi-streaming beams. As will be shown below, these distributions are consistent with instability mechanisms proposed for the observed waves. The results provide insights into wave coupling near the magnetopause and provide additional evidence to the event in Chapter 4 that coupling processes may be more important than usually thought.

6.2 Overview of Event

An example of simultaneously observed waves during a magnetopause crossing made by probe E of the THEMIS mission on 23 August 2010 is shown in this section. The spacecraft was located at a radius of 9.3 Re, [X, Y, Z]=[7.2, 5.5, -1.8]Re in GSM, Lat = 5.8°, MLT = 14.4 hr and L = 9.3 Re around the time when the waves were observed. This event was identified through auditory analysis [1]. It stood out to ears while listening through audified THEMIS electric field data.

Figure 6.1 shows a 4 hrs interval of the field and plasma observations made by THEMIS-E on 23 August 2010. The spacecraft travels from the outer magnetosphere (SP) through the magnetopause boundary layer (BL) and the magnetopause (MP) into the magnetosheath (SH). The characteristics of the fields and plasmas during 15:50:00 UT and 16:40:00 UT shown in Figure 6.1 look like those of a low-latitude boundary layer. The light green band and orange band indicate the outer and inner boundary layer of the magnetopause, respectively. The simultaneous waves (indicated by the vertical purple line) were identified from the EFW burst in the inner boundary layer during

16:22:32.64 UT - 16:22:32.71 UT when densities (Figure 6.1c) and temperatures (Figures 6.1e and 6.1f) had large fluctuations. The waves were not observed in the burst magnetic field.

The magnetopause crossing can be seen in the change in Bz from positive to negative (Figure 6.1a). It can also be seen in the fluctuations of ion bulk flow (Figure 6.1d). The differential energy flux of ions in Figure 6.1g shows that in the magnetosphere, where Bz was positive, high-energy ions were encountered; while in the magnetosheath, where Bz was negative, lower-energy ions were measured. The differential energy flux of electrons in Figure 6.1i shows similar characteristics. The spacecraft passed from the lower plasma density mangetosphere to the higher density (factor of 100) magnetosheath via a region of mixed magnetosheath/magnetospheric plasmas comprising the low-latitude boundary layer as shown in Figure 6.1c. In the inner boundary layer, the ratio of electron temperature over ion temperature is ~ 0.1 (Figure 6.1k) and the plasma beta is ~ 0.2 (Figure 6.1m). The ratio of electron parallel temperature over electron perpendicular temperature fluctuates between 0.5 and 1.0 (Figure 6.1l).

Figure 6.2 describes differential energy flux of ions and electrons. It can be seen from Figures 6.2d, 6.2e, 6.2f and 6.2g that ions with energies less than 600 eV have temperature anisotropy of $T_{i\perp} > T_{i\|}$. However, electrons with energies less than 150 eV have temperature anisotropy of $T_{e\|} > T_{e\perp}$ as shown in Figures 6.2k and 6.2l.

6.3 Simultaneously Observed Waves

The waveform and wave power spectra of the simultaneously observed waves are shown in Figure 6.3. Figure 6.3a shows the perpendicular and parallel components of the electric field low-pass filtered at 100 Hz. The corresponding wave power spectra shown in Figures 6.3b, 6.3c and 6.3d indicate that there is more power enhancement in the perpendicular directions than the parallel direction near the lower hybrid frequency ($f_{lh} \sim 40$ Hz). Figures 6.3e plots the perpendicular and parallel components of the

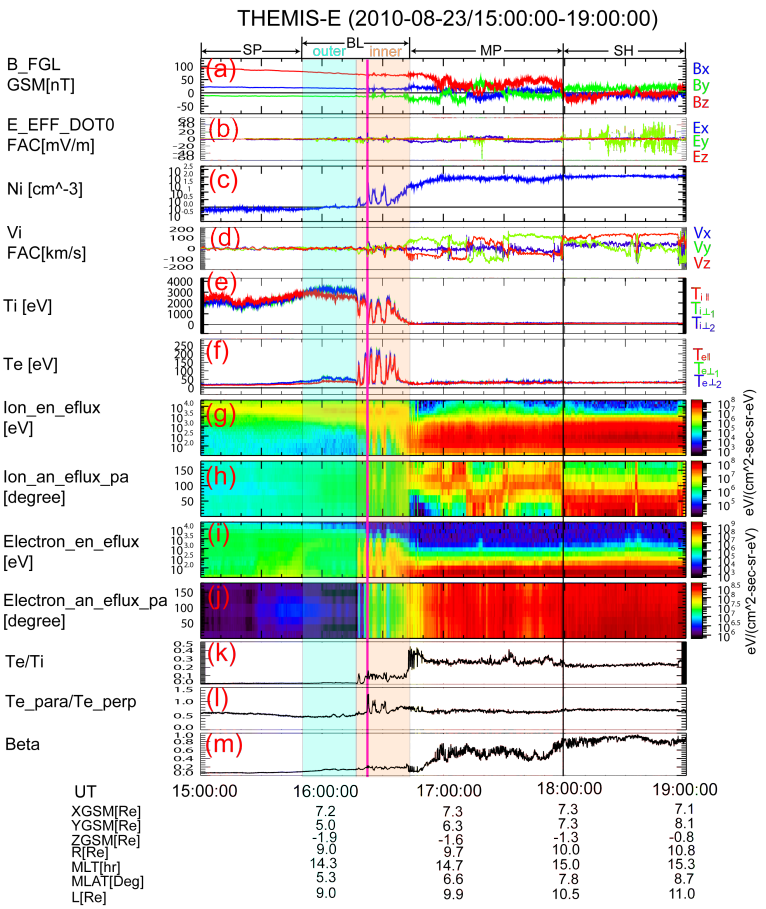

Figure 6.1: Field and plasma measurements mady by THEMIS-E during a magnetopause crossing on 23 August 2010. (a) Spin-resolution (∼3s) magnetic field in GSM. (b) Electric field at 128 samples/s in FAC. (c) Ion density. (d) ion and electron bulk flow velocity in GSM, respectively. (e and f) Ion and electron temperatures. (g) Differential energy flux for ions measured by ESA. (h) Ion pitch angle spectra for lower energy ions measured by ESA. (i) Differential energy flux for electrons measured by ESA. (j) Electron pitch angle spectra for lower energy electrons measured by ESA. (k) Ratio of electron temperature to ion temperature. (l) Ratio of the parallel to perpendicular electron temperature. (m) Plasma beta. The vertical purple line indicates when the simultaneous waves were observed.

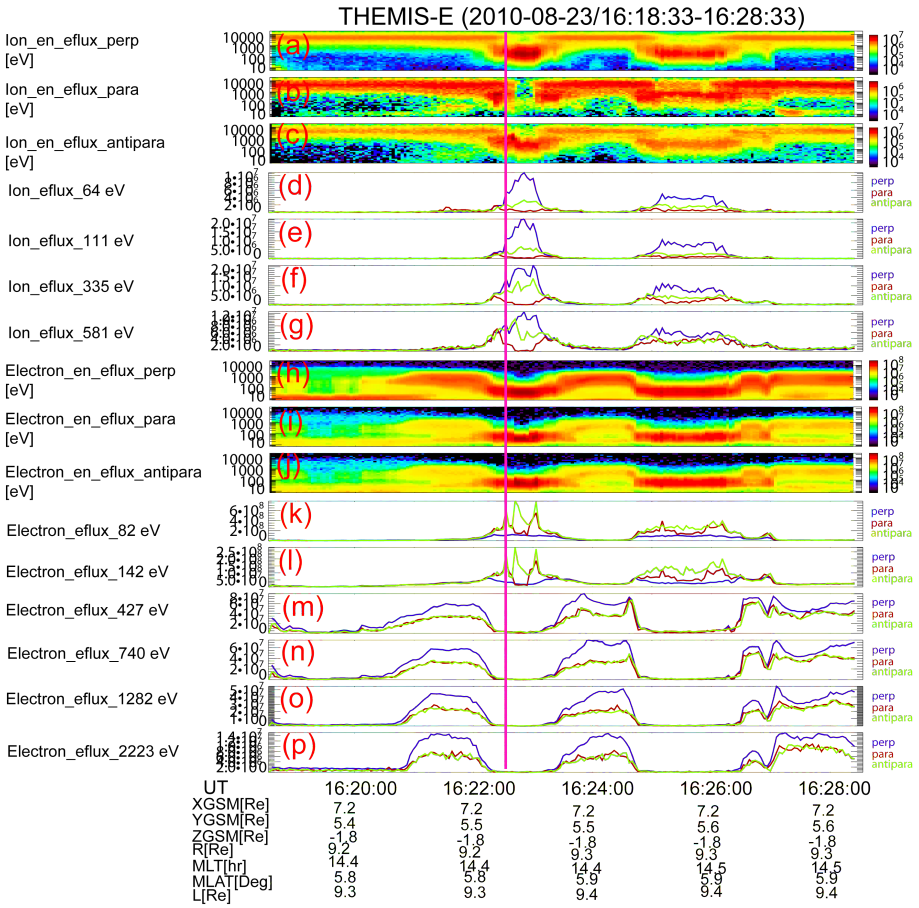

Figure 6.2: Differential energy flux of ions and electrons. (a, b and c) Differential energy flux of ions in perpendicular, parallel and anti-parallel directions, respectively. (d, e, f and g) Differential energy flux for ions at 64 eV, 111 eV, 335 eV and 581 eV, respectively. (h, i and j) Differential energy flux of electrons in perpendicular, parallel and anti-parallel directions, respectively. (k, l, m, n, o and p) Differential energy flux for electrons at 82 eV, 142 eV, 427 eV, 740 eV, 1282 eV and 2223 eV, respectively. The vertical purple line indicates when the simultaneous waves were observed.

electric field high-pass filtered at 100 Hz. Wave power enhances in the perpendicular directions on the band of 2000-3000 Hz just above the electron cyclotron frequency ($f_{ce} \sim$ 2000 Hz) as shown in Figures 6.3f and 6.3g. This wave mode is identified as electron cyclotron waves. Electrostatic solitary waves are indicated by the bipolar pulses in the parallel component of the electric field as well as the broadband power in the parallel electric field spectrum shown in Figure 6.3h (16:22:32.675 UT - 16:22:32.705 UT). Wave power at $\sim$ 1000 Hz (near half of f_{ce}) corresponds to the whistler-mode waves. For the whistler-mode waves, the parallel electric field component dominates.

6.4 Distribution Functions

Figure 6.4 shows the distribution functions of lower-energy ions measured by ESA. Figures 6.4a, 6.4b and 6.4c correspond to times preceding, during and after the time of simultaneously observed waves. Figures 6.4d, 6.4e and 6.4f are the cuts of the distribution functions corresponding to Figures 6.4a, 6.4b and 6.4c. It can be seen from Figure 6.4e that the ions during the time interval of the simultaneously observed waves are anisotropic with $T_{i\perp} > T_{i\parallel}$.

Figure 6.5 shows the distribution functions of lower-energy electrons measured by ESA. Figures 6.5a, 6.5b and 6.5c correspond to times preceding, during and after the time of simultaneously observed waves. Figures 6.5d, 6.5e and 6.5f are the cuts of the distribution functions corresponding to Figures 6.5a, 6.5b and 6.5c. It can be seen from Figure 6.5e that the electrons show what appears to be a double-peaked distribution (i.e., possibly bi-streaming beams) at 3000-4000 km/s ($\sim$ 30 eV) in the bulk flow rest frame. Thus, at low energies ($\lesssim$ 300 eV) the electrons are anisotropic with $T_{e\parallel} > T_{e\perp}$. Electron distributions preceding and after the time interval of the simultaneously observed waves don't have this feature as shown in Figures 6.5d and 6.5f.

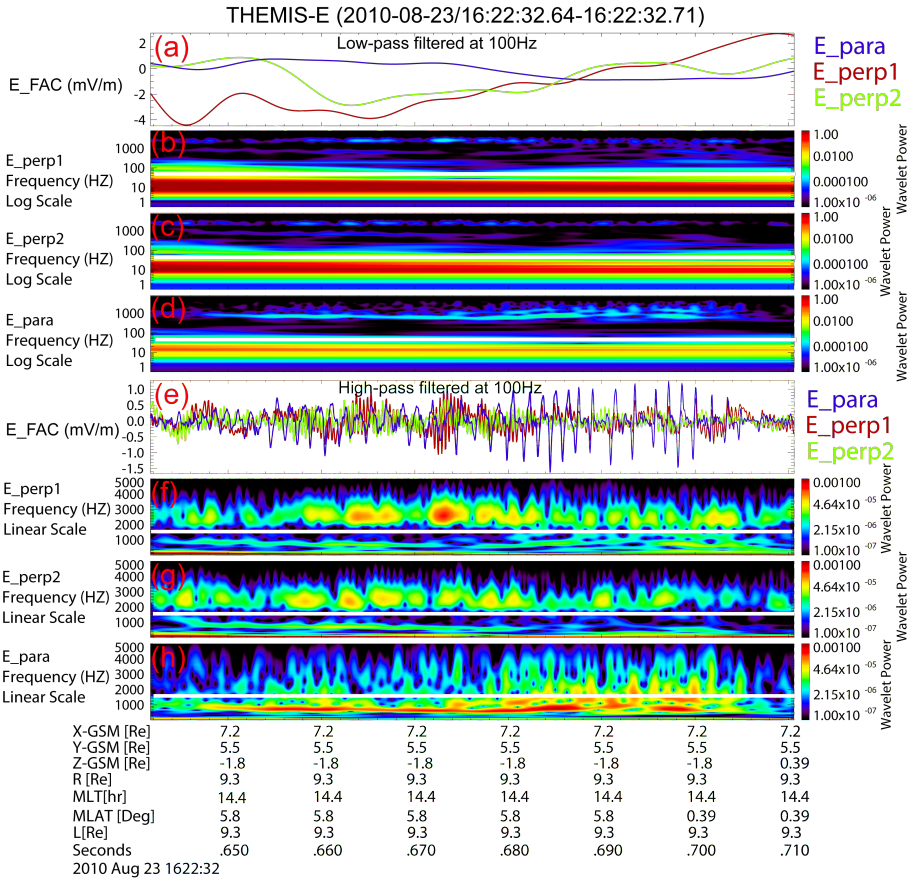

Figure 6.3: Waveform and wave power spectrum plots of the simultaneously observed waves. (a) Parallel and perpendicular components of electric field low-pass filtered at 100Hz. (b, c and d) Wave power spectra of the electric field in perpendicular and parallel directions in log scale. The white lines indicate lower-hybrid frequency. (e) Parallel and perpendicular components of electric field high-pass filtered at 100Hz. (f, g and h) Wave power spectra of the electric field in perpendicular and parallel directions in linear scale. The white lines indicate electron cyclotron frequency.

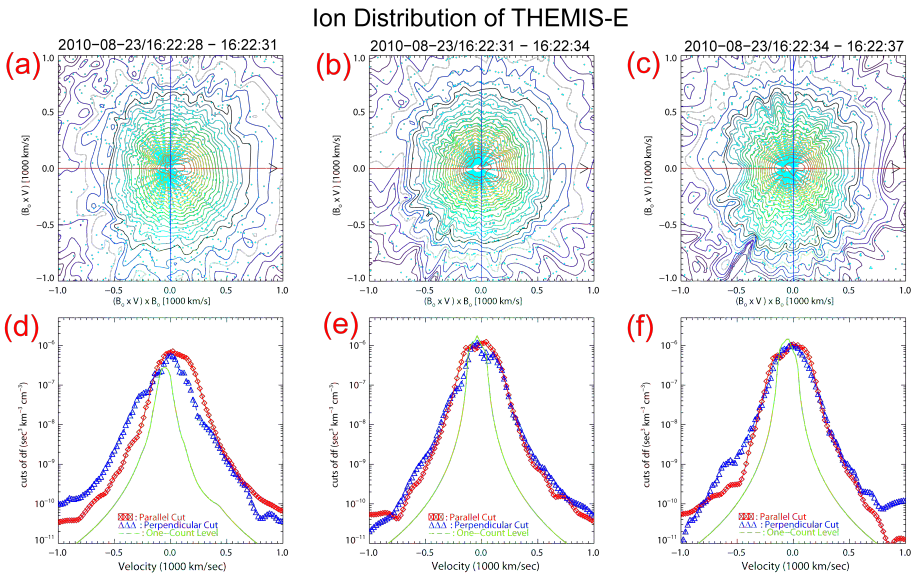

Figure 6.4: Distribution functions of lower-energy ions measured by ESA. (a, b and c) Distribution functions of lower-energy ions at times preceding, during and after the time of simultaneously observed waves. The horizontal axis is perpendicular to the ambient magnetic field and the bulk velocity defines the plane. (d, e and f) Cuts of distribution functions of lower-energy ions corresponding to a, b and c.

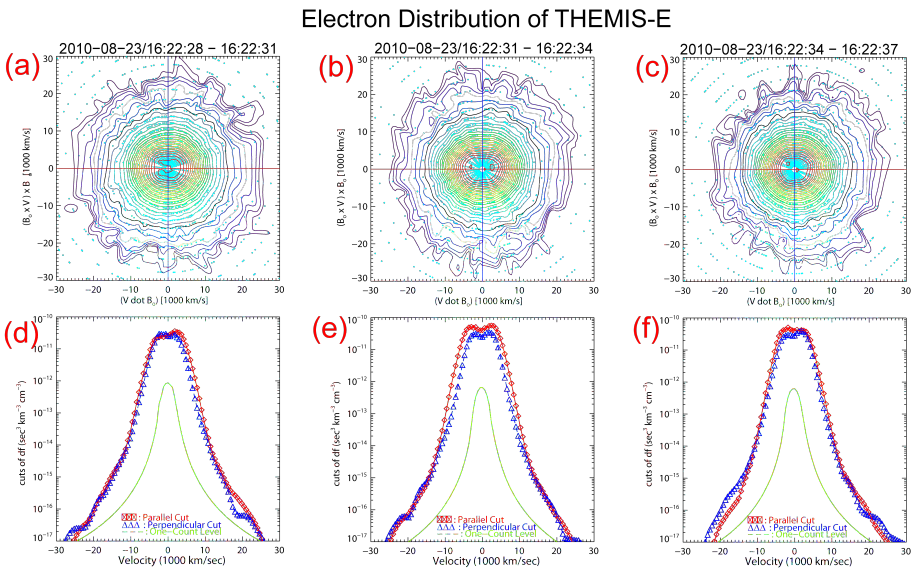

Figure 6.5: Distribution functions of lower-energy electrons measured by ESA. (a, b and c) Distribution functions of lower-energy electrons at times preceding, during and after the time of simultaneously observed waves. The horizontal axis is parallel to the ambient magnetic field and the bulk velocity defines the plane. (d, e and f) Cuts of distribution functions of lower-energy electrons corresponding to a, b and c.

6.5 Discussion and Conclusions

We have reported here the first simultaneous observations of lower-hybrid waves, whistler-mode waves, electrostatic solitary waves and electron cyclotron waves at the low-latitude boundary layer of the Earth's magnetopause.

The particle distribution functions show that lower-energy ions (<1.3 keV) are anisotropic with $T_{i\perp} > T_{i\parallel}$ while lower-energy (<300 eV) electrons are anisotropic with $T_{e\perp} < T_{e\parallel}$. In addition, lower-energy electrons show a double-peaked distribution, i.e., bi-streaming beams, consistent with possible source mechanisms for electrostatic electron cyclotron waves. These distributions are consistent with instability mechanisms proposed for the observed waves. The results provide insights into wave coupling near the magnetopause and suggest that coupling processes may be more important than previously thought.

The variations in the solar wind condition may correspond to the changes in the fields and plasma observed by THEMIS-E one hour later. It usually takes only a few minutes for a spacecraft to cross a magnetopause [144, 146]. However, the magnetopause crossing in this event took more than 1 hr.

The wave electric field of the lower-hybrid waves is mainly perpendicular to B_0 consistent with lower-hybrid drift waves. This wave mode may be excited by the observed density gradient. The lower-energy electrons with anisotropic distributions of $T_{e\parallel} > T_{e\perp}$ may have been heated by the observed lower-hybrid waves, consistent with the suggestion that lower-hybrid waves lead to electron heating in the parallel direction [16].

The wave electric field of electron cyclotron waves is mainly contained in the plane perpendicular to B_0 while the wave power of whistler-mode waves enhances in the parallel to B_0 direction. The 30 eV electrons may be trapped and bunched by the parallel electric field of the whistler-mode waves. The trapped electrons may excite electrostatic waves via the resistive medium instability, which is a type of bi-stream instability. The bi-streaming beams are consistent with possible source mechanisms proposed for

electrostatic electron cyclotron waves. The observation of high frequency electrostatic waves is the only and strongest indication for the presence of electron beams flowing along the magnetic field. Presumably these beams are emanating from the reconnection site at the cusp magnetopause along the magnetic separatrices.

High frequency electrostatic electron cyclotron waves may evolve into electrostatic solitary waves. The solitary waves with amplitudes up to 2.5 mV/m may cause the observed perpendicular ion heating, consistent with Ergun et al. [42].

Chapter 7

Summary and Future Work

Magnetic reconnection is a ubiquitous process occurring in the universe. It is considered to be an important mechanism by which magnetic energy is dissipated in the universe [39]. The microphysics of magnetic reconnection is poorly understood although it has been studied for over 50 years. The effect of different wave modes on the reconnection process has been a problem of longstanding interest.

7.1 Summary

The work presented in this thesis has summarized the in situ observations of plasma wave modes, at frequencies near the ion cyclotron frequency and up to the plasma frequency near the Earth's dayside magnetopause. The magnetopause is of particular importance as it is believed to play a major role in magnetic reconnection with the subsequent injection of solar wind plasma into the magnetosphere. There are many observational studies dealing with individual wave modes. We present results when different wave modes were simultaneously observed. In the first case study, we identified intense whistler-mode waves and electrostatic waves and associated electron heating in a well-defined electron diffusion region for the first time. In the second case study, we observed electrostatic ion cyclotron waves and associated ion heating in a magnetopause reconnection layer for the first time. In the third case study, we identified simultaneous observations of four wave modes with evidence of bi-stream electrons in a magnetopause

boundary layer for the first time. The results provide insights into generation mechanisms of waves, roles of waves in reconnection and boundary layer formation and wave interactions near the magnetopause.

Electron beams generated in the reconnection process may be a major free energy source that can generate different wave modes. Density gradients as well as different kinds of distribution functions are also important. Electrostatic solitary waves are observed associated strongly with electron cyclotron waves. We suggest that electron cyclotron waves may evolve into electrostatic solitary waves at the magnetopause. This might be a novel mechanism for the generation of electrostatic solitary waves. More work is needed to verify this suggestion.

The waves play crucial roles in the reconnection onset and supporting the reconnection, in anomalous resistivity and diffusion. The diffusive resistivity may be due to the combined effects of different wave modes. The low-frequency wave modes may play a crucial role in reconnection by providing anomalous resistivity. The high-frequency wave modes are generated by unstable electron distributions and thus provide detailed information about the electron-scale dynamics. Whistler-mode waves have the ability to propagate over large distances away from the reconnection site without appreciable damping. This property makes whistler-mode waves a great tool for remote sensing of reconnection sites as well as transporting information from the reconnection site to other places in the plasma.

The work presented in this thesis has helped validate and improve simulations of reconnection, as well as guide investigations with the Magnetospheric Multiscale (MMS) mission, which is designed to study the microphysics of reconnection and associated particle energization in the Earth's magnetosphere. Magnetic reconnection plays an important role in particle energization and in driving explosive phenomena in the universe. These processes are a direct influence on the health of astronauts, longevity of spacecraft and performance of modern technological systems such as telecommunications networks, GPS navigation and electrical power grids. Understanding magnetic reconnection can help understand and predict space weather and its impacts on Earth. The fundamental

knowledge of the microphysics of reconnection is also critical to improving magnetic confinement in fusion reactors in laboratories.

7.2 Future Work

Some of the previous observations suggest that these waves are most intense along the separatrices emanating from the reconnection sites. However, it's still not clear how are different wave modes located with respect to the inner structure of the current sheet and the separatrices. We will perform a statistical study to investigate how are different wave modes distributed in the reconnecting current sheet by using THEMIS and Polar data (at magnetopause) and Cluster data (in magnetotail).

Future work is to expand the scope of reconnection regions in space and laboratories and wave survey for both simulation and observation studies. The MMS mission was launched on 12 March 2015. The four identically instrumented spacecraft of MMS would provide plasmas, fields, and particles data with unprecedented (milliseconds) time resolution and accuracy needed to reveal the small-scale three-dimensional structure and dynamics of the elusively thin and fast-moving electron diffusion region. The work presented in this thesis would help validate and guide investigations with the MMS mission.

References

[1] R. L. Alexander, S. O'Modhrain, D. A. Roberts, J. A. Gilbert, and T. H. Zurbuchen. The bird's ear view of space physics: Audification as a tool for the spectral analysis of time series data. *J. Geophys. Res. Space Physics*, 119:52595271, July 2014.

[2] W. E. Amatucci, D. N. Walker, G. Ganguli, J. A. Antoniades, D. Duncan, J. H. Bowles, V. Gavrishchaka, and M. E. Koepke. Plasma Response to Strongly Sheared Flow. *Physical Review Letters*, 77:1978–1981, September 1996.

[3] W. E. Amatucci, D. N. Walker, G. Ganguli, D. Duncan, J. A. Antoniades, J. H. Bowles, V. Gavrishchaka, and M. E. Koepke. Velocity-shear-driven ion-cyclotron waves and associated transverse ion heating. *J. Geophys. Res.*, 103:11711–11724, June 1998.

[4] R. R. Anderson, T. E. Eastman, C. C. Harvey, M. M. Hoppe, B. T. Tsurutani, and J. Etcheto. Plasma waves near the magnetopause. *J. Geophys. Res.*, 87:2087–2107, April 1982.

[5] V. Angelopoulos. The THEMIS Mission. *Space Sci. Rev.*, 141:5–34, December 2008.

[6] N. Aunai, M. Hesse, C. Black, R. Evans, and M. Kuznetsova. Influence of the dissipation mechanism on collisionless magnetic reconnection in symmetric and asymmetric current layers. *Physics of Plasmas*, 20(4):042901, April 2013.

[7] H. U. Auster, K. H. Glassmeier, W. Magnes, O. Aydogar, W. Baumjohann, D. Constantinescu, D. Fischer, K. H. Fornacon, E. Georgescu, P. Harvey, O. Hillenmaier, R. Kroth, M. Ludlam, Y. Narita, R. Nakamura, K. Okrafka, F. Plaschke, I. Richter, H. Schwarzl, B. Stoll, A. Valavanoglou, and M. Wiedemann. The THEMIS Fluxgate Magnetometer. *Space Sci. Rev.*, 141:235–264, December 2008.

[8] S. D. Bale, F. S. Mozer, and T. Phan. Observation of lower hybrid drift instability in the diffusion region at a reconnecting magnetopause. *Geophys. Res. Lett.*, 29(24):2180, dec 2002.

[9] E. V. Belova, J. Blenski, M. Denis, L. M. Zelenyj, and S. P. Savin. Excitation of ion cyclotron waves at the boundary of the magnetosphere. *Fizika Plazmy*, 17:555–560, August 1991.

[10] R. Bergmann. Electrostatic ion (hydrogen) cyclotron and ion acoustic wave instabilities in regions of upward field-aligned current and upward ion beams. *J. Geophys. Res.*, 89:953–968, February 1984.

[11] R. Bergmann and M. K. Hudson. Decay of electrostatic hydrogen cyclotron waves into ion acoustic modes in auroral field lines. *J. Geophys. Res.*, 92:2495–2504, March 1987.

[12] J. Blecki, K. Kossaki, B. Popielawska, S. I. Klimov, and S. A. Romanov. ELF plasma waves associated with plasma jets near the earth magnetopause as observed by Prognoz-8. *Phys. Scr.*, 37:623–631, April 1988.

[13] J. W. Bonnell, F. S. Mozer, G. T. Delory, A. J. Hull, R. E. Ergun, C. M. Cully, V. Angelopoulos, and P. R. Harvey. The Electric Field Instrument (EFI) for THEMIS. *Space Sci. Rev.*, 141:303–341, December 2008.

[14] A. Bratenahl and C. M. Yeates. Experimental Study of Magnetic Flux Transfer at the Hyperbolic Neutral Point. *Physics of Fluids*, 13:2696–2709, November 1970.

[15] L. J. Cahill and P. G. Amazeen. The Boundary of the Geomagnetic Field. *J. Geophys. Res.*, 68:1835–1843, April 1963.

[16] I. H. Cairns and B. F. McMillan. Electron acceleration by lower hybrid waves in magnetic reconnection regions. *Physics of Plasmas*, 12(10):102110, October 2005.

[17] C. Cattell. The relationship of field-aligned currents to electrostatic ion cyclotron waves. *J. Geophys. Res.*, 86:3641–3645, May 1981.

[18] C. Cattell, R. Bergmann, K. Sigsbee, C. Carlson, C. Chaston, R. Ergun, J. McFadden, F. S. Mozer, M. Temerin, R. Strangeway, R. Elphic, L. Kistler, E. Moebius, L. Tang, D. Klumpar, and R. Pfaff. The association of electrostatic ion cyclotron waves, ion and electron beams and field-aligned currents: FAST observations of an auroral zone crossing near midnight. *Geophys. Res. Lett.*, 25:2053–2056, 1998.

[19] C. Cattell, J. Crumley, J. Dombeck, J. R. Wygant, and F. S. Mozer. Polar observations of solitary waves at the Earth's magnetopause. *Geophys. Res. Lett.*, 29(5):050000–1, March 2002.

[20] C. Cattell, J. Dombeck, J. Wygant, J. F. Drake, M. Swisdak, M. L. Goldstein, W. Keith, A. Fazakerley, M. André, E. Lucek, and A. Balogh. Cluster observations of electron holes in association with magnetotail reconnection and comparison to simulations. *Journal of Geophysical Research (Space Physics)*, 110(A9):1211, January 2005.

[21] C. Cattell, F. S. Mozer, I. Roth, R. R. Anderson, R. C. Elphic, W. Lennartsson, and Ungstrup E. ISEE 1 observations of electrostatic ion cyclotron waves in association with ion beams on auroral field lines from 2.5 to 4.5 RE. *J. Geophys. Res.*, 96:11421–11439, July 1991.

[22] C. Cattell, J. Wygant, F. S. Mozer, T. Okada, K. Tsuruda, S. Kokubun, and T. Yamamoto. ISEE 1 and Geotail observations of low-frequency waves at the magnetopause. *J. Geophys. Res.*, 100:11823, July 1995.

[23] C. Cattell, J. R. Wygant, K. Goetz, K. Kersten, P. J. Kellogg, T. von Rosenvinge, S. D. Bale, I. Roth, M. Temerin, M. K. Hudson, R. A. Mewaldt, M. Wiedenbeck, M. Maksimovic, R. Ergun, M. Acuna, and C. T. Russell. Discovery of very large amplitude whistler-mode waves in Earth's radiation belts. *Geophys. Res. Lett.*, 35:1105, January 2008.

[24] C. A. Cattell and F. S. Mozer. Experimental determination of the dominant wave mode in the active near-earth magnetotail. *Geophys. Res. Lett.*, 13(3):221–224, mar 1986.

[25] C. A. Cattell, F. S. Mozer, R. R. Anderson, E. W. Hones, and R. D. Sharp. ISEE observations of the plasma sheet boundary, plasma sheet, and neutral sheet: 2. Waves. *J. Geophys. Res.*, 91:5681–5688, May 1986.

[26] S. Chapman and V. C. A. Ferraro. A new theory of magnetic storms. *Terrestrial Magnetism and Atmospheric Electricity (Journal of Geophysical Research)*, 36:77, 1931.

[27] C. C. Chaston, T. D. Phan, J. W. Bonnell, F. S. Mozer, M. Acuña, M. L. Goldstein, A. Balogh, M. Andre, H. Reme, and A. Fazakerley. Drift-Kinetic Alfvén Waves Observed near a Reconnection X Line in the Earth's Magnetopause. *Phys. Rev. Lett.*, 95(6):065002, August 2005.

[28] H. Che, J. F. Drake, and M. Swisdak. A current filamentation mechanism for breaking magnetic field lines during reconnection. *nature*, 474:184–187, June 2011.

[29] F. V. Coroniti. On the tearing mode in quasi-neutral sheets. *J. Geophys. Res.*, 85:6719–6728, December 1980.

[30] F. V. Coroniti. Space plasma turbulent dissipation - Reality or myth? *Space Sci. Rev.*, 42:399–410, October 1985.

[31] L. Dai, J. R. Wygant, C. Cattell, J. Dombeck, S. Thaller, C. Mouikis, A. Balogh, and H. Rème. Cluster observations of surface waves in the ion jets from magnetotail reconnection. *Journal of Geophysical Research (Space Physics)*, 116:12227, December 2011.

[32] Lei Dai. Collisionless magnetic reconnection via alfvén eigenmodes. *Phys. Rev. Lett.*, 102:245003, Jun 2009.

[33] W. Daughton. Electromagnetic properties of the lower-hybrid drift instability in a thin current sheet. *Phys. Plasmas*, 10(8):3103–3119, August 2003.

[34] R. C. Davidson and N. T. Gladd. Anomalous transport properties associated with the lower-hybrid-drift instability. *Physics of Fluids*, 18:1327–1335, October 1975.

[35] X. H. Deng and H. Matsumoto. Rapid magnetic reconnection in the Earth's magnetosphere mediated by whistler waves. *Nature*, 410:557–560, March 2001.

[36] J. F. Drake, O. V. Agapitov, and F. S. Mozer. The development of a bursty precipitation front with intense localized parallel electric fields driven by whistler waves. *Geophys. Res. Lett.*, 2015.

[37] J. F. Drake, M. Swisdak, C. Cattell, M. A. Shay, B. N. Rogers, and A. Zeiler. Formation of Electron Holes and Particle Energization During Magnetic Reconnection. *Science*, 299:873–877, February 2003.

[38] W. E. Drummond and M. N. Rosenbluth. Anomalous Diffusion Arising from Microinstabilities in a Plasma. *Physics of Fluids*, 5:1507–1513, December 1962.

[39] J. W. Dungey. Interplanetary Magnetic Field and the Auroral Zones. *Phys. Rev. Lett.*, 6:47–48, January 1961.

[40] T. E. Eastman and E. W. Hones, Jr. Characteristics of the magnetospheric boundary layer and magnetopause layer as observed by Imp 6. *"J. Geophys. Res."*, 84:2019–2028, May 1979.

[41] T. E. Eastman, E. W. Hones, Jr., S. J. Bame, and J. R. Asbridge. The magnetospheric boundary layer - Site of plasma, momentum and energy transfer from the magnetosheath into the magnetosphere. *"Geophys. Res. Lett."*, 3:685–688, November 1976.

[42] R. E. Ergun, C. W. Carlson, J. P. McFadden, F. S. Mozer, L. Muschietti, I. Roth, and R. J. Strangeway. Debye-Scale Plasma Structures Associated with Magnetic-Field-Aligned Electric Fields. *Physical Review Letters*, 81:826–829, July 1998.

[43] D. H. Fairfield. Average and unusual locations of the Earth's magnetopause and bow shock. *J. Geophys. Res.*, 76:6700, 1971.

[44] W. M. Farrell, M. D. Desch, M. L. Kaiser, and K. Goetz. The dominance of electron plasma waves near a reconnection X-line region. *Geophys. Res. Lett.*, 29(19):190000–1, October 2002.

[45] W. M. Farrell, M. D. Desch, K. W. Ogilvie, M. L. Kaiser, and K. Goetz. The role of upper hybrid waves in magnetic reconnection. *Geophys. Res. Lett.*, 30:2259, December 2003.

[46] W. M. Farrell, D. A. Gurnett, J. D. Menietti, H. K. Wong, and C. S. Lin. Wave intensifications near the electron cyclotron frequency within the polar cusp. *J. Geophys. Res.*, 95:6493–6504, May 1990.

[47] W. Fox, M. Porkolab, J. Egedal, N. Katz, and A. Le. Laboratory Observation of Electron Phase-Space Holes during Magnetic Reconnection. *Phys. Rev. Lett.*, 101(25):255003, December 2008.

[48] K. Fujimoto and R. D. Sydora. Whistler waves associated with magnetic reconnection. *Geophys. Res. Lett.*, 35:19112, October 2008.

[49] S. A. Fuselier and W. S. Lewis. Properties of Near-Earth Magnetic Reconnection from In-Situ Observations. *Space Sci. Rev.*, 160:95–121, October 2011.

[50] G. Ganguli, Y. C. Lee, and P. Palmadesso. A new mechanism for excitation of electrostatic ion cyclotron waves and associated perpendicular ion heating. *Geophys. Res. Lett.*, 12:643–646, October 1985.

[51] G. Ganguli, Y. C. Lee, and P. J. Palmadesso. Kinetic theory for electrostatic waves due to transverse velocity shears. *Physics of Fluids*, 31:823–838, April 1988.

[52] S. P. Gary and T. E. Eastman. The lower hybrid drift instability at the magnetopause. *J. Geophys. Res.*, 84:7378–7381, December 1979.

[53] N. T. Gladd and J. D. Huba. Finite beta effects on the drift-cyclotron instability. *Physics of Fluids*, 22:911–922, May 1979.

[54] M. V. Goldman, D. L. Newman, G. Lapenta, L. Andersson, J. T. Gosling, S. Eriksson, S. Markidis, J. P. Eastwood, and R. Ergun. Čerenkov Emission of Quasiparallel Whistlers by Fast Electron Phase-Space Holes during Magnetic Reconnection. *Physical Review Letters*, 112(14):145002, April 2014.

[55] M. V. Goldman, D. L. Newman, and P. Pritchett. Vlasov simulations of electron holes driven by particle distributions from PIC reconnection simulations with a guide field. *Geophys. Res. Lett.*, 35:22109, November 2008.

[56] J. T. Gosling, J. R. Asbridge, S. J. Bame, W. C. Feldman, G. Paschmann, N. Sckopke, and C. T. Russell. Evidence for quasi-stationary reconnection at the dayside magnetopause. *J. Geophys. Res.*, 87:2147–2158, April 1982.

[57] J. T. Gosling, R. M. Skoug, D. J. McComas, and C. W. Smith. Direct evidence for magnetic reconnection in the solar wind near 1 AU. *Journal of Geophysical Research (Space Physics)*, 110:1107, January 2005.

[58] J. T. Gosling, M. F. Thomsen, S. J. Bame, T. G. Onsager, and C. T. Russell. The electron edge of the low latitude boundary layer during accelerated flow events. *Geophys. Res. Lett.*, 17:1833–1836, October 1990.

[59] D. B. Graham, Y. V. Khotyaintsev, A. Vaivads, M. André, and A. N. Fazakerley. Electron Dynamics in the Diffusion Region of an Asymmetric Magnetic Reconnection. *Physical Review Letters*, 112:5004, May 2014.

[60] D. A. Gurnett, R. R. Anderson, B. T. Tsurutani, E. J. Smith, G. Paschmann, G. Haerendel, S. J. Bame, and C. T. Russell. Plasma wave turbulence at the magnetopause - Observations from ISEE 1 and 2. *J. Geophys. Res.*, 84:7043–7058, December 1979.

[61] D. A. Gurnett, L. A. Frank, and R. P. Lepping. Plasma waves in the distant magnetotail. *J. Geophys. Res.*, 81:6059–6071, December 1976.

[62] J. P. Hauck, H. Bohmer, N. Rynn, and G. Benford. Ion beam excitation of ion-cyclotron waves and ion heating in plasmas with drifting electrons. *Journal of Plasma Physics*, 19:253, April 1978.

[63] M. Hesse, N. Aunai, S. Zenitani, M. Kuznetsova, and J. Birn. Aspects of collisionless magnetic reconnection in asymmetric systems. *Physics of Plasmas*, 20(6):061210, June 2013.

[64] M. Hesse, T. Neukirch, K. Schindler, M. Kuznetsova, and S. Zenitani. The Diffusion Region in Collisionless Magnetic Reconnection. *Space Sci. Rev.*, 160:3–23, October 2011.

[65] E. W. Hones, Jr., J. R. Asbridge, S. J. Bame, M. D. Montgomery, S. Singer, and S.-I. Akasofu. Measurements of magnetotail plasma flow made with Vela 4B. *J. Geophys. Res.*, 77:5503, 1972.

[66] J. D. Huba, N. T. Gladd, and K. Papadopoulos. The lower-hybrid-drift instability as a source of anomalous resistivity for magnetic field line reconnection. *Geophys. Res. Lett.*, 4:125–126, 1977.

[67] H. Ji, T. Carter, S. Hsu, and M. Yamada. Study of local reconnection physics in a laboratory plasma. *Earth, Planets, and Space*, 53:539–545, June 2001.

[68] H. Ji, S. Terry, M. Yamada, R. Kulsrud, A. Kuritsyn, and Y. Ren. Electromagnetic Fluctuations during Fast Reconnection in a Laboratory Plasma. *Phys. Rev. Lett.*, 92(11):115001, March 2004.

[69] H. Ji, M. Yamada, S. Hsu, and R. Kulsrud. Experimental Test of the Sweet-Parker Model of Magnetic Reconnection. *Physical Review Letters*, 80:3256–3259, April 1998.

[70] H. Karimabadi, W. Daughton, and K. B. Quest. Role of electron temperature anisotropy in the onset of magnetic reconnection. *Geophys. Res. Lett.*, 31:18801, September 2004.

[71] P. J. Kellogg. Flow of Plasma around the Earth. *J. Geophys. Res.*, 67:3805–3811, September 1962.

[72] C. F. Kennel and M. Ashour-Abdalla. *Electrostatic waves and the strong diffusion of magnetospheric electrons*, pages 245–344. 1982.

[73] C. F. Kennel and H. E. Petschek. Limit on Stably Trapped Particle Fluxes. *J. Geophys. Res.*, 71:1, January 1966.

[74] C. F. Kennel, F. L. Scarf, R. W. Fredricks, J. H. McGehee, and F. V. Coroniti. VLF electric field observations in the magnetosphere. *J. Geophys. Res.*, 75:6136–6152, November 1970.

[75] Y. V. Khotyaintsev, A. Vaivads, A. Retinò, M. André, C. J. Owen, and H. Nilsson. Formation of Inner Structure of a Reconnection Separatrix Region. *Physical Review Letters*, 97(20):205003, November 2006.

[76] A. V. Khrabrov and B. U. Ö. Sonnerup. Error estimates for minimum variance analysis. *J. Geophys. Res.*, 103:6641–6652, April 1998.

[77] J. M. Kindel and C. F. Kennel. Topside current instabilities. *J. Geophys. Res.*, 76:3055–3078, May 1971.

[78] P. M. Kintner. On the distinction between electrostatic ion cyclotron waves and ion cyclotron harmonic waves. *Geophys. Res. Lett.*, 7:585–588, August 1980.

[79] P. M. Kintner, M. C. Kelley, and F. S. Mozer. Electrostatic hydrogen cyclotron waves near one earth radius altitude in the polar magnetosphere. *Geophys. Res. Lett.*, 5:139–142, February 1978.

[80] P. M. Kintner, M. C. Kelley, R. D. Sharp, A. G. Ghielmetti, M. Temerin, C. Cattell, P. F. Mizera, and J. F. Fennell. Simultaneous observations of energetic /keV/ upstreaming and electrostatic hydrogen cyclotron waves. *J. Geophys. Res.*, 84:7201–7212, December 1979.

[81] M. G. Kivelson and C. T. Russell. *Introduction to Space Physics.* April 1995.

[82] M. G. Kivelson and C. T. Russell. *Introduction to Space Physics.* April 1995.

[83] M. E. Koepke, W. E. Amatucci, J. J. Carroll, III, and T. E. Sheridan. Experimental verification of the inhomogeneous energy-density driven instability. *Physical Review Letters*, 72:3355–3358, May 1994.

[84] M. E. Koepke, C. Teodorescu, E. W. Reynolds, C. C. Chaston, C. W. Carlson, J. P. McFadden, and R. E. Ergun. Inverse ion-cyclotron damping: Laboratory demonstration and space ramifications. *Physics of Plasmas*, 10:1605–1613, May 2003.

[85] J. Labelle and R. A. Treumann. Plasma waves at the dayside magnetopause. *Space Sci. Rev.*, 47:175–202, March 1988.

[86] J. LaBelle and R. A. Treumann. Auroral Radio Emissions, 1. Hisses, Roars, and Bursts. *Space Sci. Rev.*, 101:295–440, August 2002.

[87] J. Labelle, R. A. Treumann, G. Haerendel, O. H. Bauer, and G. Paschmann. AMPTE IRM observations of waves associated with flux transfer events in the magnetosphere. *J. Geophys. Res.*, 92:5827–5843, June 1987.

[88] G. S. Lakhina. Low-frequency electrostatic noise due to velocity shear instabilities in the regions of magnetospheric flow boundaries. *J. Geophys. Res.*, 92:12161–12170, November 1987.

[89] M. Lampe and K. Papadopoulos. Formation of fast electron tails in type II solar bursts. *Astrophys. J.*, 212:886–890, March 1977.

[90] R. L. Lysak, M. K. Hudson, and M. Temerin. Ion heating by strong electrostatic ion cyclotron turbulence. *J. Geophys. Res.*, 85:678–686, February 1980.

[91] M. E. Mandt, R. E. Denton, and J. F. Drake. Transition to whistler mediated magnetic reconnection. *Geophys. Res. Lett.*, 21:73–76, January 1994.

[92] H. Matsumoto, X. H. Deng, H. Kojima, and R. R. Anderson. Observation of Electrostatic Solitary Waves associated with reconnection on the dayside magnetopause boundary. *Geophys. Res. Lett.*, 30(6):060000–1, March 2003.

[93] H. Matsumoto and H. Usui. Intense bursts of electron cyclotron harmonic waves near the dayside magnetopause observed by GEOTAIL. *Geophys. Res. Lett.*, 24:49–52, 1997.

[94] J. P. McFadden, C. W. Carlson, D. Larson, M. Ludlam, R. Abiad, B. Elliott, P. Turin, M. Marckwordt, and V. Angelopoulos. The THEMIS ESA Plasma

Instrument and In-flight Calibration. *Space Sci. Rev.*, 141:277–302, December 2008.

[95] J. D. Menietti, J. S. Pickett, D. A. Gurnett, and J. D. Scudder. Electrostatic electron cyclotron waves observed by the plasma wave instrument on board Polar. *J. Geophys. Res.*, 106:6043–6058, April 2001.

[96] J. D. Menietti, J. S. Pickett, G. B. Hospodarsky, J. D. Scudder, and D. A. Gurnett. Polar observations of plasma waves in and near the dayside magnetopause/magnetosheath. *Planet. Space Sci.*, 52:1321–1337, December 2004.

[97] J. D. Menietti, O. Santolik, J. D. Scudder, J. S. Pickett, and D. A. Gurnett. Electrostatic electron cyclotron waves generated by low-energy electron beams. *Journal of Geophysical Research (Space Physics)*, 107:1285, October 2002.

[98] A. Miura. Anomalous transport by magnetohydrodynamic Kelvin-Helmholtz instabilities in the solar wind-magnetosphere interaction. *J. Geophys. Res.*, 89:801–818, February 1984.

[99] R. W. Motley and N. D'Angelo. Excitation of Electrostatic Plasma Oscillations near the Ion Cyclotron Frequency. *Physics of Fluids*, 6:296–299, February 1963.

[100] F. S. Mozer. Criteria for and statistics of electron diffusion regions associated with subsolar magnetic field reconnection. *J. Geophys. Res.*, 110:12222, Dec 2005.

[101] F. S. Mozer, S. D. Bale, and T. D. Phan. Evidence of Diffusion Regions at a Subsolar Magnetopause Crossing. *Phys. Rev. Lett.*, 89(1):015002, June 2002.

[102] F. S. Mozer, S. D. Bale, T. D. Phan, and J. A. Osborne. Observations of electron diffusion regions at the subsolar magnetopause. *Phys. Rev. Lett.*, 91:245002, Dec 2003.

[103] F. S. Mozer, C. W. Carlson, M. K. Hudson, R. B. Torbert, B. Parady, J. Yatteau, and M. C. Kelley. Observations of paired electrostatic shocks in the polar magnetosphere. *Physical Review Letters*, 38:292–295, February 1977.

[104] F. S. Mozer and P. L. Pritchett. Magnetic field reconnection: A first-principles perspective. *Physics Today*, 63(6):060000, 2010.

[105] F. S. Mozer and P. L. Pritchett. Electron Physics of Asymmetric Magnetic Field Reconnection. *Space Sci. Rev.*, 158:119–143, January 2011.

[106] J. Ng, J. Egedal, A. Le, W. Daughton, and L.-J. Chen. Kinetic Structure of the Electron Diffusion Region in Antiparallel Magnetic Reconnection. *Phys. Rev. Lett.*, 106(6):065002, February 2011.

[107] M. Øieroset, T. D. Phan, M. Fujimoto, R. P. Lin, and R. P. Lepping. In situ detection of collisionless reconnection in the Earth's magnetotail. *nature*, 412:414–417, July 2001.

[108] Y. Omura, H. Matsumoto, T. Miyake, and H. Kojima. Electron beam instabilities as generation mechanism of electrostatic solitary waves in the magnetotail. *J. Geophys. Res.*, 101:2685–2698, February 1996.

[109] E. N. Parker. *Cosmical magnetic fields: Their origin and their activity.* 1979.

[110] G. Paschmann, M. Øieroset, and T. Phan. In-Situ Observations of Reconnection in Space. *Space Sci. Rev.*, 178:385–417, October 2013.

[111] G. Paschmann, I. Papamastorakis, N. Sckopke, G. Haerendel, B. U. O. Sonnerup, S. J. Bame, J. R. Asbridge, J. T. Gosling, C. T. Russel, and R. C. Elphic. Plasma acceleration at the earth's magnetopause - Evidence for reconnection. *nature*, 282:243–246, November 1979.

[112] P. Petkaki, M. P. Freeman, and A. P. Walsh. Cluster observations of broadband electromagnetic waves in and around a reconnection region in the Earth's magnetotail current sheet. *Geophys. Res. Lett.*, 33:16105, August 2006.

[113] P. Petkaki, C. E. J. Watt, R. B. Horne, and M. P. Freeman. Anomalous resistivity in non-Maxwellian plasmas. *Journal of Geophysical Research (Space Physics)*, 108:1442, December 2003.

[114] H. E. Petschek. Magnetic Field Annihilation. *NASA Special Publication*, 50:425, 1964.

[115] T. D. Phan, J. F. Drake, M. A. Shay, F. S. Mozer, and J. P. Eastwood. Evidence for an elongated (> 60 ion skin depths) electron diffusion region during fast magnetic reconnection. *Phys. Rev. Lett.*, 99:255002, Dec 2007.

[116] T. D. Phan, J. T. Gosling, M. S. Davis, R. M. Skoug, M. Øieroset, R. P. Lin, R. P. Lepping, D. J. McComas, C. W. Smith, H. Reme, and A. Balogh. A magnetic reconnection X-line extending more than 390 Earth radii in the solar wind. *nature*, 439:175–178, January 2006.

[117] T.-D. Phan, M. Oieroset, and M. Fujimoto. Reconnection at the dayside low-latitude magnetopause and its nonrole in low-latitude boundary layer formation during northward interplanetary magnetic field. *Geophys. Res. Lett.*, 32:17101, September 2005.

[118] P. L. Pritchett. Collisionless magnetic reconnection in an asymmetric current sheet. *Journal of Geophysical Research (Space Physics)*, 113:6210, June 2008.

[119] P. L. Pritchett and F. S. Mozer. Asymmetric magnetic reconnection in the presence of a guide field. *Journal of Geophysical Research (Space Physics)*, 114:11210, November 2009.

[120] Z. Y. Pu, C. J. Xiao, X. G. Zhang, Z. Y. Huang, S. Y. Fu, Z. X. Liu, M. W. Dunlop, Q. G. Zong, C. M. Carr, H. Réme, I. Dandouras, A. Fazakerley, T. Phan, T. L. Zhang, H. Zhang, and X. G. Wang. Double Star TC-1 observations of component reconnection at the dayside magnetopause: a preliminary study. *Annales Geophysicae*, 23:2889–2895, November 2005.

[121] A. Retinò, M. B. Bavassano Cattaneo, M. F. Marcucci, A. Vaivads, M. André, Y. Khotyaintsev, T. Phan, G. Pallocchia, H. Rème, E. Möbius, B. Klecker, C. W. Carlson, M. McCarthy, A. Korth, R. Lundin, and A. Balogh. Cluster multispacecraft observations at the high-latitude duskside magnetopause: implications for continuous and component magnetic reconnection. *Annales Geophysicae*, 23:461–473, February 2005.

[122] A. Retinò, A. Vaivads, M. André, F. Sahraoui, Y. Khotyaintsev, J. S. Pickett, M. B. Bavassano Cattaneo, M. F. Marcucci, M. Morooka, C. J. Owen, S. C.

Buchert, and N. Cornilleau-Wehrlin. Structure of the separatrix region close to a magnetic reconnection X-line: Cluster observations. *Geophys. Res. Lett.*, 33:6101, March 2006.

[123] L. Rezeau and G. Belmont. Magnetic turbulence at the magnetopause, a key problem for understanding the solar wind/ magnetosphere exchanges. *Space Sci. Rev.*, 95:427–441, January 2001.

[124] P. Ricci, J. U. Brackbill, W. Daughton, and G. Lapenta. New role of the lower-hybrid drift instability in the magnetic reconnection. *Phys. Plasmas*, 12(5):055901, May 2005.

[125] B. N. Rogers, R. E. Denton, and J. F. Drake. Signatures of collisionless magnetic reconnection. *Journal of Geophysical Research (Space Physics)*, 108:1111, March 2003.

[126] S. S. Rossolenko, E. E. Antonova, Y. I. Yermolaev, I. P. Kirpichev, N. L. Borodkova, and E. Y. Budnik. Formation and characteristics of low latitude boundary layer. *Advances in Space Research*, 41:1545–1550, 2008.

[127] A. Roux, O. Le Contel, C. Coillot, A. Bouabdellah, B. de La Porte, D. Alison, S. Ruocco, and M. C. Vassal. The Search Coil Magnetometer for THEMIS. *Space Sci. Rev.*, 141:265–275, December 2008.

[128] V. Roytershteyn, W. Daughton, H. Karimabadi, and F. S. Mozer. Influence of the Lower-Hybrid Drift Instability on Magnetic Reconnection in Asymmetric Configurations. *Physical Review Letters*, 108(18):185001, May 2012.

[129] C. T. Russell and R. C. Elphic. ISEE observations of flux transfer events at the dayside magnetopause. *Geophys. Res. Lett.*, 6:33–36, January 1979.

[130] C. T. Russell and R. J. Walker. Flux transfer events at Mercury. *J. Geophys. Res.*, 90:11067, November 1985.

[131] N. Rynn, D. R. Dakin, D. L. Correll, and G. Benford. Ion Heating by the Current-Driven Electrostatic Ion-Cyclotron Instability. *Physical Review Letters*, 33:765–768, September 1974.

[132] M. Scholer, I. Sidorenko, C. H. Jaroschek, R. A. Treumann, and A. Zeiler. Onset of collisionless magnetic reconnection in thin current sheets: Three-dimensional particle simulations. *Physics of Plasmas*, 10:3521–3527, September 2003.

[133] J. D. Scudder, R. D. Holdaway, W. S. Daughton, H. Karimabadi, V. Roytershteyn, C. T. Russell, and J. Y. Lopez. First Resolved Observations of the Demagnetized Electron-Diffusion Region of an Astrophysical Magnetic-Reconnection Site. *Phys. Rev. Lett.*, 108(22):225005, June 2012.

[134] R. R. Shaw and D. A. Gurnett. Electrostatic noise bands associated with the electron gyrofrequency and plasma frequency in the outer magnetosphere. *J. Geophys. Res.*, 80:4259–4271, November 1975.

[135] P. Song, C. T. Russell, R. C. Elphic, J. T. Gosling, and C. A. Cattell. Structure and properties of the subsolar magnetopause for northward IMF - ISEE observations. *J. Geophys. Res.*, 95:6375–6387, May 1990.

[136] P. Song, C. T. Russell, N. Lin, R. J. Strangeway, and J. T. Gosling. *Wave and particle properties of the subsolar magnetopause*, pages 463–476. 1990.

[137] Y. Song and R. L. Lysak. Paradigm Transition in Cosmic Plasma Physics, Magnetic Reconnection and the Generation of Field-Aligned Current. *Washington DC American Geophysical Union Geophysical Monograph Series*, 118:11, 2000.

[138] B. U. Ö. Sonnerup. Magnetopause reconnection rate. *J. Geophys. Res.*, 79:1546–1549, April 1974.

[139] B. U. O. Sonnerup. Theory of the low-latitude boundary layer. *J. Geophys. Res.*, 85:2017–2026, May 1980.

[140] B. U. O. Sonnerup, G. Paschmann, I. Papamastorakis, N. Sckopke, G. Haerendel, S. J. Bame, J. R. Asbridge, J. T. Gosling, and C. T. Russell. Evidence for magnetic field reconnection at the earth's magnetopause. *J. Geophys. Res.*, 86:10049–10067, November 1981.

[141] G. Stenberg, T. Oscarsson, M. André, A. Vaivads, M. Morooka, N. Cornilleau-Wehrlin, A. Fazakerley, B. Lavraud, and P. M. E. Décréau. Electron-scale sheets

of whistlers close to the magnetopause. *Annales Geophysicae*, 23:3715–3725, December 2005.

[142] P. A. Sweet. The neutral point theory of solar flares. In B. Lehnert, editor, *Electromagnetic Phenomena in Cosmic Physics*, pages 123–134. Cambridge Univ. Press, New York, 1958.

[143] M. Swisdak, B. N. Rogers, J. F. Drake, and M. A. Shay. Diamagnetic suppression of component magnetic reconnection at the magnetopause. *Journal of Geophysical Research (Space Physics)*, 108:1218, May 2003.

[144] X. Tang, C. Cattell, J. Dombeck, L. Dai, L. B. Wilson, III, A. Breneman, and A. Hupach. THEMIS observations of the magnetopause electron diffusion region: Large amplitude waves and heated electrons. *Geophys. Res. Lett.*, 40:2884–2890, June 2013.

[145] X. Tang, C. Cattell, R. Lysak, L. B. Wilson, III, L. Dai, and R. Alexander. First simultaneous observations of lower hybrid, whistler mode, electrostatic solitary, and electron cyclotron waves in the magnetopause boundary layer. *Geophys. Res. Lett., to be submitted in May 2015.*

[146] X. Tang, C. Cattell, R. Lysak, L. B. Wilson, III, L. Dai, and S. Thaller. THEMIS observations of electrostatic ion cyclotron waves and associated ion heating near the Earth's dayside magnetopause. *J. Geophys. Res. Space Physics*, 120, March 2015.

[147] THEMIS Science Team. http://themis.ssl.berkeley.edu/overview.shtml.

[148] M. Temerin, C. Cattell, R. Lysak, M. Hudson, R. B. Torbert, F. S. Mozer, R. D. Sharp, and P. M. Kintner. The small-scale structure of electrostatic shocks. *J. Geophys. Res.*, 86:11278–11298, December 1981.

[149] M. Temerin, M. Woldorff, and F. S. Mozer. Nonlinear steepening of the electrostatic ion cyclotron wave. *Physical Review Letters*, 43:1941–1943, December 1979.

[150] C. Torrence and G. P. Compo. A Practical Guide to Wavelet Analysis. *Bulletin of the American Meteorological Society*, 79:61–78, January 1998.

[151] R. A. Treumann and W. Baumjohann. *Advanced space plasma physics*. 1997.

[152] R. A. Treumann, J. Labelle, and T. M. Bauer. Diffusion Processes: An Observational Perspective. In P. Song, B. U. O. Sonnerup, and M. F. Thomsen, editors, *Washington DC American Geophysical Union Geophysical Monograph Series*, volume 90 of *Washington DC American Geophysical Union Geophysical Monograph Series*, page 331, 1995.

[153] R. A. Treumann, J. Labelle, and R. Pottelette. Plasma diffusion at the magnetopause - The case of lower hybrid drift waves. *J. Geophys. Res.*, 96:16009, September 1991.

[154] B. T. Tsurutani and R. M. Thorne. Diffusion processes in the magnetopause boundary layer. *Geophys. Res. Lett.*, 9:1247–1250, November 1982.

[155] E. Ungstrup, D. M. Klumpar, and W. J. Heikkila. Heating of ions to superthermal energies in the topside ionosphere by electrostatic ion cyclotron waves. *J. Geophys. Res.*, 84:4289–4296, August 1979.

[156] A. Vaivads, M. André, S. C. Buchert, J.-E. Wahlund, A. N. Fazakerley, and N. Cornilleau-Wehrlin. Cluster observations of lower hybrid turbulence within thin layers at the magnetopause. *Geophys. Res. Lett.*, 31:3804, February 2004.

[157] A. Vaivads, Y. Khotyaintsev, M. André, and R. A. Treumann. Plasma Waves Near Reconnection Sites. In J. W. Labelle and R. A. Treumann, editors, *Geospace Electromagnetic Waves and Radiation*, volume 687 of *Lecture Notes in Physics, Berlin Springer Verlag*, page 251, January 2006.

[158] A. Vaivads, A. Retinò, and M. André. Microphysics of Magnetic Reconnection. *Space Sci. Rev.*, 122:19–27, February 2006.

[159] A. Vaivads, O. Santolík, G. Stenberg, M. André, C. J. Owen, P. Canu, and M. Dunlop. Source of whistler emissions at the dayside magnetopause. *Geophys. Res. Lett.*, 34:9106, May 2007.

[160] I. Y. Vasko, O. V. Agapitov, F. S. Mozer, A. V. Artemyev, and D. Jovanovic. Magnetic field depression within electron holes. *Geophys. Res. Lett.*, 2015.

[161] H. Viberg, Y. V. Khotyaintsev, A. Vaivads, M. André, and J. S. Pickett. Mapping HF waves in the reconnection diffusion region. *Geophys. Res. Lett.*, 40:1032–1037, March 2013.

[162] D. N. Walker, W. E. Amatucci, G. Ganguli, J. A. Antoniades, J. H. Bowles, D. Duncan, V. Gavrishchaka, and M. E. Koepke. Perpendicular ion heating by velocity-shear-driven waves. *Geophys. Res. Lett.*, 24:11871190, May 1997.

[163] J. R. Wygant, C. A. Cattell, R. Lysak, Y. Song, J. Dombeck, J. McFadden, F. S. Mozer, C. W. Carlson, G. Parks, E. A. Lucek, A. Balogh, M. Andre, H. Reme, M. Hesse, and C. Mouikis. Cluster observations of an intense normal component of the electric field at a thin reconnecting current sheet in the tail and its role in the shock-like acceleration of the ion fluid into the separatrix region. *Journal of Geophysical Research (Space Physics)*, 110:9206, September 2005.

[164] M. Yamada. Review of the recent controlled experiments for study of local reconnection physics. *Earth, Planets, and Space*, 53:509–519, June 2001.

[165] M. Yamada, R. Kulsrud, and H. Ji. Magnetic reconnection. *Reviews of Modern Physics*, 82:603–664, January 2010.

[166] J. Yoo, M. Yamada, H. Ji, J. Jara-Almonte, C. E. Myers, and L.-J. Chen. Laboratory Study of Magnetic Reconnection with a Density Asymmetry across the Current Sheet. *Physical Review Letters*, 113(9):095002, August 2014.

[167] T. S. T. Young, J. D. Callen, and J. E. McCune. High-frequency electrostatic waves in the magnetosphere. *J. Geophys. Res.*, 78:1082–1099, March 1973.

[168] Y. Zhang, H. Matsumoto, and H. Kojima. Whistler mode waves in the magnetotail. *J. Geophys. Res.*, 104:28633–28644, 1999.

[169] M. Zhou, X. Deng, M. Ashour-Abdalla, R. Walker, Y. Pang, C. Tang, S. Huang, M. El-Alaoui, Z. Yuan, and H. Li. Cluster observations of kinetic structures and

electron acceleration within a dynamic plasma bubble. *Journal of Geophysical Research (Space Physics)*, 118:674–684, February 2013.

[170] M. Zhou, Y. Pang, X. H. Deng, Z. G. Yuan, and S. Y. Huang. Density cavity in magnetic reconnection diffusion region in the presence of guide field. *Journal of Geophysical Research (Space Physics)*, 116:6222, June 2011.